

Dissertation

Analysis of Light Absorbing Carbonaceous Aerosols in Varying Conditions of Combustion

Conducted for the purpose of receiving the academic title

‘Doktor der Naturwissenschaften’

Supervisor:

Ao. Univ. Prof. Dipl.-Ing. Dr. techn. Anne Kasper-Giebl

Univ. Ass. Mag. pharm. Dr. rer. nat Heidi Bauer (†)

E 164

Institute of Chemical Technologies and Analytics, Vienna, Austria

Submitted at the Vienna University of Technology, Faculty of Technical Chemistry by

Tanja Dobovičnik

0928595

Novakova ulica 1, SI-1000 Ljubljana

Vienna, November 2013

Acknowledgments

I would like to thank to my PhD advisors Prof. Anne Kasper-Giebl. I appreciate all her contributions of time, ideas to make my Ph.D. experience productive and stimulating. She was generous, supportive and has provided insightful discussions about the research. I am also very grateful to dr. Griša Močnik and dr. Anthony Hansen for their scientific advice and knowledge and many insightful discussions. I also have to thank the members of my PhD committee. I will forever be thankful to my former research advisor, dr. Heidi Bauer. She was and remains my mentor, and life teacher. I would also like to thank prof. Puxbaum. He convinced me for the PhD research and without him I would not have this book. Here I would also like to thank to special person for all the comments and great advices.

A special thank goes to funding agency (SPIRIT Slovenia - Public Agency of the Republic of Slovenia for the Promotion of Entrepreneurship, Innovation, Development, Investment and Tourism) which has financially support me during my Ph.D.. Operation in part was financed by the European Union, European Social Fund (P-MR-09/1).

The most special thank goes to my best friend Polona Zavratnik for an expertly proofreading and correction of my english in the PhD thesis.

I would also like to thank my colleagues from Aerosol Company for support and technical advices during the research and study.

Lastly, I would like to thank my family for all their love and encouragement. My parents supported me in all my pursuits and enormous thanks go also to all my friends.

Abstract

Measurements of particulate matter from traffic emissions and wood-burning emissions are emerging trends in aerosol science. Angstrom exponent (α) is nowadays a common parameter to differentiate between these emission sources.

Within the CAST experiment different carbon-to-oxygen ratios (C/O ratios) were used in the CAST burner, to generate black and brownish aerosols. In this experiment, the two-component Aethalometer model (Sandradewi et al., 2008) was extended to all seven wavelengths available in the new Aethalometer instrument to provide more information besides BC concentration. The resulting Aethalometer model enabled the detection of the amount of BC and BrC in the black and brownish samples. The results were compared with another optical method, the integrating sphere. Aethalometer data were compensated with different compensation principles (Weingartner et al., 2003, Arnott et al., 2005 and Kirchstetter et al., 2007) and the Weingartner principle was used for further discussions. The Angstrom exponent α was calculated with the help of the compensated data. For BC α was found to be around 1.2 ± 0.3 , and α for brown carbon reached values up to 6.02 ± 1.0 .

In the second experiment, the wood-burning emissions were put into focus. Different types of wood (hardwood, softwood and pellets) and different stoves (wood-stove and pellets stove) were used in laboratory measurements. Emissions of the residential stoves (7kW power) were analysed with off-line (quartz filters) and on-line measurements (Aethalometer). When observing the filter samples of wood-burning visually, comparisons could be made with CAST experiment conditions at the C/O ratios of 0.21 or 0.31. Angstrom exponent calculated for wood (beech and spruce) reached an average value of $\alpha \sim 1.5 \pm 0.2$ and α of pellets was around 1.0 ± 0.05 . Anhydrosugars are well known tracers for wood smoke, especially levoglucosan, which was a major organic compound found in the wood smoke samples using liquid chromatography.

Emissions from wood burning are known to be important sources of ambient particulate matter in the Austrian and Slovenian regions. Due to these findings, ambient measurements were carried out as a part of PMinter project for 2011/12 and 2012/13 winter periods. Observation was focused on source apportionment, which means that again Aethalometer model was used to differentiate between BC fractions: BC_{wb} originated from wood smoke emissions and BC_{ff} was BC emitted by burning diesel or gasoline, heating oil and coal, which was neglected being a minor emission source (1%). Two measurement stations were chosen: an urban region (Klagenfurt – Völkermarkterstrasse) and a rural region (Zell – Ebenthal). In Klagenfurt, the BC_{ff} portion was about 88%, while in Zell it decreased to 69%. The amount of BC_{wb} was higher in Zell

(31%) than in Klagenfurt (12%) during the 2011/12 winter period. The percentages of BC_{ff} and BC_{wb} were similar also in the winter 2012/13. The values of the Angstrom exponents α used for Aethalometer model were set to $\alpha = 1.0$ for traffic and $\alpha = 2.0$ for wood-burning, based on the laboratory measurements described above. With the test of sensibility of the method (model), high deviation was observed by moving $\alpha \pm 10\%$. Setting the α of wood-burning for -10% may double the portion of BC_{wb} . Anhydrosugars were again analyzed to compare levoglucosan concentrations with BC_{wb} fraction..

The Aethalometer model gives us a new mechanism that can determine the contribution of biomass burning emissions in real time.

Kurzfassung

Die Messungen der Emissionen des Straßenverkehrs und der Emissionen, die bei der Verbrennung von Holz entstehen, sind wichtige Trends der Aerosolforschung. Häufig wird der Angström Exponent (α) verwendet, um zwischen diesen Emissionsquellen zu unterscheiden. Das erste Ziel der Doktorarbeit war das Vermessen von lichtabsorbierenden kohlenstoffhaltigen Partikeln mit dem Aethalometer.

Im CAST Experiment wurde durch die Verwendung unterschiedlicher Verhältnisse von Kohlenstoff zu Sauerstoff (C/O Verhältnisse) im CAST-Brenner die Möglichkeit geschaffen, schwarze und braune Aerosole zu generieren. Bei diesem Experiment wurde das auf zwei Wellenlängen basierende Aethalometermodell (Sandradewi et al., 2008) auf alle sieben Wellenlängen, die im neuen Aethalometer angeboten werden ausgeweitet, um neben der BC Konzentration noch weitere Informationen zu liefern. Mit dem Aethalometer konnten wir den Anteil von BC und BrC in den schwarzen und braunen Proben erfassen. Die Ergebnisse wurden mit einer weiteren optischen Methode, der Ulbricht-Kugel, verglichen. Die Aethalometerdaten wurden nach verschiedenen Prinzipien korrigiert, wobei die Kompensation über das Weingartner Prinzip (Weingartner et al., 2003) für die weiteren Diskussion benutzt wurden. So wurde der Angström Exponent α mit Hilfe von kompensierten Daten berechnet und lag für BC war bei ungefähr 1.2 ± 0.3 und bei BrC erreichten die Werte bis 6.02 ± 1.0 .

Im zweiten Experiment standen die Emissionen, die bei der Verbrennung von Holz entstehen, im Mittelpunkt. Diesbezüglich wurden die Partikel aus der Verbrennung von verschiedenen Holzsorten (Nadelholz, Laubholz und Pellets) in verschiedenen Ofenarten (Holzofen und Pelletofen) gemessen. So wurden Heizöfen (Leistung: 7kW) mit off-line Messungen (Quartz Filter) und on-line Messungen (Aethalometer) untersucht. Wenn man die Filterproben aus der Holzverbrennung mit bloßem Auge betrachtet, kann man Vergleiche mit dem CAST Experiment bei den C/O Verhältnissen von 0.21 und 0.31 ziehen. Der Angström Exponent berechnet für Holz (Buche und Fichte) erreichte einen durchschnittlichen Wert von $\alpha \sim 1.5 \pm 0.2$ und α für Pellets lag bei ungefähr 1.0 ± 0.05 . Anhydrozucker, besonders Levoglucosan aber auch Mannosan und Galactosan, sind Tracer für die Holzverbrennung, und wurden mittels Ionenchromatographie in den Holzrauchproben bestimmt.

In den letzten Jahren wurde in der Grenzregion Österreich-Slowenien die Holzverbrennung als wichtige Feinstaubquelle charakterisiert. Daher wurden als ein Teil des PMinter Projekts für den Winter 2011/12 und 2012/13 Messungen durchgeführt. Wieder wurde das Aethalometermodell für die Unterscheidung zwischen den BC Fraktionen benutzt. BC_{wb} stammte aus Holzrauchemissionen und BC_{ff} kennzeichnete BC-Emissionen aus Dieselkraftstoff-, Benzin-, Heizöl und Kohlenverbrennung – diese wurden wegen ihrer geringeren Rolle (1%) nicht beachtet. Zwei Messstationen wurden ausgewählt: eine städtische Station (Klagenfurt – Völkermarkterstrasse) und eine ländliche Station (Zell – Ebenthal). Der BC_{ff} Anteil in Klagenfurt lag bei 88%, in Zell sank er aber auf 69%. Die Menge des BC_{wb} im Winter 2011/12 war größer in Zell (31%) als in Klagenfurt (12%). Der Prozentsatz von BC_{ff} und BC_{wb} war ähnlich auch im Winter 2012/13. Die α Werte für das Aethalometer Modell wurden, gemäß den zuvor durchgeführten Laborexperimenten, auf $\alpha = 1.0$ für Verkehr und $\alpha = 2.0$ für Holzverbrennung eingestellt. Mit einem

Empfindlichkeitstest der Methode (Model), wurden bei einer Änderung von α für $\pm 10\%$ erhebliche Abweichungen beobachtet. Eine Senkung von α für 10% für die Holzverbrennung kann den Teil von BC_{wb} verdoppeln. Auch Anhydrozucker wurde analysiert und die Levoglucosankonzentration mit der BC_{wb} Fraktion verglichen. Das Aethalometer Model gibt uns einen neuen Mechanismus, der den Anteil von Feinstaub der aus der Holzverbrennung resultiert in Echtzeit bestimmen kann..

Contents

CHAPTER 1.....	1
Introduction	1
1.1. Definition of carbonaceous species.....	2
Black carbon and elemental carbon	2
Organic carbon	3
Brown carbon	3
1.2. Relevance for health and climate	4
1.3. Light absorbing carbonaceous aerosols and their source apportionment in general	5
1.4. Motivation	5
CHAPTER 2.....	8
Methodology	8
2.1. Off-line measurements.....	9
2.1.1. Filters.....	9
2.1.2. Thermal-optical methods.....	9
2.1.3. Optical methods.....	14
2.1.4. Anhydrosugars	16
2.2. On-line measurements	18
2.2.1. Nephelometer (Model 3563, TSI)	18
2.2.2. Aethalometer® (Model AE 31, Magee Scientific)	20
2.2.3. Data post-processing of Aethalometer data	22
CHAPTER 3.....	29
The CAST experiment.....	29
3.1. The CAST propane burner and the experiment	30
3.2. Results.....	36

3.2.1. Comparison of BC and EC data obtained with different methods	38
3.2.2. Composition of light absorbing carbonaceous aerosols.....	46
3.2.3. Analysis made by two-component Aethalometer model (absorption vs. wavelength) to determine two carbonaceous components: BC and BrC	49
CHAPTER 4.....	54
The wood-burning experiment.....	54
4.1. Emissions from household heating	55
4.1.1. Wood-burning sampling system	55
4.1.2. Combustion chamber – a wood-burning stove.....	59
4.1.1. Combustion procedures	60
4.2. Type of wood	63
4.3. Results.....	64
4.3.1. Organic carbon, elemental carbon, black carbon and brown carbon concentration dependence on various types of wood.....	67
4.3.2. Determination of the absorption Angstrom exponent.....	78
4.3.3. Anhydrosugar analysis – tracers of wood-burning emissions.....	82
CHAPTER 5.....	86
Ambient measurements.....	86
5.1. Measurement stations	87
5.2. Sources of energy and emissions	90
5.3. Results.....	93
5.3.1. Urban and rural emissions – black carbon measurements	93
5.3.2. Source apportionment – residential combustion and traffic	97
5.3.3. Anhydrosugars – tracers of wood-burning.....	102
5.3.4. Sensitivity of the Aethalometer model when changing the absorption Angstrom exponent of wood-burning (α_{wb}) and fossil fuels (α_{ff}) for 10%	103
CHAPTER 6.....	106

Summary and conclusions.....106

Bibliography..... 111

List of Figures

Figure 1: TEM pictures of soot particles generated under a) C/O ratio = 0.21, and b) C/O ratio = 0.60 (Kim et al., 2013).....	3
Figure 2: Particle deposition as a function of particle diameter in various regions of the lung. The nasopharyngeal region consists of the nose and throat; the tracheobronchial (T-bronchial) region consists of the windpipe and large airways; and the pulmonary region consists of the small bronchi and the alveolar sacs. Source: Task Group on Lung Dynamics (1996). Health Physics. 12: 173. (http://www.onlineethics.org/cms/23617.aspx – 06/10/ 13).....	4
Figure 3: The structure of OC-EC Dual-optical analyzer (http://www.cdc.gov/niosh/docs/2003-154/pdfs/5040f3.pdf . – 01/15/13).....	10
Figure 4: Example of thermogram. Peaks correspond to organic (OC), carbonate (CC), pyrolytic (PC), and elemental (EC) carbon. The last peak is a methane calibration (CH ₄) – the NIOSH 5040 temperature protocol (http://www.cdc.gov/niosh/docs/2003-154/pdfs/5040f3.pdf – 01/15/13).	11
Figure 5: Temperature diagrams of the two temperature protocols used in the wood-burning experiment: a) NIOSH 5040, and b) EUSAAR 2. The arrow indicates the oxygen (O ₂) input...13	
Figure 6: The thermal-optical transmission method with linear temperature program (TLT) http://www.cta.tuwien.ac.at/epa/ea/ – 02/14/2012).	14
Figure 7: The integrating sphere method (Wonaschütz et al., 2009).	15
Figure 8: The nephelometer measuring system.	18
Figure 9: Light path in the optical chamber of the Aethalometer.	20
Figure 10: The absorption Angstrom exponent (α) values of the operating condition with C/O ratio = 0.21 (with the mixing gas - N ₂). α are the results of raw data (dotted line) and fixed α (solid line) are data compensated with the Weingartner principle.....	25
Figure 11: Set of all instruments during the CAST experiment.....	30
Figure 12: The CAST burner (Jing-CAST Technology).	31
Figure 13: The working principle of the CAST burner (http://www.sootgenerator.com/documents/Zahoransky.pdf – 02/14/2012).	32
Figure 14: Four sets of filters under different operating conditions. The left pair in the set was sampled when no mixing gas (N ₂) was present, as opposed to the right pair. The first group of four filters had a C/O ratio of 0.21, the second 0.31, the third 0.41 and the last group 0.60 (left to right).....	36
Figure 15: Dependence of EC and BC concentrations on combustion regime – C/O ratio (without mixing gas): (\diamond) the EC concentration measured with OC-EC dual-optical instrument using NIOSH 5040, (\circ) the EC concentration measured with OC-EC dual-optical instrument using EUSAAR2,	

(□) the BC concentration measured with integrating sphere, and (Δ) BC concentration measured with Aethalometer. 39

Figure 16: Thermograms of analyzed filter samples at the C/O ratio of 0.21 using the NIOSH 5040 temperature protocol: a) sample with automatically set split point (blue vertical line), and b) sample with manually set split point: violet (left vertical) line is an automatic split point and blue (right vertical) line is a manual split point). 41

Figure 17: Thermograms of analyzed filter samples with the C/O ratio of 0.31 using the NIOSH 5040 temperature protocol: a) sample with automatically set split point, and b) sample with manually set split point (violet (left) line is an automatic split point and blue (right) line is a manual split point). 42

Figure 18: Dependence of EC and BC concentrations on combustion regime – C/O ratio (without mixing gas): (◇) the EC concentration measured with OC-EC dual-optical instrument using NIOSH 5040, (○) the EC concentration measured with OC-EC dual-optical instrument using EUSAAR2, (□) the BC concentration measured with integrating sphere, and (Δ) BC concentration measured with Aethalometer. The manual split point was manipulated to obtain proper results of the OC-EC dual optical analyzer. 42

Figure 19: The EC/TC ratio dependence on combustion regime without the mixing gas: the blue line represents the results of the EC/TC ratio measured with the OC-EC dual optical instrument using the EUSAAR2 temp. protocol, the violet line represents the results of the EC/TC ratio measured with the OC-EC dual optical instrument using NIOSH 5040 temp. protocol, the green line represents the results of the EC/TC ratio measured with TLT. 44

Figure 20: Thermogram of analyzed filter sample with the C/O ratio of 0.31 (the EUSAAR2 temp. protocol); no mixing gas. Split point set by Sunset software is the violet (on the left) vertical line on the thermogram, while the blue line is a manually set split (on the right) point. 44

Figure 21: The EC/TC ratio dependence on combustion regime with the mixing gas: the blue line represents the results of the EC/TC ratio measured with the OC-EC dual optical instrument using the EUSAAR 2 temp. protocol, the violet line represents the results of the EC/TC ratio measured with the OC-EC dual optical instrument using NIOSH 5040 temp. protocol, the green line represents the results of the EC/TC ratio measured with TLT. 45

Figure 22: A filter sample analyzed by the OC-EC dual-optical instrument using two different temperature protocols at the C/O ratio of 0.31: a) the NIOSH 5040 temperature protocol, and b) the EUSAAR 2 temperature protocol. 46

Figure 23: Absorption Angstrom exponents of different compensation principles: the Kirchstetter principle (green), the Weingartner principle (pink), and the Arnott principle (blue) for all operating conditions (C/O ratio = 0.21, 0.31, 0.41, and 0.60) where “0.21” is a sample with the C/O ratio 0.21 without the mixing gas and “0.21+ N2” is a sample with the C/O ratio of 0.21 with the mixing gas (Error bars are standard deviations).* Repeated condition with the C/O ratio of 0.21. 48

Figure 24: Black carbon concentration measured with Aethalometer and absorption Angstrom exponent dependence of the C/O ratio in operating conditions of combustion with (solid line) and without (dotted line) the added mixing gas (N ₂).	49
Figure 25: Dependence of absorption coefficient on wavelength: (o) $b_{abs,BrC}$ and $b_{abs,BC}$ at C/O ratio = 0.21, and (Δ) $b_{abs,BrC}$ and $b_{abs,BC}$ at C/O ratio = 0.60. (α_{BrC} = 5.38, without the mixing gas (N ₂)).	51
Figure 26: Dependence of absorption coefficient on wavelength: (o) $b_{abs,BrC}$ and $b_{abs,BC}$ at C/O ratio = 0.21, and (Δ) $b_{abs,BrC}$ and $b_{abs,BC}$ at C/O ratio = 0.60. (α_{BrC} = 6.20, with the mixing gas (N ₂)).	51
Figure 27: Histogram of BrC absorption coefficient ($b_{abs, BrC}$) dependence on various wavelengths (λ) and operation conditions (C/O ratio = 0.21, 0.31, 0.41 and 0.60). (Error bars are standard deviations).	52
Figure 28: Histogram of BC absorption coefficient ($b_{abs, BC}$) dependence on various wavelengths (λ) and operation conditions (C/O ratio = 0.21, 0.31, 0.41 and 0.60). (Error bars are standard deviations).	53
Figure 29: Household heating.	55
Figure 30: Chimney of the wood-burning laboratory experiment.	56
Figure 31: Dilution/cooling pipe with two-particle separators (PM ₁₀ and PM _{2.5}) and filter holders.	57
Figure 32: Wodtke wood stove and its dimensions (http://www.wodtke.si/toplozracni-polena-vision7.html#ime).	59
Figure 33: Rika pellet stove MEMO (www.rika.at).	60
Figure 34: Description of the combustion procedure in wood-burning tests: the phase 1 and phase 2.	61
Figure 35: Description of the combustion procedure of pellet-burning.	62
Figure 36: Average PM ₁₀ values of EC concentration for different types of wood that were measured with the OC-EC dual-optical instrument using NIOSH 5040 (light grey) and EUSAAR 2 (grey) temperature protocols. Average values of BC concentration using optical methods: Integrating sphere (IS-BC) and TSP values of Aethalometer (Aeth-BC). Error bars reflect the standard deviations of the variations occurring in four experiments conducted for beech and spruce and the three experiments involving pellets.	67
Figure 37: Thermogram of PM ₁₀ filter sample (beech) using the NIOSH temperature protocol and automatic setting of split point.	68
Figure 38: Average PM _{2.5} values of EC concentration for different types of wood that were measured with the OC-EC dual-optical instrument using NIOSH 5040 (light grey) and EUSAAR 2 (grey) temperature protocols. Average values of BC concentration using optical methods: Integrating sphere (IS-BC) and TSP values of Aethalometer (Aeth-BC). Error bars reflect the	

standard deviations of the variations occurring in four experiments conducted for beech and spruce and the three experiments involving pellets.....	69
Figure 39: PM ₁₀ concentrations of organic carbon (OC) and elemental carbon (EC) measured with the OC-EC dual-optical instrument, and black carbon (BC-IS) and brown carbon (BrC-IS) concentrations measured with integrating sphere in various wood-burning tests using beech wood.....	70
Figure 40: PM _{2.5} concentrations of organic carbon (OC) and elemental carbon (EC) measured with the OC-EC dual-optical instrument, and black carbon (BC-IS) and brown carbon (BrC-IS) concentrations measured with integrating sphere in various wood-burning tests using beech wood.....	71
Figure 41: PM ₁₀ concentrations of organic carbon (OC) and elemental carbon (EC) measured with the OC-EC dual-optical instrument, and black carbon (BC-IS) and brown carbon (BrC-IS) measured with integrating sphere in different wood-burning tests using spruce wood. The Spruce IV* sample has a moisture content of 16%.....	72
Figure 42: PM _{2.5} concentrations of organic carbon (OC) and elemental carbon (EC) measured with the OC-EC dual-optical instrument, and black carbon (BC-IS) and brown carbon (BrC-IS) measured with integrating sphere in different wood-burning tests using spruce wood. The Spruce IV* sample has a moisture content of 16%.....	73
Figure 43: PM ₁₀ concentrations of organic carbon (OC) and elemental carbon (EC) measured with the OC-EC dual-optical instrument, and black carbon (BC-IS) and brown carbon (BrC-IS) measured with integrating sphere in different stove capacity tests using pellets.....	74
Figure 44: PM _{2.5} concentrations of organic carbon (OC) and elemental carbon (EC) measured with the OC-EC dual-optical instrument, and black carbon (BC-IS) and brown carbon (BrC-IS) measured with integrating sphere in different capacity tests using pellets.....	74
Figure 45: Average OC values of various wood types when using the two temperature protocols (NIOSH 5040 and EUSAAR 2) – PM _{2.5} (Error bars are standard deviations).....	76
Figure 46: Average EC values of various wood types when using the two temperature protocols (NIOSH 5040 and EUSAAR 2) – PM _{2.5} (Error bars are standard deviations).....	76
Figure 47: Average OC values of various wood types using the two temperature protocols (NIOSH 5040 and EUSAAR 2) – PM ₁₀ (Error bars are standard deviations).	77
Figure 48: Average EC values of various wood types using two the temperature protocols (NIOSH 5040 and EUSAAR 2) – PM ₁₀ (Error bars are standard deviations).	78
Figure 49: The Angstrom exponent dependence on various burning phases: phase 1 (blue) and phase 2 (green). *Pellet results are presented with only one bar because they were analyzed according to the stove capacity. Error bars are standard deviations of averaged Aethalometer data of 5-minute time base.....	79
Figure 50: The Angstrom exponent dependence on time for each cycle of beech burning: blue (□) is burning phase 1 and green (○) is burning phase 2.	80

Figure 51: The Angstrom exponent dependence on time for each cycle of spruce burning: blue (□) is burning phase 1 and green (○) is burning phase 2.	81
Figure 52: The Angstrom exponent dependence on time for each cycle of pellet burning: blue (□) is a 100% burning efficiency and green (○) is a 30% burning efficiency.	82
Figure 53: Average deposition mass of anhydrosugars (levoglucosan, mannosan, galactosan) for various types of wood (beech, spruce, pellets) – PM ₁₀ . Error bars are standard deviations. .	83
Figure 54: Average deposition mass of anhydrosugars (levoglucosan, mannosan, galactosan) for various types of wood (beech, spruce, pellets) – PM _{2.5} . Error bars are standard deviations. .	84
Figure 55: Southern part of Austria with the locations of measurement stations – Klagenfurt and Zell (Google maps).....	87
Figure 56: Land covered with waters, buildings or forests, or used for gardens and agriculture/surface (Source: Year Book, Klagenfurt 2012).	88
Figure 57: Urban measurement station in the Klagenfurt city center, Völkermarkter Strasse – marked with the red dot (Source: Google maps – 05/22/13).	89
Figure 58: Rural measurement station in the village of Zell – marked with the red dot (Source: Google maps – 05/22/13).	89
Figure 59: Sources of energy in Carinthia for the years 2005 and 2010 (Source: Environmental Report Carinthia 2012 – 4/6/13).	90
Figure 60: NO _x and PM ₁₀ emissions from industry/trade/heating plants, traffic and small consumers in Carinthia (Source: Environmental Report Carinthia 2012).....	91
Figure 61: Black carbon concentration measured in urban (Klagenfurt) and rural (Zell) areas with Aethalometer during 2011/12 winter period.	94
Figure 62: Black carbon concentration measured in urban (Klagenfurt) and rural (Zell) areas with Aethalometer during 2012/13 winter period.	95
Figure 63: BC fractions of wood-burning (BC _{wb}) and fossil fuel (BC _{ff}) in Klagenfurt and Zell for a) winter 2011/12, and b) winter 2012/13.	96
Figure 64: Diurnal plots of BC concentrations/fractions for workdays and weekends in Klagenfurt –2012/13 winter period.	98
Figure 65: Diurnal plots of BC concentrations/fractions for workdays and weekends in Zell – 2012/13 winter period.	99
Figure 66: Diurnal plots of the absorption Angstrom exponent values for Klagenfurt and Zell in the 2011/12 winter period.....	100
Figure 67: Diurnal plots of absorption Angstrom exponent (AAE) values for Klagenfurt and Zell in the 2011/12 winter period.....	101
Figure 68: Source apportionment for Klagenfurt and Zell in a) winter 2011/12, and b) winter 2012/13.	102

Figure 69: Sugar analyses: BC concentration dependence of wood-burning emissions (BC_{wb}) from levoglucosan measured with Aethalometer, and analyzed with HPLC method: a) Klagenfurt – Völkermarkter Strasse, and b) Zell – Ebenthal..... 103

List of Tables

Table 1: A schematic overview of the PhD research.....	7
Table 2: The temperature and duration of the steps – the difference between the EUSAAR 2 and NIOSH 5040 protocols used in the OC-EC dual-optical lab instrument (Cavalli et al., 2010). .	12
Table 3: Values of sigma (σ), the specific attenuation parameter, for all seven wavelengths using “Magee BC” calibration.....	21
Table 4: Values used in Eq. (10) to calculate light absorption from optical BC measurements (Arnott et al., 2005).....	24
Table 5: Mean 24-hour-average parameters of CM and C ₂	27
Table 6: Operating conditions during the CAST experiment – “CAST X.Y”, where X represents the number of the test, and Y gives the information about the presence of the mixing gas. When Y = 0, the mixing gas is not present, and when Y = 1 the mixing gas is added to the process.	33
Table 7: The CAST experiment results of off-line and on-line analyses at various C/O ratios (C/O = 0.21, 0.31, 0.41 and 0.60).* The column “Duration of sampling” refers to filter sampling, while Aethalometer data were sampled separately (2-minute time base) from filter sampling.	37
Table 8: Angstrom exponent in light of different compensation principles: the Weingartner and Arnott principles are calculated by using the existing formulas (Weingartner et al., 2003 and Arnott et al., 2005), while the Kirchstetter principle is empirical (Kirchstetter et al., 2007). .	47
Table 9: Stock average moisture content and number of tests with different wood types (* tests containing spruce with 16% moisture – spruce IV).....	63
Table 10: PM ₁₀ , PM _{2.5} and TSP results of on-line and off-line analyses for all types of wood (beech, spruce, pellets) and burning stages. Aethalometer data are presented in a slightly different way in the table; (p1) are average BC concentrations in phase 1, and (p2) are average BC concentrations in phase 2.....	65
Table 11: Average deposition mass of anhydrosugars (levoglucosan, mannosan, galactosan) loaded on the filter samples of various wood types (beech, spruce, pellets); with the ratio between levoglucosan and mannosan.....	84
Table 12: Number of PM ₁₀ exceedences (TMW>50 $\mu\text{g}\cdot\text{m}^{-3}$) per month and year.....	92
Table 13: The average values of the Angstrom exponent (α) and black carbon concentration (BC) during winter periods of 2011/12 and 2012/13 with standard deviations and median values.	96
Table 14: Five different calculations resulting from a change in the absorption Angstrom exponent of fossil fuel (α_{ff}) and the absorption Angstrom exponent of wood-burning (α_{wb}) for $\pm 10\%$	104
Table 15: The wood-burning contribution to ambient emissions in the 2011/12 winter period when using the source apportionment model.	104

Table 16: Wood-burning contribution to ambient emissions in the 2012/13 winter period when using the source apportionment model. 105

Acronym List

A – deposit area

α – Angstrom exponent

α_{BC} – Angstrom exponent of black carbon

α_{BrC} – Angstrom exponent of brown carbon

ATN - attenuation

B – flux of light detected sensor

BC – black carbon

BrC – brown carbon

BS – “British smoke”

b_{abs} – absorption coefficient

$b_{abs,uncorr}$ – uncorrected absorption coefficient

b_{ag} – gas absorption coefficient

b_{ap} – particle absorption coefficient

b_{ATN} – attenuation coefficient

b_{ext} – extinction coefficient

b_{rg} – Rayleigh (gas) scattering coefficient

b_{scat} – scattering coefficient

b_{sp} – particle scattering coefficient

C – calibration constant

CAST – combustion aerosol standard

CM_{total} –total carbonaceous material

CM_{BC} – non-brown carbon containing carbonaceous material

CM_{Brc} – brown carbon containing carbonaceous material

CO₂ – carbon dioxide

CPC – condensation particle counter

C/O ratio – fuel-to-air ratio

C₃H₈ – propane

EC – elemental carbon

f_{air} – standard volumetric flow of synthetic air

f_p – standard volumetric flow of the propane

HEPA -

HPLC – high-performance liquid chromatography

I – intensity of light passing through the filter spot

I₀ – intensity of light passing through the pristine part of the filter

IR – infra-red

k – correcting parameter

LACA – light absorbing carbonaceous aerosols

MAAP – multiangle absorption photometer

NaOH – sodium hydroxide

NO_x – nitrogen oxides

N₂ – nitrogen

OC- organic carbon

OM – organic matter

OPC – optical particle counter

O₂ – Oxygen

PAH – polycyclic aromatic hydrocarbons

PC – pyrolytic carbon

PE – polyethylene

PM₁₀ – particulate matter (diameter of 10 micrometers)

PM_{2.5} – particulate matter (diameter of 2.5 micrometers)

PSAP – particle soot absorption photometer

Q – flow

R – empirical correction

R.H. – relative humidity

SMPS – scanning mobility particle sizer

t – sampling time (min)

TC – total carbon

TLT – transmission method with linear temperature program

UV – ultraviolet

[X] – concentration of carbonaceous species

y – vertical distance from light source to sensor

λ – wavelength

σ – mass absorption cross section

CHAPTER 1

Introduction

Contents

1.1. Definition of carbonaceous species	2
Black carbon and elemental carbon	2
Organic carbon	3
Brown carbon	3
1.2. Relevance for health and climate	4
1.3. Light absorbing carbonaceous aerosols and their source apportionment in general	5
1.4. Motivation	5

1.1. Definition of carbonaceous species

Carbonaceous fractions of atmospheric aerosols play an important role in atmospheric environment. In the present work, the focus will be set on black carbon, elemental carbon, organic carbon, and brown carbon; terms will be explained in detail further on. When working with carbonaceous aerosols, it is important to know that the terms used to classify them depend upon the measurement method (Bond et al., 2004).

Atmospheric particles originate from natural and anthropogenic sources. Particles directly emitted from the source are primary particles and particles formed in the process of nucleation, condensation, and heterogeneous or multiphase chemical reactions are secondary particles. Direct sources of primary particles include combustion of biomass and fossil fuels, volcanic eruptions, mineral dust, sea salt, wind-driven suspension of soil and biological materials.

The particles can come in almost any shape or size. Depending on their size, they are frequently divided into two major groups called $PM_{2.5}$ and PM_{10} . $PM_{2.5}$ denotes fine particulate matter, defined as the integrated mass of aerosol with aerodynamic equivalent diameters up to 2.5 μm , whereas PM_{10} denotes particulate matter, defined as the integrated mass of aerosol with aerodynamic equivalent diameters up to 10 μm .

Black carbon and elemental carbon

Black carbon (BC) contains microcrystalline graphitic structure which is produced by incomplete combustion of fossil fuels and wood-burning. It is a direct tracer for combustion aerosols because it cannot be formed, significantly transformed or destroyed by atmospheric processes (Hansen et al., 1990). The presence of BC can be determined with combustion or optical methods, but lately optical methods prevail. Several instruments can detect or measure BC, such as Aethalometer, integrating sphere (IS), Multiangle Absorption Photometer (MAAP), Particle Soot Absorption Photometer (PSAP). Usually, the attenuation or absorption coefficient of BC are measured and afterwards converted to BC concentration.

BC is sometimes equated with elemental carbon (EC); however the difference between them lies in the measurement method. BC is detected with optical methods, and is thus defined optically by measuring the change in light transmittance or reflection caused by particles (Gundel et al., 1984; Hansen et al., 1984) or absorption (Heitzenberg, 1982; Hitzemberger et al., 1996). EC is measured with thermal or thermo-optical methods; i.e. the measurement depends strongly on combustion properties and the combustion temperature of the carbonaceous aerosols. Methods for the determination of EC include the OC-EC dual-optical lab instrument (lit.) or thermal methods using a precombustion step (Cachier et al., 1996).

Organic carbon

Organic carbon (OC) usually refers to the carbonaceous fraction of the aerosol that is not refractory. This term is an oversimplification because organic carbon may contain hundreds or thousands of different organic compounds with varying atmospheric behavior. OC is the quantity that results from thermal analysis. Often not just the concentration of organic carbon or the mass of non-black carbon are significant, but also the mass of organic matter. Organic matter (OM) includes a hydrogen and oxygen bound to this carbon. In order to estimate the mass concentration of particles and the effects on radiative forcing, the mass of organic matter is needed; the ratio between organic matter and organic carbon is source-dependent (Bond et al., 2004). Methods to determine OC also include the OC-EC dual-optical lab instrument (lit.) or thermal methods using a precombustion step (Cachier et al., 1996); in this case the OC is calculated from the difference of total carbon (TC) and EC and not directly.

Brown carbon

Carbon that absorbs light may not be black, yet it is nevertheless colored, often brownish. Brown carbon (BrC) features light absorption at short wavelengths (blue and UV). It influences the split between organic carbon and elemental carbon in the thermal methods due to charring and through its light absorption characteristic leads to overestimation of BC concentration (Wonaschütz et al., 2009). Typical source of brown carbon is biomass smoke (e.g. residential heating or special events like Easter bonfires). Pyrolytic carbon generated during the OC-EC analysis when the organic fractions chars, is a special type of BrC (Andreae et al., 2006).

In **Figure 1**, an example of particles evolved during the CAST experiment is shown (see Chapter 3 – The CAST experiment). At low C/O ratio (**Figure 1**, a) the emergence of BC is expected, and at high C/O ratio (**Figure 1**, b) the emergence of BrC and other organics is expected.

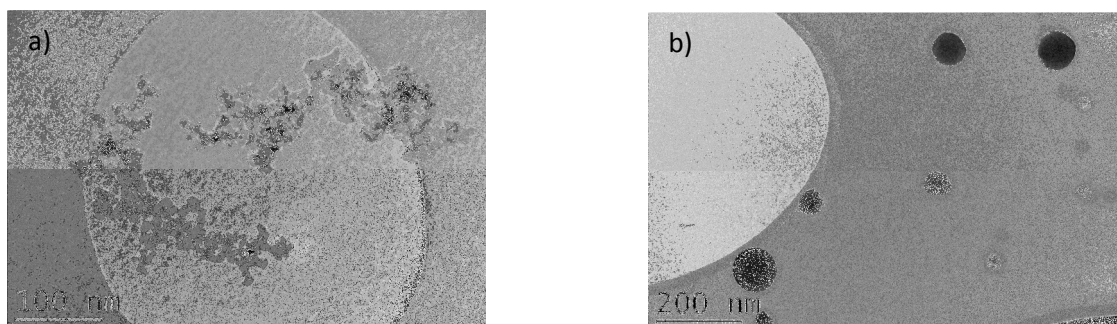


Figure 1: TEM pictures of soot particles generated under a) C/O ratio = 0.21, and b) C/O ratio = 0.60 (Kim et al., 2013).

1.2. Relevance for health and climate

The health effects of combustion-related air pollution caused by black particles were identified decades ago, when the monitoring of black smoke (or “British smoke” – BS) was a widespread method for air quality assessment in Europe. The evidence for the health effects of this type of pollution primarily affecting the respiratory system was used to recommend the first guidelines for exposure limits to such particles consistent with the protection of public health (WHO, 1979).

New scientific evidence has led to recognition of the important role of black particles (black carbon – BC) as one of the short-lived climate forcers. Measures focusing on BC and methane reduction are expected to achieve a significant short-term reduction in global warming (Jacobson et al., 1998). The same measures accompanied with the reduction of CO₂ emissions could also directly benefit global health and food security (WHO, 2012).

Figure 2 shows a description of the respiratory tract and particle deposition as a function of particle diameter.

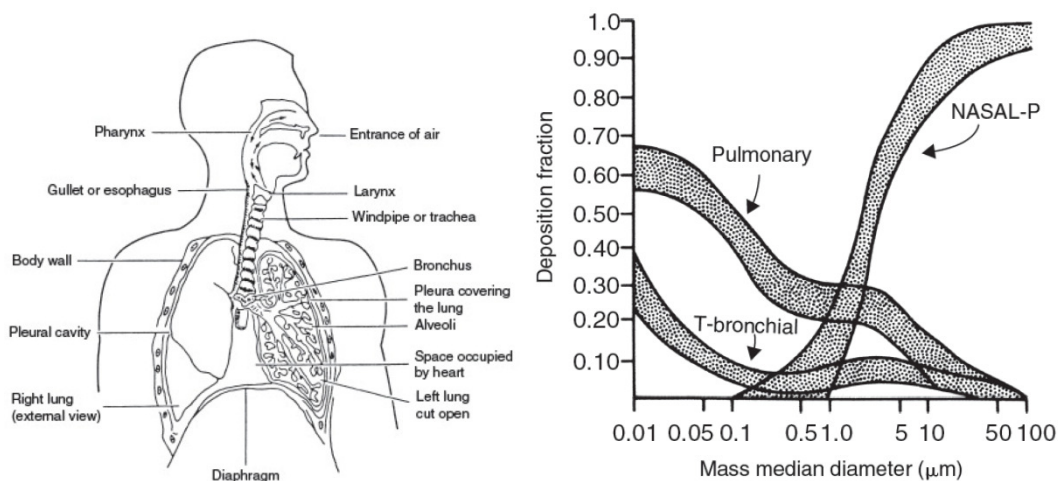


Figure 2: Particle deposition as a function of particle diameter in various regions of the lung. The nasopharyngeal region consists of the nose and throat; the tracheobronchial (T-bronchial) region consists of the windpipe and large airways; and the pulmonary region consists of the small bronchi and the alveolar sacs. *Source:* Task Group on Lung Dynamics (1996). Health Physics. 12: 173. (<http://www.onlineethics.org/cms/23617.aspx> – 06/10/ 13).

As evident from **Figure 2** the smallest particles are deposited deep in the lungs, while the larger ones are already retained in the nasal cavity or other respiratory ducts leading to the lungs.

1.3. Light absorbing carbonaceous aerosols and their source apportionment in general

Recent research (Andreae et al., 2006) has shed light on the uncertainties in the detection of different carbonaceous aerosols in wood smoke. It has been shown that the organic carbon from wood smoke contains large amounts of “brown carbon”, i.e. organic substances with a significant absorption in the visible and UV spectral range. The presence of these substances needs to be explained by the optical characterization of carbonaceous aerosols and the effect they have on the thermal-optical analysis. These substances tend to char at low temperatures when thermal methods are used, which results in an associated artificial increase in the EC signal. With the development of a dual or multi-wavelength Aethalometer, it became possible to investigate the wavelength dependence of the absorption coefficients of pure BC (e.g. from flame soot) and of wood smoke, and to invoke a dual component calibration for the “fossil fuel” BC (BC_{ff}) and “wood smoke” BC (BC_{wb}) from ambient observations using a multi wavelength Aethalometer and other more specific instruments for discriminating traffic and wood smoke emissions (Babich et al., 2004; Lanz et al., 2008; Sandradewi et al., 2008). Furthermore, it has been demonstrated that a two-component calibration can be applied to apportion the contribution of a black carbon and brown carbon source to observe BC levels (Wonaschütz et al., 2009). Therefore the operational definition (Bond et al., 2004) for the light absorbing fraction of the carbonaceous atmospheric aerosols was extended and referred to as light absorbing carbonaceous aerosols (LACA).

The finding of a wavelength dependence of different LACA sources is of vital importance because recent studies indicate that during the cold period, when the EU ambient air quality standard for PM_{10} is exceeded most frequently, biomass smoke – in particular wood smoke – acts as a major contributor. In European countries with large areas of forest stands, wood smoke has been observed to constitute 20–50% of the $PM_{2.5}$ organic carbon under wintry conditions (e.g. Puxbaum et al., 2007; Caseiro et al., 2009). These observations were obtained by selective measurements of specific wood smoke tracers (levoglucosan, mannosan, and galactosan) in emission studies (e.g. Schmidl et al., 2008a, 2008b) and at ambient rural and urban sites.

1.4. Motivation

Emerging trends in aerosol science and technologies comprise measurements of traffic emissions and wood-burning emissions, detection of the Angstrom exponent (α) for various light absorbing aerosols, and measurements of concentrations of black carbon (BC) or brown carbon (BrC) at different combustion conditions – primary and secondary aerosols.

The Angstrom exponent is now widely used to differentiate between emission sources (traffic emissions $\alpha = 1.0$, and wood-burning emissions $\alpha \sim 2.0$; Kirchstetter et al., 2004). What is more, the awareness of BC and BrC concentrations is important not only for source apportionment, but also for climate changes and health effects. When using these parameters, it is possible to predict the biggest pollutants of the environment and thus find solutions to reduce them. The Angstrom exponent is calculated by using the following equation: $b_{\text{abs}} \sim \lambda^{-\alpha}$ (a more detailed explanation of the Angstrom exponent is provided in the section on methodology). In this case, a device is needed to provide us with data on wavelength and absorption values.

This is Aethalometer, an instrument, which, when it was developed in 1987, measured black carbon at 880 nm. In 1999, LED's emitting in the UV was found and a dual-wavelength Aethalometer (denoted AE-21) was created, in which the illumination was switched between 370 and 880 nm sequentially in each time base period. Later that year, five additional 'colors' of LED to create the 7-wavelength Aethalometer (denoted AE-31) were added. In 1999, BC emission from biomass burning was not considered to be important, and the concept of the Angstrom exponent of optical absorption was brand new (Kirchstetter et al., 2004). Now we know that biomass burning is an important source of air pollution, therefore the potential of the Aethalometer instrument to provide more information besides BC concentrations is investigated in this PhD thesis.

As already mentioned, at the beginning the Aethalometer was applied as an instrument that measures the BC concentration at 880 nm wavelength as a tracer of diesel exhaust sources and other black material. With the development of the instrument, Aethalometer is now able to measure seven wavelengths. Since Sandradewi et al. (2008) already implemented two wavelengths (470 nm and 950 nm) in the Aethalometer model to discriminate inefficient wood-burning from traffic emissions, a similar two-component Aethalometer model was used in this work as well to differentiate between brown carbon (BrC) and black carbon (BC) because our aim was to demonstrate that the Aethalometer can also be used to detect light absorbing aerosols at short wavelengths, such as brown carbon.

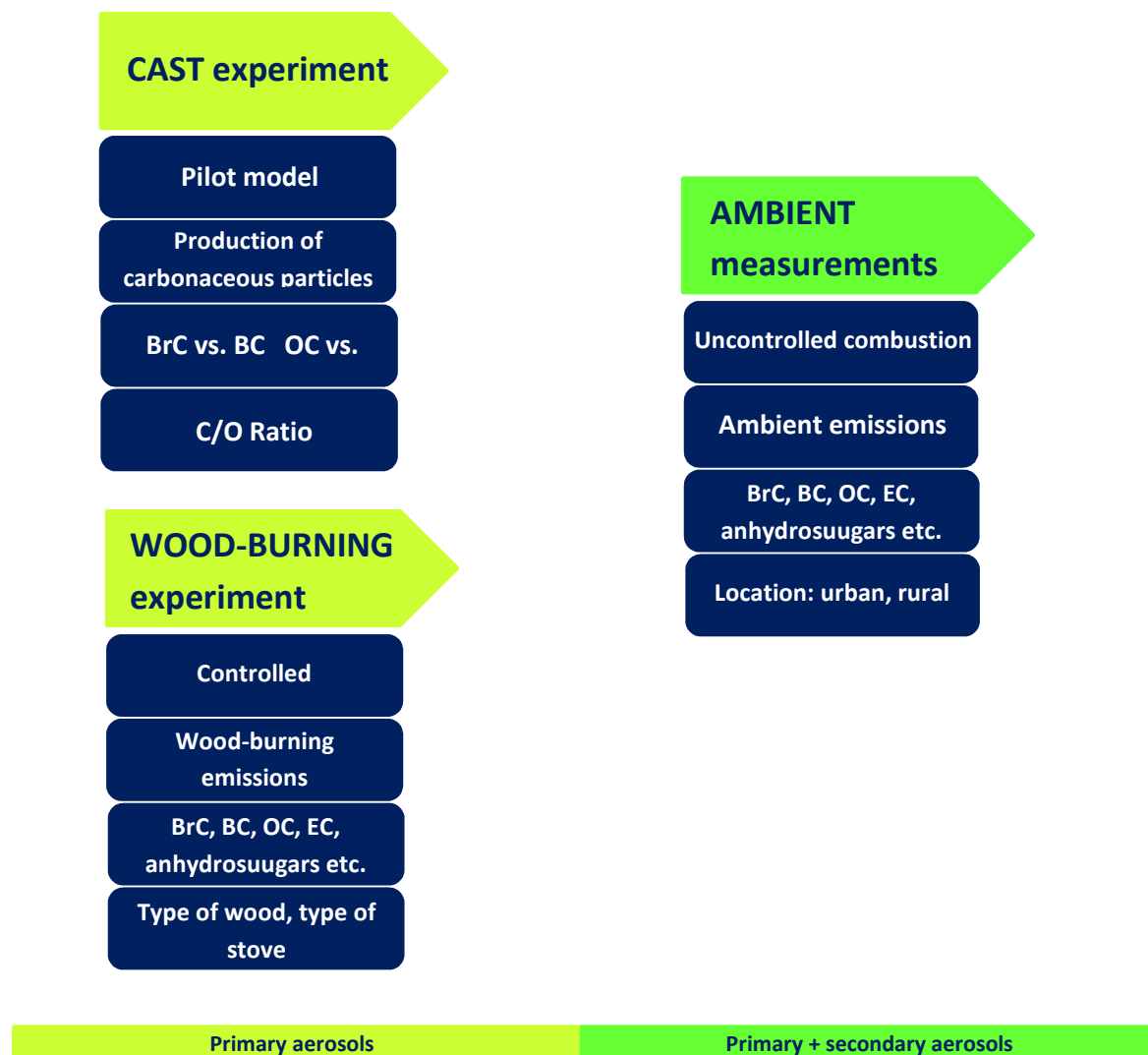
Black carbon and brown carbon in this research were defined by their optical properties: BC is an aerosol, absorbing across a broad optical spectrum from ultraviolet (UV) to infrared (IR) with the absorption Angstrom exponent $\alpha_{\text{BC}} \sim 1.0-1.1$ (a value consistent with the Mie theory and close to the value given for pure diesel emissions, Schnaiter et al., 2003), while BrC is defined as UV and blue absorbing matter, with a high value of the absorption Angstrom exponent, either measured in the experiment or determined from the ambient data.

The research conducted for this PhD thesis is schematically described in the **Table 1**. In the CAST experiment, attention will be put on the optical properties, ranging from oxygen rich

conditions to oxygen poor (fuel rich) conditions. In the wood-burning experiment, the primary emissions will be examined, while in ambient measurement both the primary and secondary emissions will be observed. The value ranges determined in the wood-burning experiments will be compared to field values. This comparison will enable the development of a robust on-line field methodology for quantitative speciation of aerosol and source apportionment on a time scale of minutes – orders of magnitude lower than achievable by existing techniques.

A schematic overview of the PhD research is shown in **Table 1**.

Table 1: A schematic overview of the PhD research.



CHAPTER 2

Methodology

Contents

2.1. Off-line measurements	9
2.1.1. Filters.....	9
2.1.2. Thermal-optical methods	9
2.1.2.1. OC-EC dual-optical instrument (Sunset Laboratory Inc.).....	9
2.1.2.2. Thermal-optical transmission method with linear temperature program (TLT – Vienna University of Technology).....	13
2.1.3. Optical methods.....	14
2.1.3.1. Integrating sphere (University of Vienna)	14
2.1.4. Anhydrosugars	16
2.2. On-line measurements	18
2.2.1. Nephelometer (Model 3563, TSI).....	18
2.2.2. Aethalometer® (Model AE 31, Magee Scientific).....	20
2.2.3. Data post-processing.....	22
2.2.3.1. Compensation principles.....	22
2.2.3.2. The Aethalometer model	25

For all three experiments, i.e. the CAST experiment, the wood-burning experiment and the ambient measurements, the methods described in this chapter were used. Filters were analyzed with thermal-optical methods, optical methods and chromatography for sugar analyses. Aethalometer measurements were compensated and, using the Aethalometer model, separated in different carbonaceous fractions.

2.1. Off-line measurements

2.1.1. Filters

Quartz filters (type: Tissuquartz 2500QAT-UP, 47 mm) were used for combustion aerosols sampling and characterization of the ambient aerosols. These filters are suitable for aerosol sampling in high temperature and aggressive atmospheres. They tolerate high temperature use for analysis and high flow rate.

First, the filters were preheated to 460 °C. They were exposed to this temperature for at least 6 hours and afterwards cooled down in a desiccator with a water vapor saturated atmosphere to minimize adsorption of gaseous compounds containing carbon, which could increase blank readings.

The filters were weighed before and after the sampling. Gravimetric analysis of quartz filters was performed with a microbalance (Sartorius M5P with range up to 1 g, reading to ± 0.5 mg) after a 24–48 h equilibration in an air-conditioned room (20 ± 1 °C, $50 \pm 5\%$ R.H.).

2.1.2. Thermal-optical methods

2.1.2.1. OC-EC dual-optical instrument (Sunset Laboratory Inc.)

The instrument used for thermal-optical analysis of carbonaceous aerosols was the OC-EC dual-optical lab instrument (Sunset Laboratory Inc.) (Birch and Cary, 1996). The thermal-optical method consists of two stages. First, a filter sample (punch of the quartz filter, 10 mm in diameter) is inserted in a sample oven. Then the heating in an inert atmosphere (He-mode) starts. At this stage, organic carbon (OC) is evolved as well as carbonate carbon (CC) and pyrolytic carbon (PC). In the oxygen-containing atmosphere, PC is usually detected as elemental carbon (EC) and it is evolved due to charring of organic matter. This means that thermally unstable organic compounds pyrolyze in the He-mode.

In the second stage, the oven temperature is reduced and a mixture of oxygen and helium (He/O₂-mode) is introduced into the sample oven. In the oxygen-containing atmosphere, the remaining carbonaceous material is combusted, while the temperature is increasing again and this way EC is evolved.

The laser signal is recorded, which allows optical correction of results. Transmission and reflectance can be evaluated from its values. The point at which the filter transmittance or reflectance for the laser light reaches its initial value is called the OC-EC split point (**Figure 4**).

Carbon evolved before the split point is considered to be OC (and may include carbonate, depending on the protocol), and carbon detected after the split point is considered to be EC. Incorrect accounting for PC formation can significantly influence the discrimination between OC and EC (Schmid et al., 2001).

Different temperature protocols can be used for the thermal-optical method. Two of them will be explained in detail further on.

The accurate discrimination between OC and EC according to the split point, as described above, relies upon the following assumption: PC (in He-mode, *Figure 4*) has the same specific mass absorption cross section (σ) as the atmospheric EC and all PC formed during the He-mode is assumed to evolve from the filter before the native EC throughout the analysis (Cavalli et al., 2010).

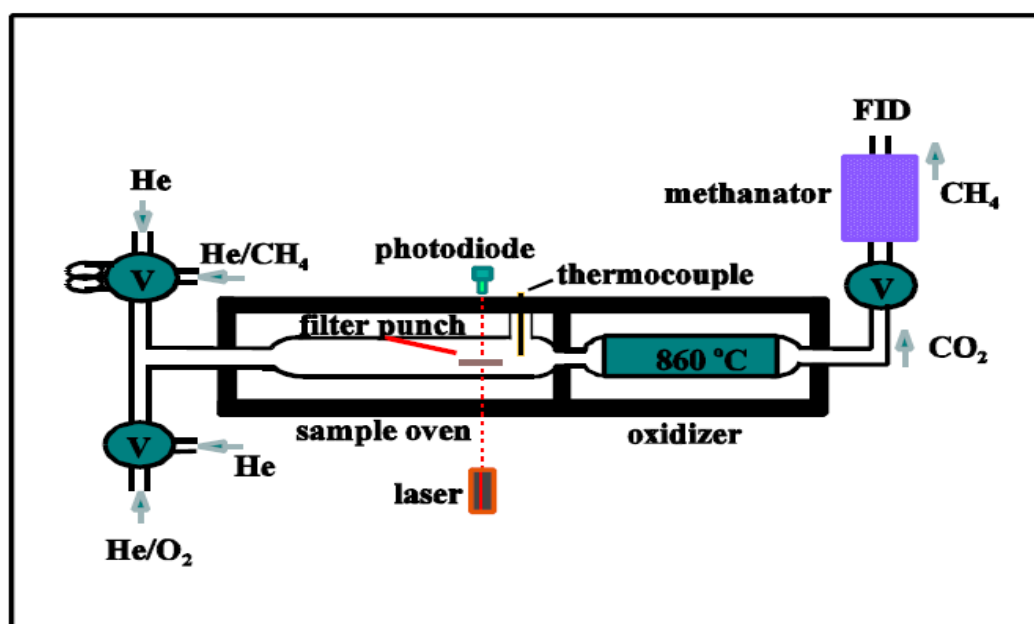


Figure 3: The structure of OC-EC Dual-optical analyzer (<http://www.cdc.gov/niosh/docs/2003-154/pdfs/5040f3.pdf>. – 01/15/13).

Figure 4 depicts an example of thermogram. The chart features a temperature line (black line); laser transmittance (red line); flame ionization detector signal (FID); OC-EC split point; He-mode (yellow line) and O₂/He-mode (green line).

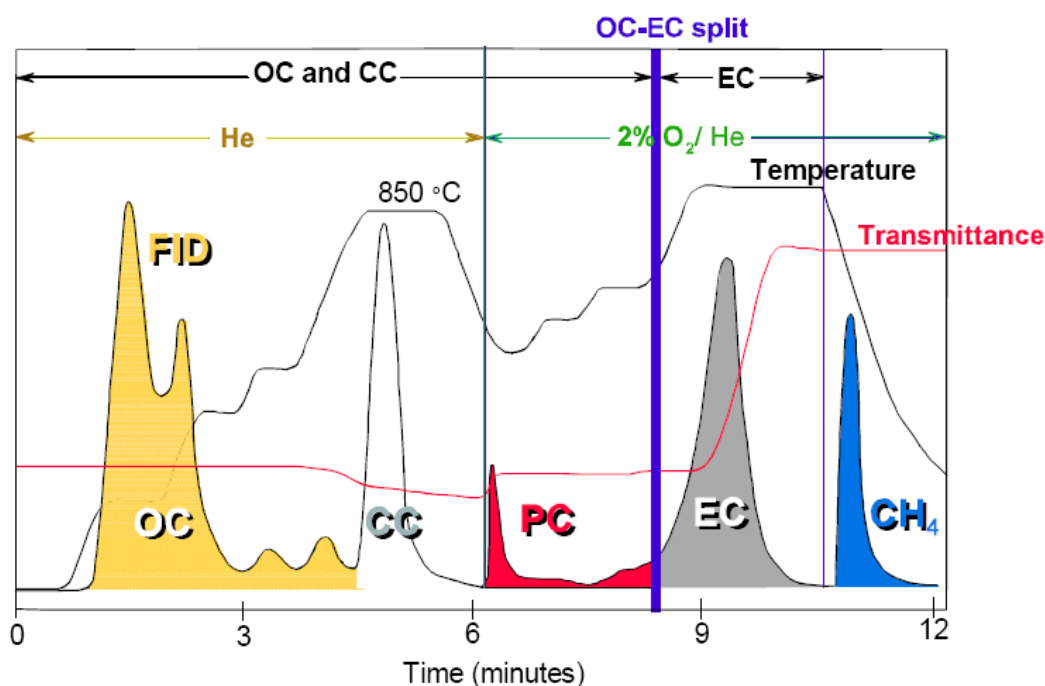


Figure 4: Example of thermogram. Peaks correspond to organic (OC), carbonate (CC), pyrolytic (PC), and elemental (EC) carbon. The last peak is a methane calibration (CH₄) – the NIOSH 5040 temperature protocol (<http://www.cdc.gov/niosh/docs/2003-154/pdfs/5040f3.pdf> – 01/15/13).

The thermal-optical analysis was performed by using two temperature protocols: EUSAAR 2 (Cavalli et al., 2010) and NIOSH 5040 (Peterson and Richards, 2002).

The NIOSH 5040 temperature protocol vs. the EUSAAR 2 temperature protocol

The use of different temperature protocols (EUSAAR 2 and NIOSH 5040) can result in a wide elemental-to-total carbon variation (Cavalli et al., 2010). In the following table (Table 2), the temperature set points and residence times of the two temperature protocols are shown, whereas Figure 5 visualizes these conditions.

Table 2: The temperature and duration of the steps – the difference between the EUSAAR 2 and NIOSH 5040 protocols used in the OC-EC dual-optical lab instrument (Cavalli et al., 2010).

Atmosphere	EUSAAR 2		NIOSH 5040	
	Time (s)	Temp (°C)	Time (s)	Temp (°C)
He	120	200	60	310
	150	300	60	480
	180	450	60	615
	180	650	90	870
He/O ₂	120	500	35	600
	120	550	45	675
	70	700	45	750
	80	850	45	825
			120	870

The NIOSH 5040 protocol is recognized as a de-facto standard method for the determination of organic and elemental carbon in particulates collected on quartz fiber filters (Birch and Cary, 1996). For the IMPROVE network, a different thermal protocol was used (Chow et al., 2007). Later Cavalli et al., (2010) presented a new protocol – EUSAAR 2. Their approach improved the accuracy of the discrimination between OC and EC and tried to establish the following:

1. Minimizing the potential negative bias in EC determination due to early evolution of light absorbing carbon species at high temperature in the He-mode;
2. Minimizing the potential positive bias in EC regarding the incomplete evolution of OC during the He-mode, which then evolves during the He/O₂-mode, potentially after the split point;
3. Minimizing the uncertainty due to the position of the OC/EC split point in the FID response profile by introducing multiple desorption steps in the He/O₂-mode.

With this in mind, the following key parameters were investigated when designing the optimized EUSAAR 2 thermal protocol (Cavalli et al., 2010):

- The steps at low temperature;
- The He-mode's maximum temperature;
- The residence time of each temperature step;
- The temperature steps in the HE/O₂-mode.

The temperature steps with corresponding residence time are shown in **Figure 5**.

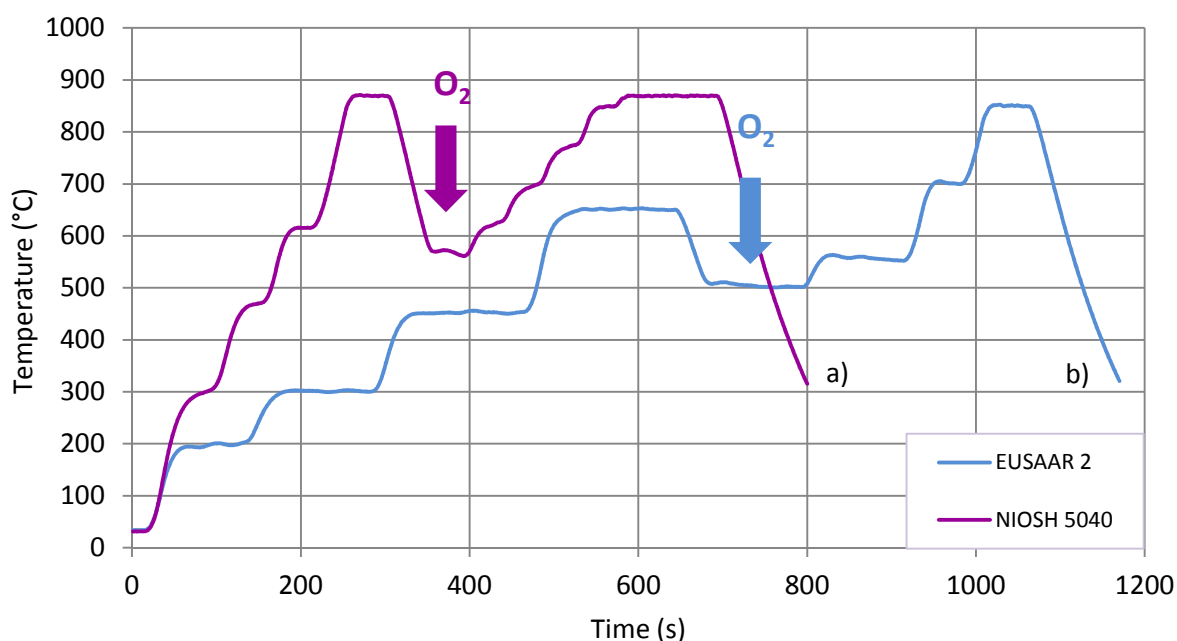


Figure 5: Temperature diagrams of the two temperature protocols used in the wood-burning experiment: a) NIOSH 5040, and b) EUSAAR 2. The arrow indicates the oxygen (O_2) input.

Filters used in the CAST experiment and wood-burning experiment were analyzed with both temperature protocols, i.e. NIOSH 5040 and EUSAAR 2. One point of observation was the influence of both the temperature steps and corresponding residence time on the amount of evolved EC or OC. Although we applied both the EUSAAR 2 and NIOSH 5040 temperature protocols, as they are most commonly used worldwide, the values from the NIOSH 5040 protocol were consistently used for the final data analyses.

2.1.2.2. Thermal-optical transmission method with linear temperature program (TLT – Vienna University of Technology)

The thermal-optical transmission method with linear temperature program (TLT, **Figure 6**) is based on a method described by Puxbaum (1979), and later modified to simultaneous laser transmission measurement (wavelength 632.8 nm) and detection of CO_2 concentration by NDIR (Method # 9b in Schmid et al., 2001).

The filter sample (punch of quartz filter, 12 mm in diameter) is inserted in a FROK 200/50/1000 (AHT Austria) horizontal furnace. In the beginning, the furnace is cooled down to room temperature that increases linearly for $20\text{ }^\circ\text{C}\cdot\text{min}^{-1}$ until the maximum temperature of the process is reached, which is $800\text{ }^\circ\text{C}$. A manganese oxide is presented as a catalyst in

the process. It is heated to 700 °C to oxidize all carbonaceous gases to carbon dioxide (CO₂). Organic carbon and elemental carbon are separated due to different thermal stabilities. Transmittance through the filter sample is recorded continuously using an NDIR analyzer (Maihak UNOR 6N) during the heating procedure.

The change of the transmittance gives information about charring phenomena which can lead to increased blackness of the filter, and also about the temperature range of the burn-off of the EC, allowing identification of EC in the TLT-plot (Jankowski et al., 2008).

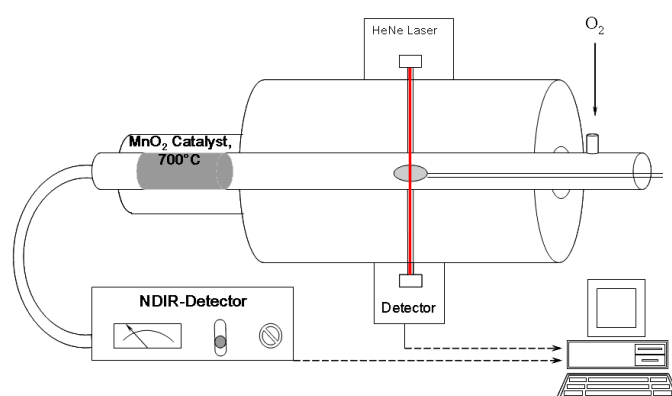


Figure 6: The thermal-optical transmission method with linear temperature program (TLT) <http://www.cta.tuwien.ac.at/epa/ea/-02/14/2012>.

2.1.3. Optical methods

2.1.3.1. Integrating sphere (University of Vienna)

The integrating sphere instrument (manufactured by Labsphere, *Figure 7*) was used to analyze filter samples by employing a method originally developed by Heintzenberg (1982) and later extended by Hitzenberger et al. (1996, 2001).

The sphere is coated internally with Spectrafect, which diffusely reflects more than 99.9% of the incident light. A light of incandescent source (a 75 W halogen lamp) passes through opal glass plate, an interference filter (550 nm), and a further diffuser and enters the sphere through inside port. The detector (Si photodiode) is placed at the bottom port and shielded from directly entering light by a baffle (Wonaschütz et al., 2009).

The filter sample (punch of quartz filter, 8 mm in diameter) is immersed in the liquid suspension – a solvent prepared with 2 ml of acetone and 2 ml of water/isopropanol (80:20)

– and put into transparent PE vials. PE vials are positioned in the center of the sphere using a sample holder introduced through the top port. A laser diode is mounted at the port directly opposite the incandescent light source which is switched off when the laser diode is in operation and vice versa. A reference vial (empty PE vial) is measured/analyzed at the beginning to set the value for each wavelength (red, green, or blue); afterwards two samples, one after the other, are measured, which is followed by the measurements of the reference vial.

Absorption cannot be measured directly in the integrating sphere. Calibration standards have to be used to convert the measured signals to amounts of absorbing material. The term “signal” is used for $-\ln\left(\frac{I}{I_0}\right)$, where I_0 is the intensity with a PE vial containing blank filter and solvent, and I is the intensity with PE vial containing filter sample and solvent. The signal decrease caused by BC is converted to BC concentration using a calibration curve obtained with a commercial carbon black (Elftex 124, Cabot Corporation). A humic acid sodium salt is used as a standard for brown carbon (BrC). Calibration curves are obtained for carbon black masses of 1–10 μg and humic acid salt masses of 5–40 μg at all three wavelengths (blue, green and red).

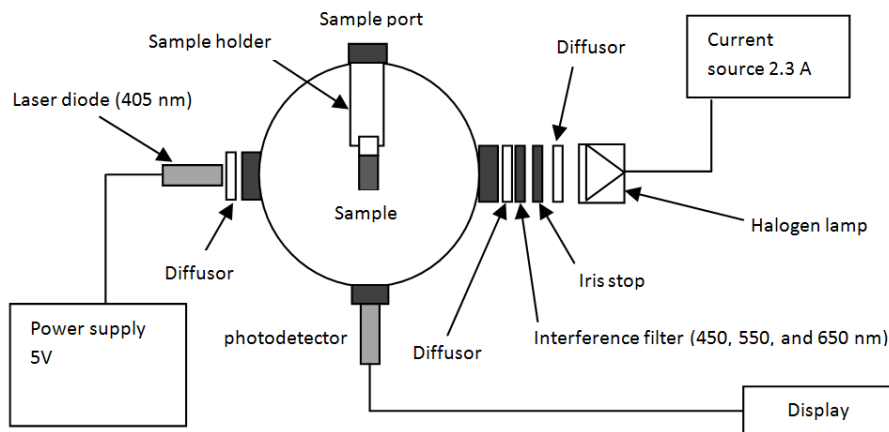


Figure 7: The integrating sphere method (Wonaschütz et al., 2009).

Results of filter analyses were recorded as the BC and BrC concentration in $\mu\text{g}\cdot\text{m}^{-3}$, and were used for further evaluation. Results of CAST samples were analyzed by the Faculty of Physics, University of Vienna, Austria (Hitzenberger et al., 2013 – unpublished data).

2.1.4. Anhydrosugars

To determine the saccharides in wood smoke and ambient atmospheric samples, liquid chromatography is used, i.e. the anion chromatography combined with pulsed amperometric detection. The method is able to quantify the following saccharides: five primary monosaccharides (arabinose, galactose, fructose, glucose and mannose), one disaccharide (sucrose), four sugar alcohols (arabitol, mannitol, sorbitol and xylitol) and three anhydrosugars (galactosan, levoglucosan, and mannosan).

Water used to prepare the standard solutions and to extract the samples was $18.2 \text{ M}\Omega\cdot\text{cm}^{-1}$ (Milli-Q, Millipore) water. The following standards were purchased from the suppliers:

- Levoglucosan: Aldrich 316 555 1G, CAS 498-07-7
- Galactosan: Sigma-Aldrich A-5180, CAS 644-76-8
- Mannosan: Sigma-Aldrich A-7429, CAS 14168-65-1
- Fructose: Sigma-Aldrich F 0127, CAS 57-48-7
- Galactose: Sigma G 0750, CAS 59-23-4
- Glucose: Sigma-Aldrich G 8270, CAS 50-99-7
- Mannose: Sigma 63580, CAS 3458-28-4
- Sucrose: Merck 8966, CAS 57-50-1
- Arabitol: Sigma 10880, CAS 50-70-4
- Mannitol: Merck 5769, CAS 69-65-8
- Xylitol: Sigma 95649, CAS 87-99-0

The standard solutions were prepared by dissolving 100 mg of each compound in water and diluting it to 100 ml.

The filter sample (punch of quartz filter, 8 mm in diameter) was extracted in 3 ml of Milli-Q water and put into ultrasonic bath agitation for 45 min. Undissolved sample material and filter pieces were removed from the sample solution by centrifugation (15 min at 13.4×10^3 rpm) and filtration (35 μm and 5 μm , Dionex) prior to injection.

A chromatography system by Dionex (Dionex ICS 3000) was used for analysis of wood-burning samples. Saccharides are separated in the MA-1 column (4 x 50 mm). NaOH gradient is used in the column. Its initial concentration is 480 mM and increases up to 650 mM. (Iinuma et al., 2009). Anhydrosugars are detected with an electrochemical detector with pulsed amperometric detection. The detector cell has a gold working electrode and pH electrode as reference (both from Dionex). The method is described by Iinuma et al. (2009).

The sample (150 μL) was flushed through the sample loop (20 μL) by the Basic Marathon auto sampler from Spark (The Netherlands). The fine particles were removed from the

injected sample by in-line filters – a 35 μm filter followed by a 5 μm filter (in one unit). In-line filters were placed after the auto sampler.

Diluted sodium hydroxide solutions were used as a mobile phase. NaOH solution was diluted, 10.5 ml to 1 L, to give a 1 molar solution. Exposure of these solutions to atmospheric CO_2 must be minimized; otherwise carbonate will absorb on the column and lead to deterioration in performance. (Caseiro et al., 2007)

All four reservoirs (bottles) of the Dionex pump were filled with Mili-Q water and 1 molar sodium hydroxide. The solutions were degassed by applying vacuum to the sonicated eluent for 10 min. After gently pouring the NaOH solution into the reservoirs (B) and (C), all four bottles were purged with helium at approx. 5 psi for another 10 min to prevent absorption of CO_2 (Caseiro et al., 2007).

2.2. On-line measurements

2.2.1. Nephelometer (Model 3563, TSI)

The nephelometer (**Figure 8**) is an instrument that measures aerosol light scattering. It detects scattering properties by measuring light scattered by the aerosol and subtracting light scattered by the gas, the walls of the instrument and the background noise in the detector. The three-wavelength model (TSI 3563) splits the scattered light into red (700 nm), green (550 nm), and blue (450 nm) wavelengths. The TSI nephelometer measures back-scattered light at these wavelengths as well (http://www.esrl.noaa.gov/gmd/aero/instrumentation/neph_desc.html – 05/11/11).

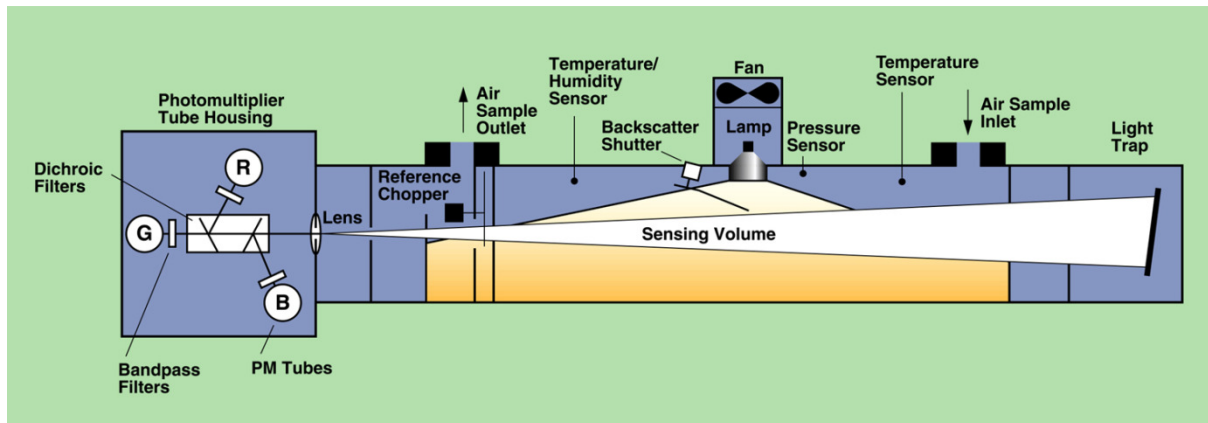


Figure 8: The nephelometer measuring system.

The backscatter shutter allows blocking of the angles from 7° to 90° so that only backscattering is measured. The light trap provides a dark reference against which the scattered light can be determined. The property that the nephelometer measures, is the scattering of light over a distance. Extinction is caused by both scattering and absorption of light by particles. The extinction coefficient b_{ext} is the sum of these, and is given by the formula

$$b_{ext} = b_{scat} + b_{abs} = - \frac{\ln\left(\frac{I}{I_0}\right)}{x} \quad (1)$$

x = length of light path

I = intensity of light after distance

I_0 = initial intensity of light

b_{scat} and b_{abs} are the scattering and absorption coefficients. Each is divided into two components (http://www.esrl.noaa.gov/gmd/aero/instrumentation/neph_desc.html – 05/11/11).

$$b_{scat} = b_{rg} + b_{sp} \quad (2)$$

$$b_{abs} = b_{ag} + b_{ap} \quad (3)$$

b_{rg} = Rayleigh (gas) scattering coefficient

b_{sp} = particle scattering coefficient

b_{ag} = gas absorption coefficient

b_{ap} = particle absorption coefficient

The nephelometer measures b_{scat} and b_{rg} and subtracts to get b_{sp} . b_{ag} is usually negligible. The equation derived by Middleton (1958) and Butcher and Charlson (1972) governing the instrument is

$$B = \frac{I_0}{y} \cdot \frac{b_{scat}}{2\pi} \quad (4)$$

y = vertical distance from light source to sensor

B = flux of light detected by sensor

The nephelometer counts photons using the photomultiplier tubes. The photon counts are converted to counting frequencies and then scattering coefficients using calibration constants (http://www.esrl.noaa.gov/gmd/aero/instrumentation/neph_desc.html – 05/11/11).

Data obtained from the nephelometer were used only as an aid for calculating the absorption Angstrom exponent with the Weingartner compensation principle (Weingartner et al., 2003).

2.2.2. Aethalometer® (Model AE 31, Magee Scientific)

Aethalometer (AE) is an instrument that uses the optical method (**Figure 9**) to provide real-time BC concentration at 880 nm.

The air enters the Aethalometer through the inlet and reaches the optical chamber. The aerosols are sampled on a part of the quartz fiber filter tape. The light from the LED source of the Aethalometer AE31-ER (seven wavelengths from ultraviolet to infrared: 370 nm, 470 nm, 520 nm, 590 nm, 660 nm, 880 nm, 950 nm) passes through the filter tape.

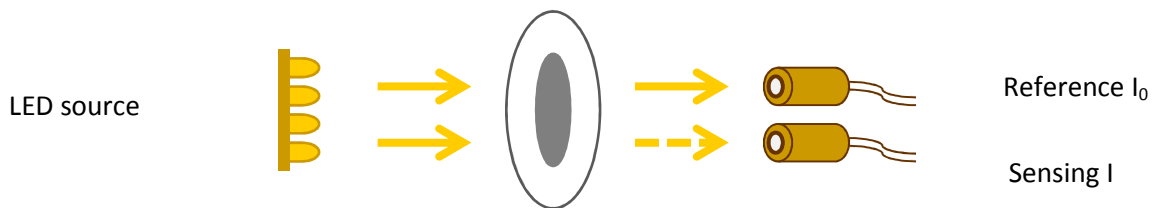


Figure 9: Light path in the optical chamber of the Aethalometer.

There are two detectors below the filter tape (**Figure 9**), one measuring transmission of light through a pristine part of the filter (reference), and the other one through the part of the filter on which aerosols are sampled (sensing). The BC concentration is calculated from the change rate of attenuation of detected light. The attenuation (ATN) is defined as:

$$ATN = 100 \cdot \ln \left(\frac{I_0}{I} \right) \quad (5)$$

I_0 is the intensity of light passing through the pristine part of the filter, and I is the intensity of light passing through the filter spot on which aerosols are sampled. The aerosol attenuation coefficient of the sampled aerosol particles b_{ATN} can be calculated using the

change in light attenuation ΔATN as a function of time, the flow rate Q and the filter spot area A (Hansen et al., 1982 and 1984):

$$b_{ATN} = \frac{A}{Q} \cdot \frac{\Delta ATN}{\Delta t} \quad (6)$$

$$BC_0 = \frac{b_{ATN}}{\sigma} \quad (7)$$

BC_0 is the concentration obtained from Aethalometer raw data ($\text{ng}\cdot\text{m}^{-3}$) and σ is specific attenuation ($\text{m}^2\cdot\text{g}^{-1}$). If the aerosols are fresh, the calculation of the BC concentration needs to be compensated with the compensation principles described in the next section. The “Classic Magee BC” calibration ($\sigma = 19.9 \text{ m}^2\cdot\text{g}^{-1}$ – factor originally derived in the early 1980’s) converts optical attenuation to a “mass of black carbon”, based on the Novakov methods for BC determination as published in Gundel, Dod et al. (Gundel et al., 1984). Mie theory for small uniform spheres predicts that to first order, sigma (σ) is inversely proportional to the optical wavelength λ . We therefore use the following values:

For “Magee BC” calibration: $\sigma = 14625 / \lambda$

For the optical sources used in the Aethalometer values in **Table 3** applied:

Table 3: Values of sigma (σ), the specific attenuation parameter, for all seven wavelengths using “Magee BC” calibration.

Lamp	λ (nm)	$\sigma(\text{m}^2\cdot\text{g}^{-1})$
UV	370	39.5
Blue	470	31.1
Green	520	28.1
Yellow	590	24.8
Red	660	22.2
IR-1	880	16.6
IR-2	950	15.4

As already mentioned, the Aethalometer used in this study measures the BC concentration at 880 nm. Since Aethalometer has seven wavelengths, it allows us to get more information about colored aerosols.

2.2.3. Data post-processing of Aethalometer data

2.2.3.1. Compensation principles

All filter based absorption measurements feature different intertwined effects which need to be taken into account when determining the absorption coefficient of ambient aerosols (Liousse et al., 1993; Petzold et al., 1997; Bond et al., 1999, Weingartner 2003, Virkkula 2007, Coen 2010). These effects include scattering of filter fibers and aerosols, and loading effects. Scattering of fibers is a multiplication factor due to the increased optical path of light in the filter matrix and depends on the filter optical properties. Aerosol scattering and loading effects depend on the aerosol properties.

Three algorithms for compensation of these effects were applied to infer the aerosol absorption coefficient b_{abs} of airborne particles from b_{ATN} (Weingartner et al., 2003, Arnott et al., 2005) or to determine the BC concentration directly (Kirchstetter et al., 2007).

The “Weingartner compensation”

Weingartner et al. (2003) proposed an empirical correction R for the attenuation effect due to the filter-loading and determined the calibration constant C for different aerosol types to correct the multiple scattering in the filter matrix. The absorption coefficient b_{abs} is given by:

$$b_{abs} = \frac{b_{ATN}}{C \cdot R} = \frac{b_{ATN,n}}{C \cdot \left[\left(\frac{1}{f} - 1 \right) \cdot \frac{\ln ATN - \ln(10\%)}{\ln(50\%) - \ln(10\%)} + 1 \right]} \quad (8)$$

The Weingartner filter loading correction R takes $ATN = 10$ as a reference point: 10% is attenuation $ATN = 10$ and 50% is attenuation $ATN = 50$. A parameter f is introduced which characterizes the slope between $b_{ATN,n}$ and $\ln(ATN_n)$ and parameterizes the filter-loading correction R :

$$f = m \cdot (1 - \omega_0) + 1 \quad m = 0.86, \quad \omega_0 = \frac{b_{scatt}}{b_{abs} + b_{scatt}} \quad (9 \text{ a, b})$$

m is an empirical number, ω_0 is single scattering albedo and b_{scatt} was used from nephelometer measurements (uncorrected data). Weingartner et al. (2003) determined f values for different aerosol types; for Palas soot particles $f = 1.5$ – 1.9 .

The Weingartner correction parameter R can depend on the light wavelength, but C does not. Therefore, a constant C value ($C = 2.14$) over the wide spectral range (370–950 nm) was chosen.

The “Arnott compensation”

The Arnott filter-loading correction R was derived from multiple scattering theory, which shows that the exponential behavior of light absorption in the strong multiple scattering limit scales as the square root of the total absorption optical depth.

The corrected b_{abs} is given by:

$$b_{abs} = \frac{b_{ATN} - \alpha \cdot b_{scat}}{\beta} = \frac{\sigma \cdot BC - \alpha \cdot b_{scat}}{M} \cdot \sqrt{1 + \frac{\left(\frac{Vd_t}{A}\right) \sum_{i=1}^{n-1} b_{abs,i}}{\tau_{\alpha,fx}}} \quad (10)$$

M is multiple scattering correction constant, V is volumetric flow rate ($m^3 \cdot s^{-1}$), i is a counter for the i -th number of filter spots, $\tau_{\alpha,fx}$ is filter absorption optical depth for the filter fraction x that has particles embedded in it, and α is introduced as scattering fraction contribution to b_{ATN} :

$$\alpha = a^{d-1} \cdot c \cdot \lambda^{-b(d-1)} \quad (11)$$

d is exponent of the power-law dependence of b_{ATN} and b_{scat} for Arnott non-absorbing aerosol experiment and b is scattering Angstrom exponent for Arnott ammonium sulfate aerosol experiment. α is dimensionless as long as $\lambda = nm$, b_{scat} and b_{ATN} have the same unit (Arnott et al., 2005).

The aerosol light absorption optical depth of the filter, $\tau_{\alpha,p}$, reduces the net multiple scattering enhancement factor β :

$$\beta = \frac{M}{\left(1 + \frac{\tau_{\alpha,p}}{\tau_{\alpha,fx}}\right)^{1/2}} \quad (12)$$

Values of α , M , and $\tau_{a,fx}$ are given in *Table 4*.

Table 4: Values used in Eq. (10) to calculate light absorption from optical BC measurements (Arnott et al., 2005)

Wavelength (nm)	σ (m ² ·g ⁻¹)	100 α	M	$\tau_{a,fx}$
370	39.53	3.35	1.813	0.2736
470	31.12	4.57	2.073	0.2263
521	28.07	5.23	2.076	0.2181
590	24.79	6.16	2.104	0.1951
660	22.16	7.13	2.182	0.1777
880	16.62	10.38	2.226	0.1375
950	15.39	11.48	2.199	0.1390

The “Kirchstetter compensation”

The effect of particle loading on attenuation was reported in Kirchstetter et al. (2007). The Aethalometer detected decreasing BC concentrations not because the concentration or the mass absorption efficiency of the BC was changing during the experiment, but because the attenuation coefficient of the collected BC decreased as the Aethalometer filter became increasingly darkened with the light absorbing particles.

The suggestion is simple means of correcting reported concentrations by using the following equation:

$$BC = \frac{BC_0}{a \cdot Tr + (1-a)} \quad (13)$$

Transmission, Tr , can be computed directly from the ATN, measured with Aethalometer; $Tr = \exp(-ATN/100)$ and a is a slope and intercept of regression line (uncorrected data) and linear line (corrected data). As the Aethalometer’s filter collects BC and Tr decreases from unity, the denominator of Eq. (5) decreases, which accounts for the decreasing attenuation coefficient. The BC concentration reported by the Aethalometer (i.e. to BC_0) was applied in the Eq. (13), and the influence of particle loading on the attenuation was eliminated (Kirchstetter et al., 2007).

The corrected BC is then converted back to b_{ATN} (corrected) and the Angstrom exponent is calculated using the corrected b_{ATN} values.

The particle loading effect is not specific to the Aethalometer measurements; it is common to all light transmission measurements using highly scattered filters.

2.2.3.2. The Aethalometer model

If we have a mixture of absorbing aerosols from two different combustion regimes, which result in aerosols with different optical properties, we can exploit this difference to determine the composition of the aerosol mixture and quantitatively apportion the absorbing aerosols to the two combustion regimes. We treat the combustion regimes between the extremes as a linear combination of these two. The "Aethalometer model" was used to discriminate between diesel exhaust and wood-smoke in ambient air (Sandradewi et al., 2008a). The parameter specific to the combustion type and fuel was the aerosol absorption Angstrom exponent (*Figure 10*), determined from dependence of aerosol absorption on the wavelength, as measured by the Aethalometer. The model is employed to discriminate between different combustion regimes of the same type of fuel at different C/O ratios. *Figure 10* shows an example of the behavior of the Angstrom exponent in the CAST experiment as the C/O ratio was 0.21 and the mixing gas was added in the combustion system.

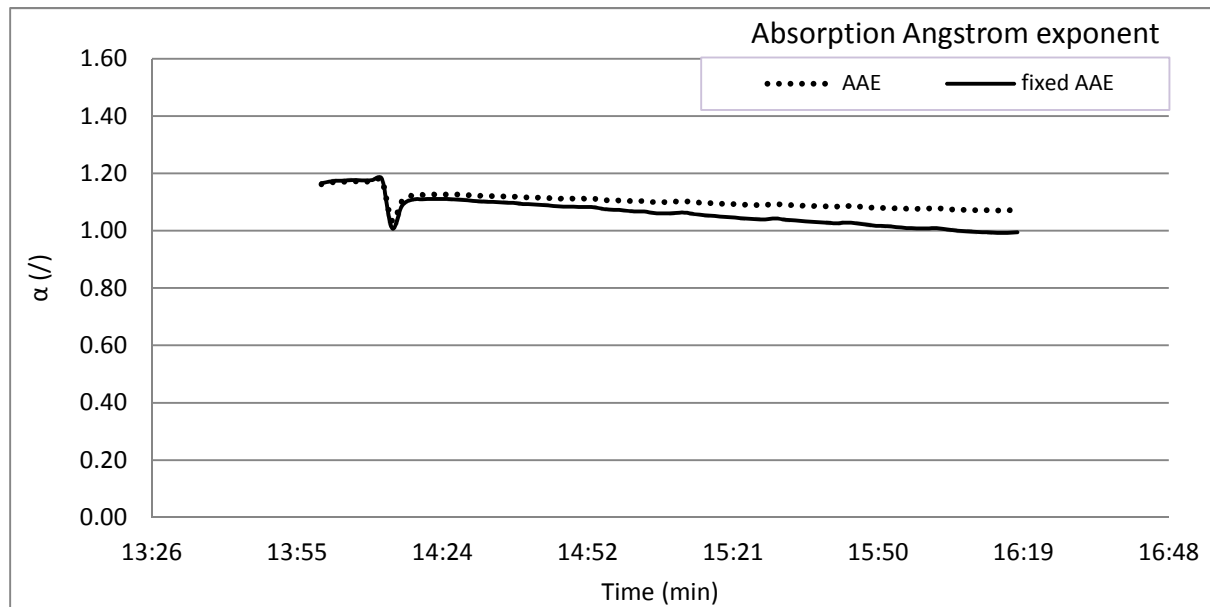


*Figure 10: The absorption Angstrom exponent (α) values of the operating condition with C/O ratio = 0.21 (with the mixing gas - N_2). α are the results of raw data (dotted line) and **fixed α** (solid line) are data compensated with the Weingartner principle.*

Several studies showed that some parts of particulate organic matter significantly absorb light at short wavelengths around 400–500 nm (e.g. Kirchstetter et al., 2004); this kind of particulate matter is now called brown carbon.

As defined in the introduction chapter (Carbonaceous species section), absorption coefficient is therefore a mixture of BC and BrC, each with a unique Angstrom exponent:

$$b_{abs}(\lambda) = b_{abs,BrC}(\lambda) + b_{abs,BC}(\lambda), \quad \lambda = 470 \text{ nm}, 880 \text{ nm} \quad (14 \text{ a, b})$$

$$\frac{b_{abs,BC}(470 \text{ nm})}{b_{abs,BC}(880 \text{ nm})} = \left(\frac{470}{880}\right)^{-\alpha_{BC}} \quad (15)$$

$$\frac{b_{abs,BrC}(470 \text{ nm})}{b_{abs,BrC}(880 \text{ nm})} = \left(\frac{470}{880}\right)^{-\alpha_{BrC}} \quad (16)$$

Solving these four equations allows us to separate the absorption coefficient due to different combustion processes at different C/O values.

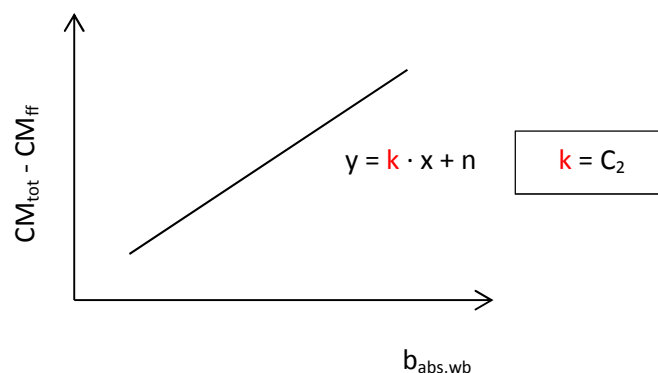
The Aethalometer model can be extended to all carbonaceous matter. A few recent studies in which Aethalometer was used to detect the presence of biomass burning aerosols in the atmosphere (Jeong et al., 2004; Sandradewi et al., 2008a) focused on the difference in optical properties based on $\lambda^{-\alpha}$. Using a multiwavelength Aethalometer and independent carbon analyses to obtain CM_{total} Sandradewi et al. (2008b) proposed two methodologies allowing the quantification of wood-burning carbonaceous aerosols. The mass concentration of all carbonaceous matter can be described as a sum of contributions from different sources:

$$CM_{total} = CM_{ff} + CM_{wb} + CM_{other} \quad (17)$$

CM_{total} is considered as a sum of all carbon-containing aerosol concentrations, CM_{ff} being the contribution from fossil fuel (traffic), CM_{wb} from brown-carbon-containing biomass smoke aerosols and CM_{others} from non-combustion aerosols. In the following equation, C_1 and C_2 are parameters, which relate the light absorption to a particulate mass of both sources ($b_{abs,wb,470nm}$ and $b_{abs,ff,950nm}$), whereas C_3 represents non-absorbing organic aerosols from other sources. In the following calculation we neglect this term (C_3) because its contribution is assumed small for our samples.

$$CM_{\text{total}} = C_1 \cdot b_{\text{abs,ff,950nm}} + C_2 \cdot b_{\text{abs,wb,470nm}} \quad (18)$$

$$CM_{\text{total}} - CM_{\text{ff}} = C_2 \cdot b_{\text{abs,wb,470nm}} \quad (19)$$



C_1 and C_2 may strongly depend on the nature of aerosols. In our case, we assume that each source has the same composition of aerosols and therefore C_1 related to fossil fuel combustion can be much less variable than C_2 which is notably influenced by the wood type and the combustion regime. Favez et al. (2010, *Table 5*) used a sensibility test (of the Aethalometer model) by varying α_{ff} from 0.9 to 1.1 and α_{wb} from 1.5 to 3.0 to show that C_1 can be generalized and used as a constant. It thus appears reasonable to use a fixed C_1 value in Eq. (18) and then calculate site-specific C_2 .

C_1 was set on $0.29 \text{ g}\cdot\text{m}^{-2}$ (Sandradewi et al., 2008; Favez et al., 2010), while C_2 has to be calculated site-specific as described above. This approach is shown in **Table 5**. C_2 corresponds to the slope of the linear regression, which was done for the OC/EC data during the period of study (January 28–March 1, 2011).

Table 5: Mean 24-hour-average parameters of CM and C_2

Station	C_2	R	CM_x/CM
Klagenfurt – Voelkermarkter Strasse	0.52	0.687	0.98
Zell - Ebenthal	0.33	0.846	0.98

We used the AethReader31 Aethalometer model software produced by Aerosol Company (L. Drinovec).

CM_{total} can be derived when combined with equations (Favez, et al. 2009):

$$CM_{total} = OM + BC \quad (20)$$

$$OM = OC \cdot f \quad , f = \frac{OM}{OC} \quad (21)$$

OC is measured with the OC-EC dual-optical instrument, while BC is measured with the Aethalometer as given before. f is a factor $f = \frac{OM}{OC}$. The value given for fresh aerosols is approximately $f = 1.2$, and around $f = 2.4$ for wood-burning (Favez et al., 2010). For ambient aerosols in Klagenfurt, a value of 1.8 was used.

CHAPTER 3

The CAST experiment

Contents

3.1. The CAST propane burner and the experiment.....	30
3.2. Results.....	36
3.2.1. Comparison of BC and EC data obtained with different methods.....	38
3.2.1.1. Manual setting of split point	40
3.2.1.2. Temperature protocol deviations	43
3.2.2. Composition of light absorbing carbonaceous aerosols.....	46
3.2.3. Analysis made by two-component Aethalometer model (absorption vs. wavelength) to determine two carbonaceous components: BC and BrC.....	49

This chapter presents systematic aerosol measurements of the CAST emissions performed under different operational conditions.

Several methods for measuring carbonaceous aerosols are combined to study the properties of emitted particles. The key question of this work is: Are there significant differences in chemical and optical properties between the combustion particles emitted from different combustion processes which then result in different Angstrom exponent values?

This set of measurements was obtained by using laminar flame propane gas burner, which is nowadays widely used in the laboratory for generating realistic combustion particles.

3.1. The CAST propane burner and the experiment

The CAST experiment was part of the EASA-funded study SAMPLE II (Studying, sampling and measuring of aircraft particulate emissions II). This experiment was aimed at the investigation of physical and chemical properties of combustion particles emitted from different combustors or burners. First part of SAMPLE II (Research project EASA.2008.OP.13) was done by a group of scientists from the Institute of Atmospheric Physics (DLR, Oberpfaffenhofen) and Cardiff University (Cardiff, UK). Their results are presented in the final report: Study on sampling and measurement of aircraft particulate emissions SAMPLE-Final report (October 2009). In the second part, we joined the aforementioned group of scientists by conducting the CAST experiment with Aethalometer measurements and filter sampling.

Several methods for measuring carbonaceous aerosols (**Figure 11**) were combined to study the relationship between chemical composition, microphysical properties and optical properties of emitted particles. The overall focus was to generate “pure” EC (BC) or BrC during a rather standardized experiment and to determine α at these “special conditions”.



Figure 11: Set of all instruments during the CAST experiment.

The following properties were observed during the experiment: aerosol absorption; aerosol scattering coefficient; total carbon, organic carbon and elemental carbon based on the thermal analysis of quartz fiber filters; morphology and microstructure; degree of graphitisation; particle number concentration; and particle size distribution. Our attention was focused on Aethalometer measurements (optical properties) and sampling on quartz fiber filters, while other devices were employed by a research group from the Institute of Atmospheric Physics (DLR Oberpfaffenhofen, Germany), the Faculty of Physics (University of Vienna, Austria), ONERA – The French Aerospace Lab (Châtillon, France) and Campus de

Luminy (Aix-Marseille Université, France). Results will be presented in the paper by Jin Kim (DLR) et al., 2013.

A Real Soot Generator RSG miniCAST 6201-C (Jing Ltd., Switzerland; hereinafter referred to as the CAST burner) was used as an aerosol generator. Propane (C_3H_8) was burned together with synthetic air (20% of oxygen – O_2) and nitrogen (N_2), which entered in the burner as a quenching or/and mixing gas (see **Figure 13**). The CAST burner was used as a model for combustion of carbonaceous fuels with varying ratios between carbon in fuel and oxygen (C/O ratio). A detailed description of the burner is given on the web page of the Jing company (<http://www.sootgenerator.com/documents/Zahoransky.pdf> - 02/14/2012).

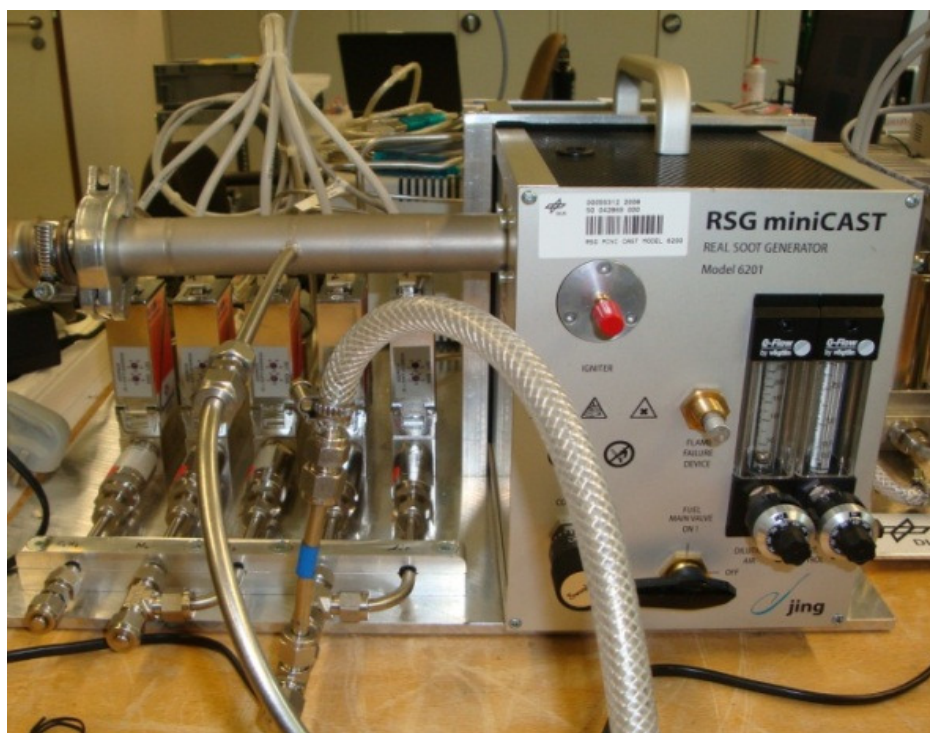


Figure 12: The CAST burner (Jing-CAST Technology).

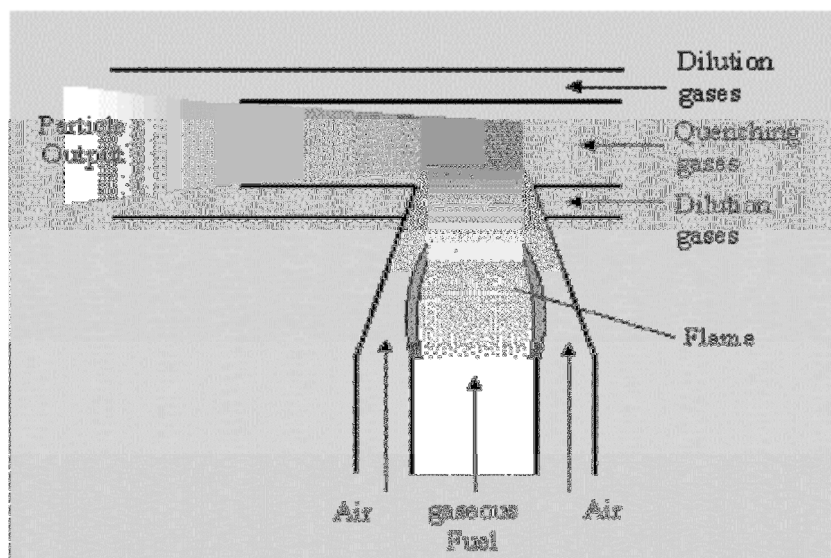


Figure 13: The working principle of the CAST burner (<http://www.sootgenerator.com/documents/Zahoransky.pdf> – 02/14/2012).

The CAST burner, the central device of our experiment, enables the soot particles to escape from the flame without further contact with oxygen. Subsequently, the particle stream is mixed with a quenching gas (N_2) in order to prevent further combustion processes in the particle stream and to stabilize the soot particles. The quenching inhibits condensation in the particle stream at ambient air conditions. To dilute the particle stream, compressed air is supplied to the quenched particle stream. In our case (CAST X.1), nitrogen as a mixing gas was used for particle stream dilution. It pre-diluted the fuel and was added to the compressed air. Then this mixture of N_2 and compressed air was introduced in the process.

For the soot particles, as for mass output, they grow when the oxygen added to the fuel gas is reduced and the flame becomes a diffusion flame. In combustion, a diffusion flame is a flame in which the oxidizer – in our case the oxygen in the synthetic air – combines with the fuel by diffusion. Diffusion flames tend to burn slower.

The CAST experiment was carried out in a laboratory at the Institute of Atmospheric Physics, DLR Oberpfaffenhofen, Germany. The experiment was set up featuring various instruments (Scheme 1). There were two dilution stages: 1:10 and 1:100. After the first dilution stage (1:10), the aerosols were measured with Optical Particle Counter (OPC), Multiangle Absorption Photometer (MAAP), and CO_2 sensor. After the 1:100 dilution, OPC, Scanning Mobility Particle Sizer (SMPS), CO_2 sensor, and four Condensation Particle Counters (CPCs – two of them were connected through a thermo-denuder) were set up. At the end of the line, two Aethalometers, Particle Soot Absorption Photometer (PSAP) and nephelometer were placed. Filters were sampled directly from the exhaust pipe. Undiluted aerosols were

collected on the filters at the end of each test (instruments were turned off during the filter sampling). Results of these measurements will not be discussed here, but will be presented in the Jin Kim et al. (2013 – yet unpublished) paper.

The CAST burner performed under various operating conditions. Each test cycle (*Table 6*) was given the name “CAST X.Y”, where X represented the number of the test, and Y the information about the presence of the mixing gas. Y equaling 0 meant that mixing gas was not present, whereas Y equaling 1 meant the mixing gas was added to the process. Each measurement cycle usually lasted around 1.5 hours.

Table 6: Operating conditions during the CAST experiment – “CAST X.Y”, where X represents the number of the test, and Y gives the information about the presence of the mixing gas. When Y = 0, the mixing gas is not present, and when Y = 1 the mixing gas is added to the process.

Conditions	C/O Ratio	Fuel $\text{C}_3\text{H}_8 - \text{l}\cdot\text{m}^{-1}$	Oxidation gas air - $\text{l}\cdot\text{m}^{-1}$	Mixing gas $\text{N}_2 - \text{l}\cdot\text{m}^{-1}$	Quenching gas $\text{N}_2 - \text{l}\cdot\text{m}^{-1}$	Dilution air air - $\text{l}\cdot\text{m}^{-1}$
CAST 1.0	0.21	0.017	0.564	-	1.24	1.08
CAST 1.1	0.21	0.017	0.564	0.015	1.24	1.08
CAST 2.0	0.31	0.017	0.396	-	1.24	1.08
CAST 2.1	0.31	0.017	0.396	0.015	1.24	1.08
CAST 3.0	0.41	0.017	0.3	-	1.24	9.00
CAST 3.1	0.41	0.017	0.3	0.015	1.24	1.08
CAST 5.0	0.6	0.025	0.3	-	1.24	1.08
CAST 5.1	0.6	0.025	0.3	0.015	1.24	1.08
CAST 7.0	0.21	0.017	0.564	-	1.24	1.08
CAST 7.1	0.21	0.017	0.564	0.015	1.24	1.08
CAST 8.0	0.31	0.017	0.396	-	1.24	1.08

We studied the reproducibility of the aerosol generator with respect to its aerosol output in terms of particle number, mass and size distribution. We wanted to get a complete set of combustion particle properties for various types of combustion processes.

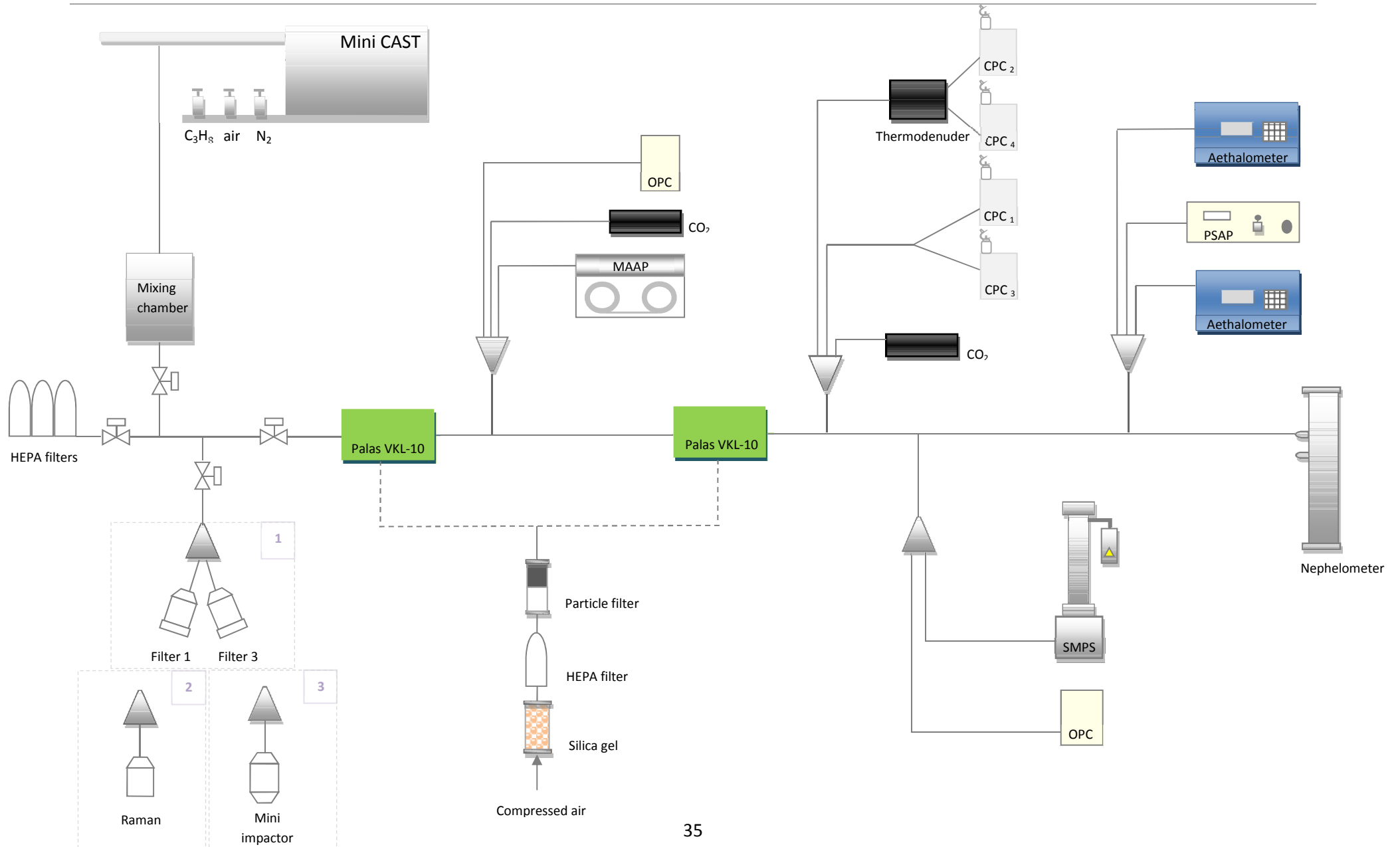
The CAST burner allows the generation of carbonaceous aerosols with OC to total carbon (TC) mass ratios which vary over a broad range from few % to 80% or more by variation of the propane-to-air ratio. The atomic ratio of carbon to oxygen (C/O ratio) in the combustion process is calculated from the actual fuel-to-air ratio, i.e. the actual flow of the propane and air taken up by the burner (Schnaiter et al., 2006):

$$C/O = 7.16 \cdot \frac{f_p}{f_{air}} \quad (22)$$

f_p and f_{air} represent the standard volumetric flows of the propane and synthetic air, respectively. Different gases are used in the combustion of the CAST burner: propane, synthetic air and nitrogen. Propane is combusted in synthetic air and nitrogen is used as a quenching or mixing gas during the combustion. In the experiment, the flow of these gases was adjusted to obtain the desired C/O ratio values.

The ratio between propane and oxygen (i.e. C/O ratio) is very important for various aerosols generations, because the quality of combustion is strongly dependent on this ratio; the less oxygen is present in the process the less incomplete the combustion is.

Scheme 1: The CAST experiment system.



3.2. Results

Our experiment should feature six modes of combustion with six different C/O ratios: 0.21, 0.31, 0.41, 0.50, 0.60, and 0.89. However, the diffusion flame was at times quite unstable, therefore we only focused on four stages of combustion (C/O ratio: 0.21, 0.31, 0.41 and 0.60) at which we were able to establish a stability state for later analyses.

Below is a photo (**Figure 14**) of the analyzed filter samples.



Figure 14: Four sets of filters under different operating conditions. The left pair in the set was sampled when no mixing gas (N_2) was present, as opposed to the right pair. The first group of four filters had a C/O ratio of 0.21, the second 0.31, the third 0.41 and the last group 0.60 (left to right).

Table 7: The CAST experiment results of off-line and on-line analyses at various C/O ratios (C/O = 0.21, 0.31, 0.41 and 0.60). * The column "Duration of sampling" refers to filter sampling, while Aethalometer data were sampled separately (2-minute time base) from filter sampling.

Filters	C/O Ratio	mixing gas (L·min ⁻¹)	Duration of sampling* (min)	flow rate (L·min ⁻¹)	SUNSET NIOSH EC/TC %	OC (mg·m ⁻³)	EC (mg·m ⁻³)	SUNSET EUSAAR2 EC/TC %	OC (mg·m ⁻³)	EC (mg·m ⁻³)	TLT EC/TC %	BrC C (mg·m ⁻³)	BC IS (mg·m ⁻³)	BC - Aeth (mg·m ⁻³)
QF 77	0.21	-	15	5.12	78.8	0.654	2.424	80.3	0.597	2.430	73.8	bdl	1.424	0.720
QF 78		-	15	5.12	74.0	0.866	2.465	78.6	0.621	2.287	76.7	bdl	1.613	
QF 79		0.015	18	5.12	55.2	0.199	0.245	58.3	0.206	0.287	51.4	bdl	0.416	0.207
QF 80		0.015	18	5.12	52.3	0.212	0.233	52.3	0.245	0.269	57.5	bdl	0.381	
QF 81	0.31	-	15	5.12	59.4	3.992	5.838	70.1	2.544	5.964	28.6	1.312	1.380	0.982
QF 82		-	15	5.12	63.3	3.526	6.094	65.0	3.108	5.759	15.7	0.770	1.773	
QF 51		0.015	3	5.12	45.8	9.877	8.342	50.2	9.244	9.319	10.1	6.308	3.852	0.498
QF 52		0.015	3	5.12	47.6	9.019	8.205	51.7	7.747	8.280	8.8	6.736	3.987	
QF 53	0.41	-	3	5.12	11.6	8.536	1.115	13.8	8.580	1.378	55.7	6.838	bdl	0.051
QF 62		-	3	5.12	12.3	7.284	1.021	16.2	7.478	1.447	54.3	6.263	bdl	
QF 63		0.015	34	5.12	6.6	0.881	0.062	7.6	0.855	0.070	50.8	0.338	bdl	0.054
QF 64		0.015	34	5.12	6.0	0.842	0.054	7.1	0.835	0.064	50.6	0.258	bdl	
QF 69	0.60	-	45	5.12	8.9	1.075	0.104	10.8	1.123	0.136	53.8	0.835	bdl	0.077
QF 70		-	45	5.12	8.7	1.167	0.111	10.2	1.046	0.119	53.7	0.817	bdl	
QF 71		0.015	35	5.12	5.0	0.532	0.028	7.7	0.589	0.049	49.0	1.707	0.071	0.036
QF 72		0.015	35	5.12	5.1	0.575	0.031	6.0	0.737	0.047	46.3	1.690		

3.2.1. Comparison of BC and EC data obtained with different methods

This study relies on the thermal behavior of the combustion aerosols emitted in the CAST experiment. Organic carbon (OC) and elemental carbon (EC) refer to the carbon fractions that thermally desorb in oxygen free and oxygen containing atmosphere and at different temperatures. Filter samples were, on one side, analyzed with two devices using thermal-optical methods: the OC-EC dual-optical instrument and TLT.

On the other side, on-line and off-line analyses with optical methods were employed using Aethalometer (on-line) and integrating sphere (off-line), where black carbon (BC) was detected. The difference between EC and BC lies only in the use of different determination methods (thermal-optical vs. optical method), as already presented at the beginning. All data were obtained with transmission laser correction. Results obtained by integrating sphere were provided by the Faculty of Physics, University of Vienna, Austria (Hitzenberger et al., 2013 – unpublished data).

In **Figure 15**, optical and thermal-optical methods are compared. All analyses, with the exception of TLT, are presented.

The results of the TLT analysis were very poor due to a laser error. There were too many disturbances during the laser measurements. TLT data will be presented in further discussion only to show the trends of OC-EC ratios.

At a low C/O ratio ($C/O = 0.31$), substantial deviations can be noticed due to the use of different methods. However, no large discrepancies can be observed using different temperature protocols; the EC concentration of $6.0 \text{ mg}\cdot\text{m}^{-3}$ is calculated using the EUSAAR 2 protocol and the EC concentration of $5.1 \text{ mg}\cdot\text{m}^{-3}$ is calculated using the NIOSH 5040 protocol ($\sim 16\%$ difference at the C/O ratio of 0.31). Therefore, in our case the temperature protocol does not affect the analyses of filters.

As for optical analysis, there were two separate sampling strategies. BC measured with Aethalometer (BC-AE) was sampled synchronously with other devices, while quartz filters were sampled at the end of each condition cycle (when all devices were turned off). Integrating sphere (BC-IS) was used to analyze those filters. The difference in measurement time slightly affects the concentration of BC and BrC measured with Aethalometer and integrating sphere. The trend of BC measurements according to the increase of C/O ratio is the same in both methods. The concentration of the BC is the highest at a low C/O ratio ($C/O = 0.21$ or/and 0.31) and decreases with increasing C/O ratio.

Values of filter analyses were expressed in $\mu\text{g}\cdot\text{cm}^{-2}$, so we changed them into mass concentrations in $\text{mg}\cdot\text{m}^{-3}$, as follows:

$$\text{Mass concentration (mg}\cdot\text{m}^{-3}) = \frac{[X] \cdot A}{Q \cdot t} \quad (23)$$

[X] represents the concentration of carbonaceous species in $\mu\text{g}\cdot\text{cm}^{-2}$, A is the deposit area, Q is the flow rate passing through the filters and t is sampling time.

In **Figure 15** BC concentration calculated with optical methods is found to be almost 3 times as low as the EC concentration of Sunset data at the C/O ratio of 0.31.

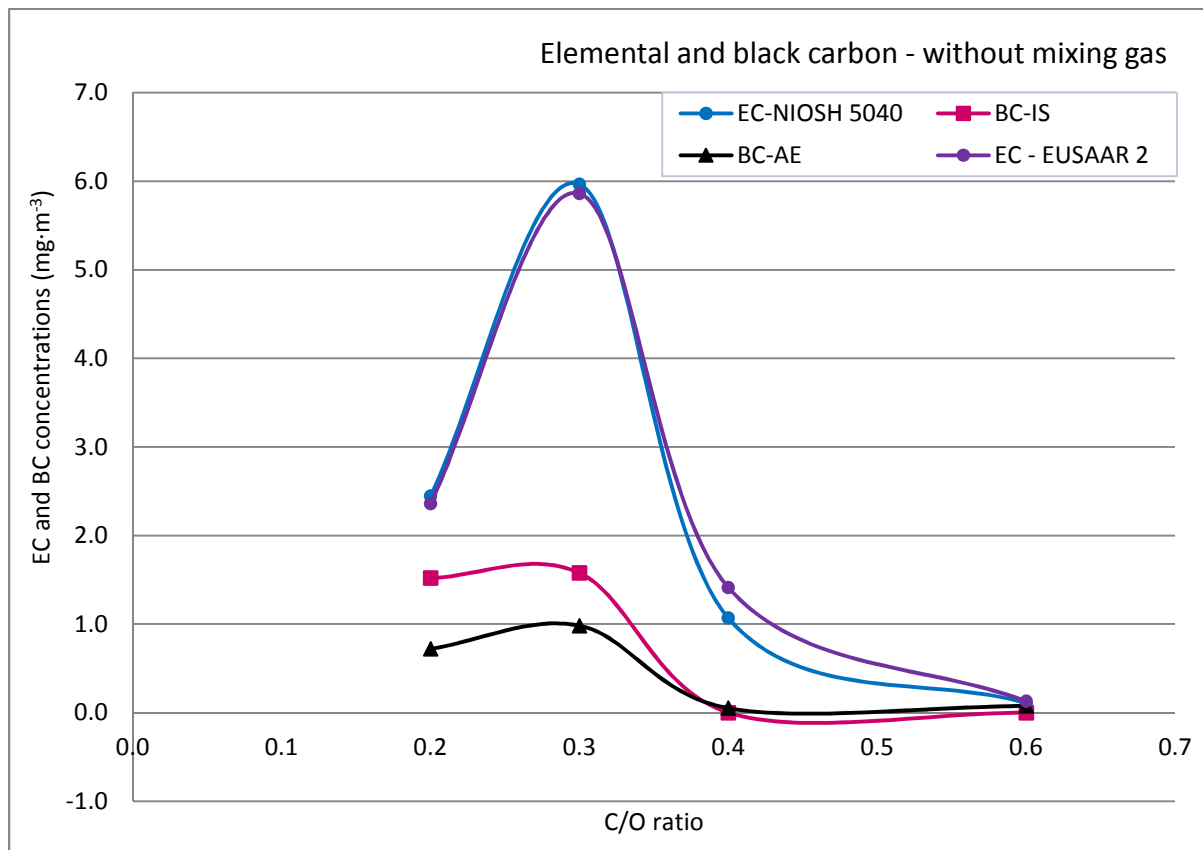


Figure 15: Dependence of EC and BC concentrations on combustion regime – C/O ratio (without mixing gas): (◊) the EC concentration measured with OC-EC dual-optical instrument using NIOSH 5040, (○) the EC concentration measured with OC-EC dual-optical instrument using EUSAAR2, (◻) the BC concentration measured with integrating sphere, and (Δ) BC concentration measured with Aethalometer.

Overestimation of the EC concentration may occur as a result of an overloaded filter and can consequently cause problems with setting the split point. The split point of results at C/O ratios of 0.21 and 0.31 was set manually, while in the rest of the results the automatic split point was taken.

As mentioned and shown in **Figure 14**, filters at low C/O ratios (C/O = 0.21 or 0.31) are very dark. The optical methods (integrating sphere and Aethalometer) are very well correlated and their lower values of BC concentrations might offer an answer on appropriate value of BC presented in the samples.

To sum up, **Figure 15** shows that at low C/O ratios (C/O = 0.21 and 0.31) EC (or BC) is generated, but by lowering the amount of oxygen in the combustion process the OC concentration increases and EC decreases. OC-EC dual-optical instrument can overestimate the EC concentration due to overloaded filters. The problem with setting the split point occurs, which will be investigated in the next section.

3.2.1.1. Manual setting of split point

As mentioned, the boundary between OC and EC is called the “split point”, marking the point at which the laser signal reaches its initial value. A split point set by Sunset software is the violet vertical line on the thermogram, while the blue line is a manually set split point. The following figures (**Figure 16** and **Figure 17**) show the thermograms of four different filter samples in two operating conditions (C/O ratio = 0.21 and 0.31).

In our case, the thermograms were plotted with the software system of the OC-EC dual-optical instrument for calculating the concentrations of OC and EC in the sample. The OC or EC concentrations were presented by using an automatic split point for samples with high C/O ratios (C/O = 0.41 and 0.60) or by using a manually set split point for samples with low C/O ratios (C/O = 0.21 and 0.31). An exception were samples with the C/O ratio of 0.31 and mixing gas added where OC and EC were also split automatically.

In **Figure 16** two thermograms of samples with the C/O ratio of 0.21 are presented; the left one (**Figure 16, a**) is the sample with automatically set split point and the right one with manually set split point. In the EC peak, a shoulder can be observed, which could be caused by the presence of brown carbon in the samples with low C/O ratio.

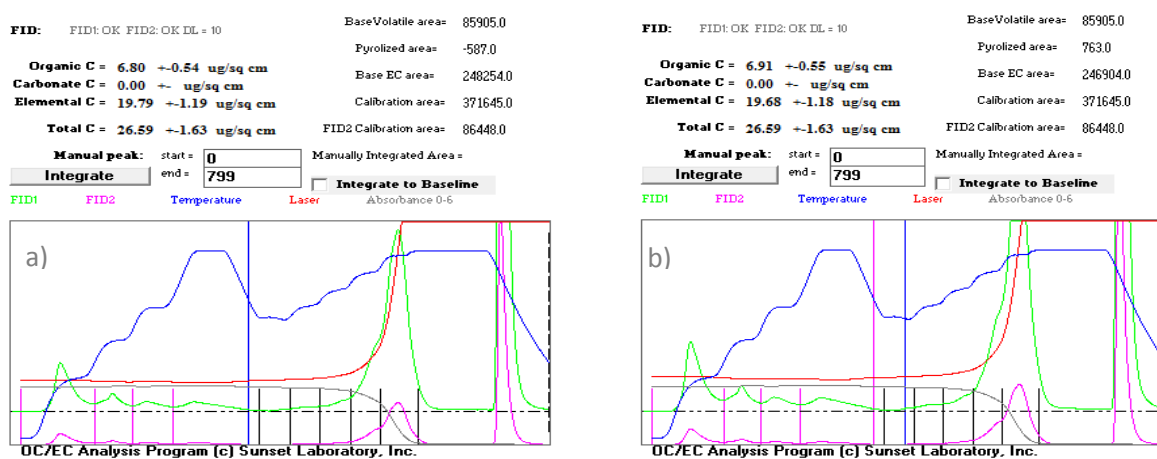


Figure 16: Thermograms of analyzed filter samples at the C/O ratio of 0.21 using the NIOSH 5040 temperature protocol: a) sample with automatically set split point (blue vertical line), and b) sample with manually set split point: violet (left vertical) line is an automatic split point and blue (right vertical) line is a manual split point).

The thermograms show that in some results, the laser signal is presented as a flat line and the Sunset software sets the split point right after the point where the oxygen enters the process (see **Figure 4**). In that case, EC concentration might be overestimated, because the laser does not reach its initial point and some pyrolytic carbon might be taken as an elemental carbon.

An overestimation of EC concentration can also be observed in **Figure 15** where a significant difference at the C/O ratio of 0.31 can be noticed when comparing different measurement methods. This overestimation occurs due to a problem when setting the split point. In the next figure (**Figure 17**), this problem will be explained.

In **Figure 17**, thermograms of samples with the C/O ratio of 0.31 are shown. On the left (**Figure 17, a**), again the sample with automatically set split point, and on the right, the sample (**Figure 17, b**) with manually set split point can be seen.

The results show that moving the split point from 559 to 580 seconds reduces the EC concentration almost for a factor of 3 (from $6.1 \text{ mg}\cdot\text{m}^{-3}$ to $2.3 \text{ mg}\cdot\text{m}^{-3}$) and in this case the difference between the methods disappears (see **Figure 18**). However, the split point should not be moved further than the initial value of laser signal.

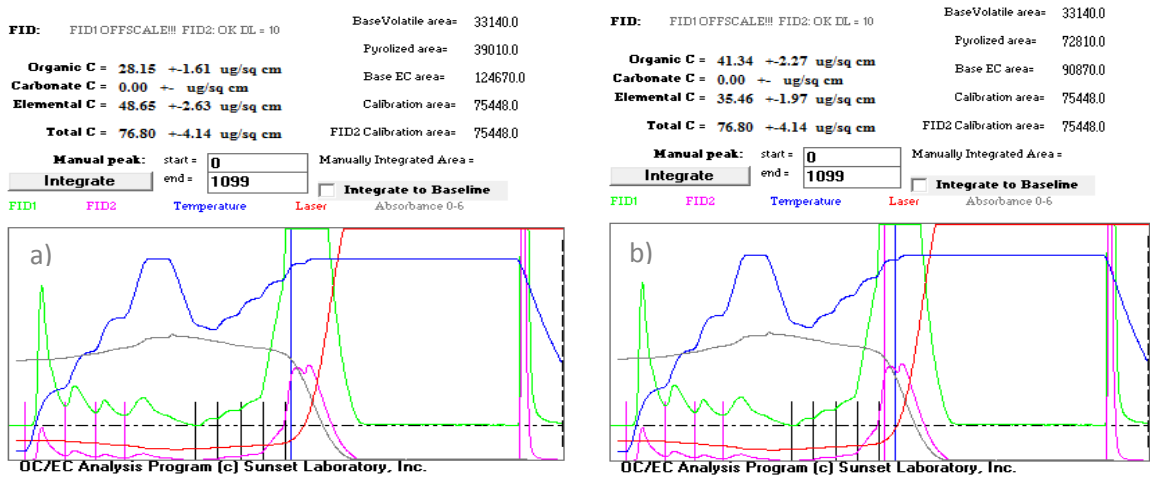


Figure 17: Thermograms of analyzed filter samples with the C/O ratio of 0.31 using the NIOSH 5040 temperature protocol: a) sample with automatically set split point, and b) sample with manually set split point (violet (left) line is an automatic split point and blue (right) line is a manual split point).

In **Figure 18**, optical and thermal-optical methods are compared and they correlate strongly due to manual setting of split point.

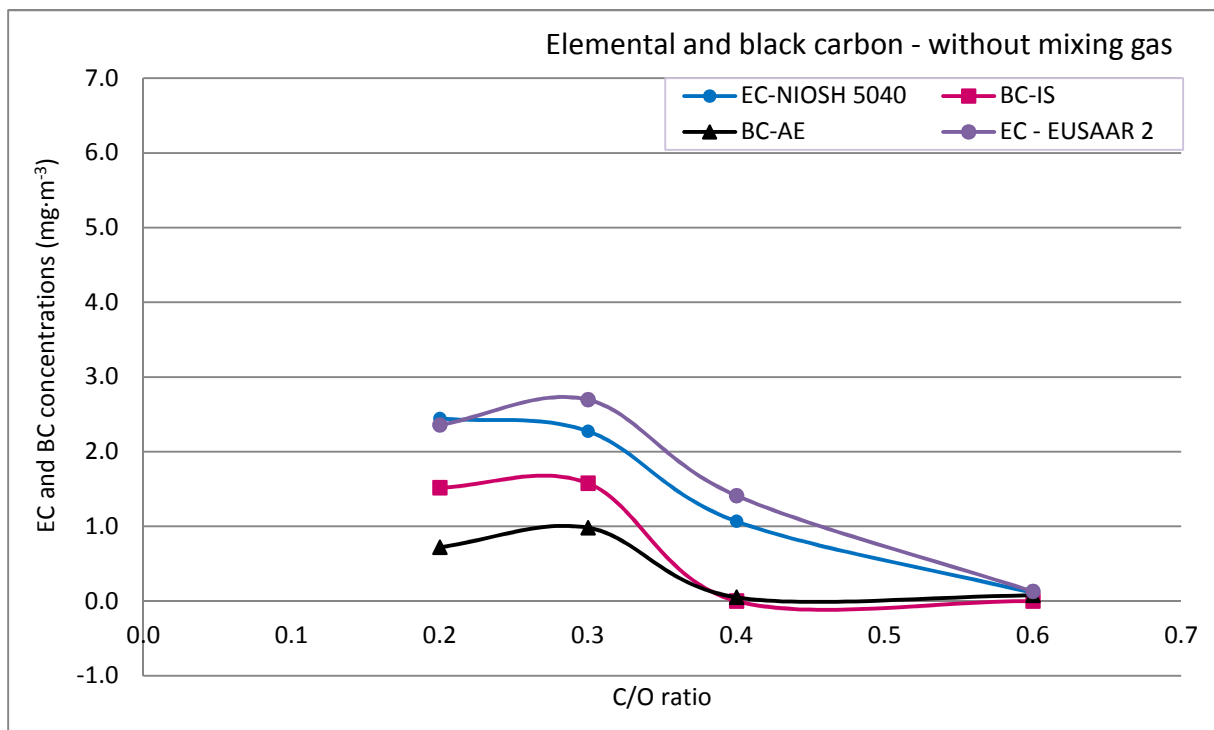


Figure 18: Dependence of EC and BC concentrations on combustion regime – C/O ratio (without mixing gas): (◊) the EC concentration measured with OC-EC dual-optical instrument using NIOSH 5040, (◊) the EC concentration measured with OC-EC dual-optical instrument using EUSAAR2, (◻) the BC concentration measured with integrating sphere, and (Δ) BC concentration measured with Aethalometer. The manual split point was manipulated to obtain proper results of the OC-EC dual optical analyzer.

As mentioned before, it is not allowed to move the split point to get good correlation, but this figure is a great example of how overestimation of EC concentration measured with OC-EC dual optical analyzer might affect the results.

In summary, **Figure 16** in which black filters were examined (C/O ratio = 0.21) shows almost identical thermograms due to automatic or manual setting of split point, while at the C/O ratio of 0.31 (**Figure 17**) the manually set split point decreases the EC concentration for almost a factor of 3 compared to automatically set split point. The results of optical and thermal-optical methods in that case match (some minor deviations are observed), which confirms the split point issue.

3.2.1.2. Temperature protocol deviations

In this section, we will take a closer look on the difference in temperature protocols for the two types of samples. **Figure 19** shows the results obtained with samples without the mixing gas (N₂) in the combustion system, while in **Figure 21**, the results of samples with mixing gas are shown.

If we observe the average values of analyzed data in conditions without the mixing gas (**Figure 19**), we can notice differences at the C/O ratio of 0.31. The results using the NIOSH 5040 temperature protocol display a larger proportion of EC than the ones using the EUSAAR 2, while the portions in terms, in which the mixing gas was presented, were nearly the same. In **Figure 19** and **Figure 21**, data from TLT can be seen. Since the TLT analysis indicates the proportion of EC and OC in the sample, it makes sense to show the obtained data, despite their experimental uncertainties. Due to instability of the laser, a big difference is noticeable, which can be seen at high C/O ratios (0.41 and 0.60).

The observed difference at the C/O ratio of 0.31 may be explained with a thermogram shown in **Figure 20**. **Figure 20** demonstrates the results of filter sample at the C/O ratio of 0.31 analyzed by the OC-EC dual-optical instrument using the EUSAAR 2 temperature protocol. This is a thermogram of filter sample where no mixing gas (N₂) was added in the combustion process.

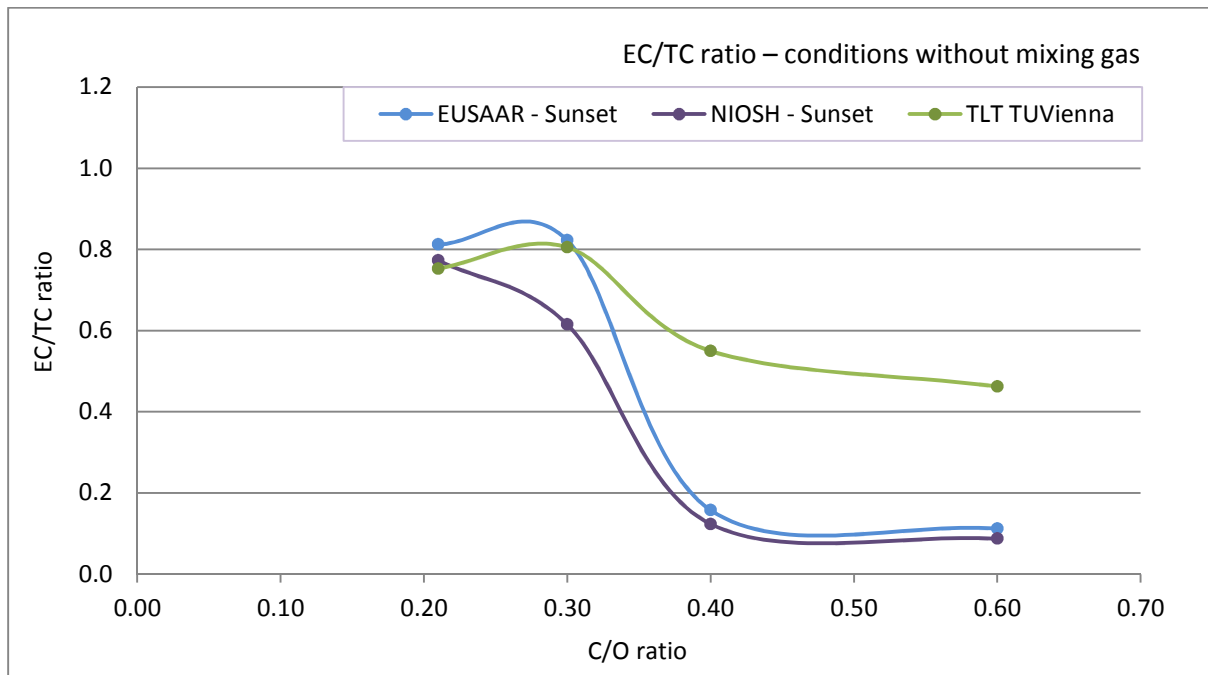


Figure 19: The EC/TC ratio dependence on combustion regime without the mixing gas: the blue line represents the results of the EC/TC ratio measured with the OC-EC dual optical instrument using the EUSAAR2 temp. protocol, the violet line represents the results of the EC/TC ratio measured with the OC-EC dual optical instrument using NIOSH 5040 temp. protocol, the green line represents the results of the EC/TC ratio measured with TLT.

Thermogram shows that there was quite a lot of material deposited on the filter, and that the split point was moved substantially in the EC area, which might have an effect on this difference.

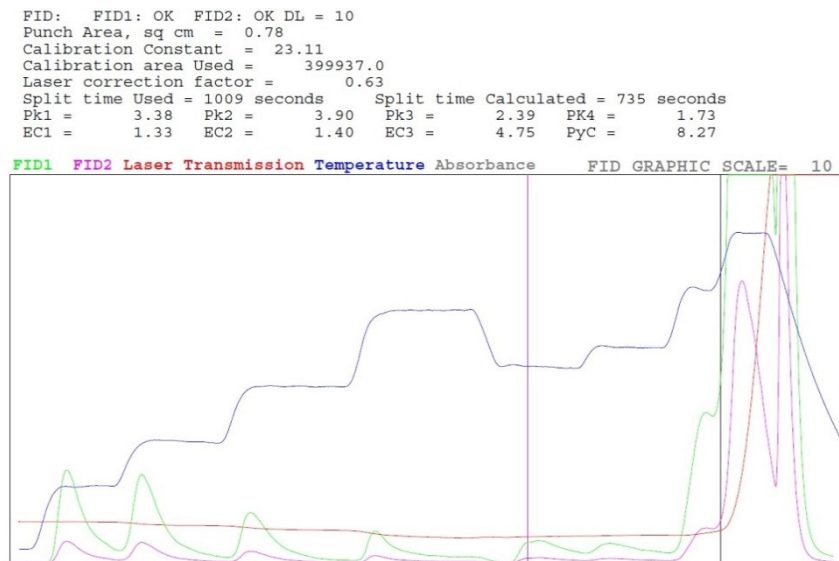


Figure 20: Thermogram of analyzed filter sample with the C/O ratio of 0.31 (the EUSAAR2 temp. protocol); no mixing gas. Split point set by Sunset software is the violet (on the left) vertical line on the thermogram, while the blue line is a manually set split (on the right) point.

In **Figure 21**, the results of thermo-optical analyses of filter samples with mixing gas in the combustion process are presented. The portion of EC is reduced in the conditions with mixing gas, which may be due to formation of NO_x . The nitrogen might react with oxygen and reduce its amount in the combustion process of carbonaceous material. Deviations between both temperature protocols are almost negligible.

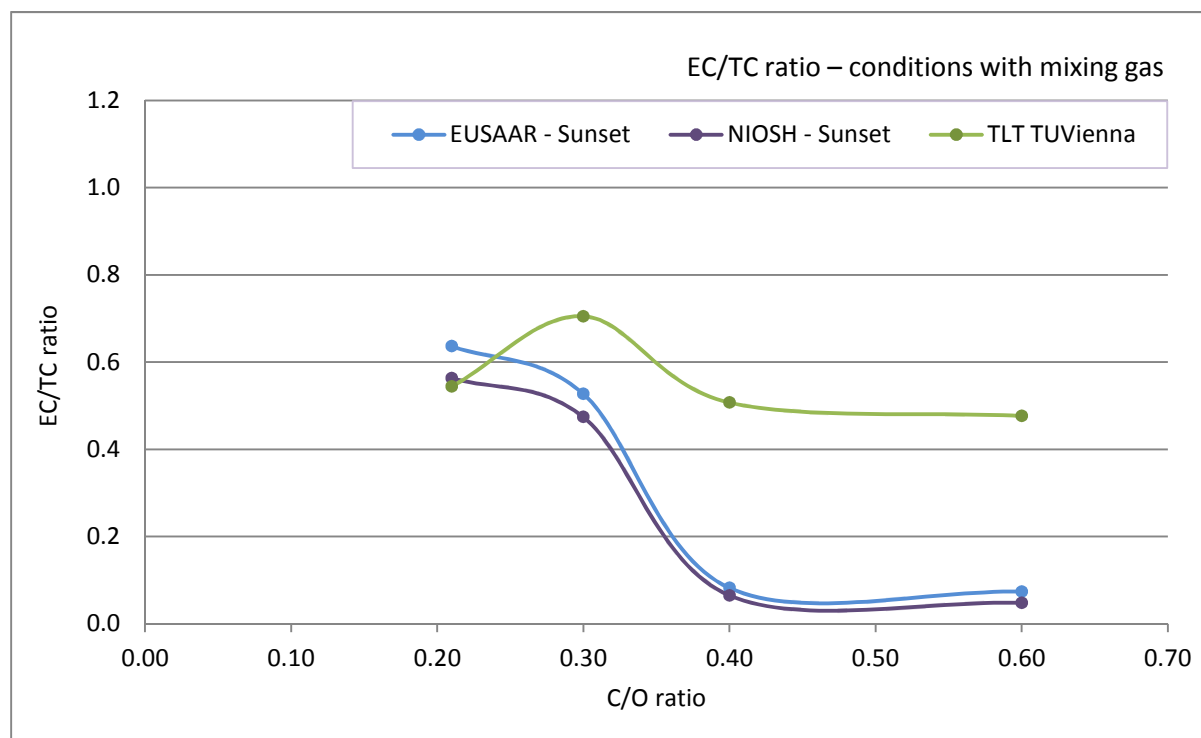


Figure 21: The EC/TC ratio dependence on combustion regime with the mixing gas: the blue line represents the results of the EC/TC ratio measured with the OC-EC dual optical instrument using the EUSAAR 2 temp. protocol, the violet line represents the results of the EC/TC ratio measured with the OC-EC dual optical instrument using NIOSH 5040 temp. protocol, the green line represents the results of the EC/TC ratio measured with TLT.

In **Figure 22**, there are two thermograms of the same filter. On the left (**Figure 22, a**), there is a sample analyzed by the OC-EC dual-optical instrument using the NIOSH 5040 temperature protocol, whereas on the right (**Figure 22, b**) the sample is analyzed by the EUSAAR 2 temperature protocol. The first noticeable difference is in the temperature stages (blue line) and residence time in each stage (**Table 2**). In both temperature protocols, the EC evolves at around 750 °C which is the temperature where also the split point is set.

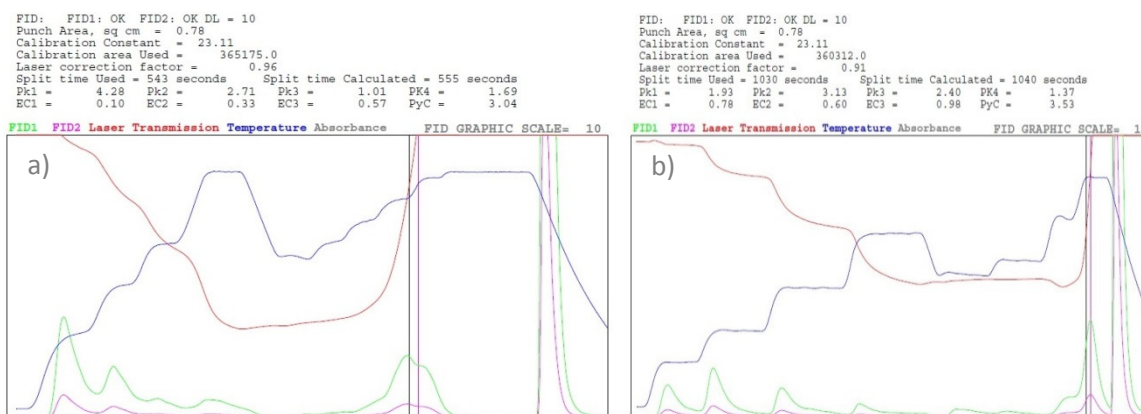


Figure 22: A filter sample analyzed by the OC-EC dual-optical instrument using two different temperature protocols at the C/O ratio of 0.31: a) the NIOSH 5040 temperature protocol, and b) the EUSAAR 2 temperature protocol.

In the thermogram portraying the NIOSH temperature protocol, the majority of OC evolves at the beginning (OC₁ – first peak, see **Figure 4**), and also in He/O₂-mode with the NIOSH protocol figure showing high peak with a shoulder, compared to the EUSAAR thermogram where OC is evolved step by step and most of the EC evolves at the end (before calibration – the last peak).

Due to higher starting temperatures of the NIOSH thermogram (**Figure 22**, a) in the He-mode (310 °C) and He/O₂-mode (600 °C), OC and EC evolve earlier than in the EUSAAR thermogram (**Figure 22**, b). Here, there are lower initial temperatures with longer times (2-times longer and more, see **Table 2**). However, when observing average concentrations of EC and OC, no considerable difference between this two temperature protocols at the CAST samples can be noticed.

In summary, the choice of temperature protocols does not drastically affect the portion of the EC measured with the OC-EC dual-optical instrument. Nevertheless, it is apparent from the graphs (**Figure 19** and **Figure 21**) that the EUSAAR 2 temperature protocol generates a higher proportion of EC than the NIOSH 5040 temperature protocol. In both cases, the trend of decreasing EC/TC ratio with increasing C/O ratio can be observed.

3.2.2. Composition of light absorbing carbonaceous aerosols

The CAST burner was used as a model for combustion of carbonaceous fuels with varying ratio of carbon in fuel and oxygen (C/O ratio), available for combustion. Aethalometer data were compensated with different compensation principles. In **Table 8**, Angstrom exponent values of compensation principles using the Weingartner et al. (2003), Arnott et al. (2005),

and Kirchstetter et al. (2007) principle are presented. This also allows the measuring of absorption coefficient over a large wavelength range, which gives some insight into the physical reasons for the absorption variability and the validity of Angstrom exponent.

Table 8: Angstrom exponent in light of different compensation principles: the Weingartner and Arnott principles are calculated by using the existing formulas (Weingartner et al., 2003 and Arnott et al., 2005), while the Kirchstetter principle is empirical (Kirchstetter et al., 2007).

CAST Conditions		Kirchstetter	Weingartner α (/)	Arnott
C/O ratio	N_2 ($l \cdot m^{-1}$)			
0.21	-	0.91	1.21	1.02
	0.015	1.06	1.55	1.29
0.31	-	1.33	1.79	1.45
	0.015	1.39	1.85	1.65
0.41	-	4.01	3.87	3.50
	0.015	7.02	6.08	5.09
0.60	-	5.06	5.38	3.77
	0.015	5.93	6.30	5.82
0.21	-	1.30	-	-
	0.018	1.43	-	-

A controlled process makes it much easier to observe various principles. The CAST experiment model was definitely one of them. When we look at **Table 8**, we realize that the compensation principles do not differ drastically from one another; with exception of the combustion cycle with the C/O ratio of 0.41 and added mixing gas where α ranges from 5.09 to 7.02. Generally, **Table 8** shows that results of the CAST experiment do not depend on how data are processed. The attention must be put on high α values at C/O ratio of 0.41, where deviations might be more considerable.

In **Figure 23**, a histogram of absorption Angstrom exponent values for the Kirchstetter principle, Weingartner principle, and Arnott compensation principle is shown. The results are presented for all operating conditions (C/O ratio = 0.21, 0.31, 0.41, and 0.60). Operating conditions are divided in two parts: "0.21" is a sample with the C/O ratio of 0.21 with no mixing gas added to combustion process and "0.21 + N₂" is a sample with the C/O ratio of 0.21 and mixing gas. Error bars are standard deviations of average α values calculated from Aethalometer data with 2-minute time base.

Angstrom exponent values of Arnott compensation principle are slightly lower than those of Weingartner principle in all conditions. When comparing the Arnott and Kirchstetter principles, the Arnott principle shows higher α values at a lower C/O ratio and lower α values at a higher C/O ratio.

When comparing the Weingartner and Kirchstetter principles, some variations can be observed at the C/O ratio of 0.41. Higher values of Angstrom exponent calculated by Kirchstetter principle were observed in this operating condition (C/O = 0.41), while in all other operating conditions the Weingartner principle always shows higher values of Angstrom exponent than the Kirchstetter principle. Based on all these results, we decided to use the Weingartner correction for the rest of the discussion.

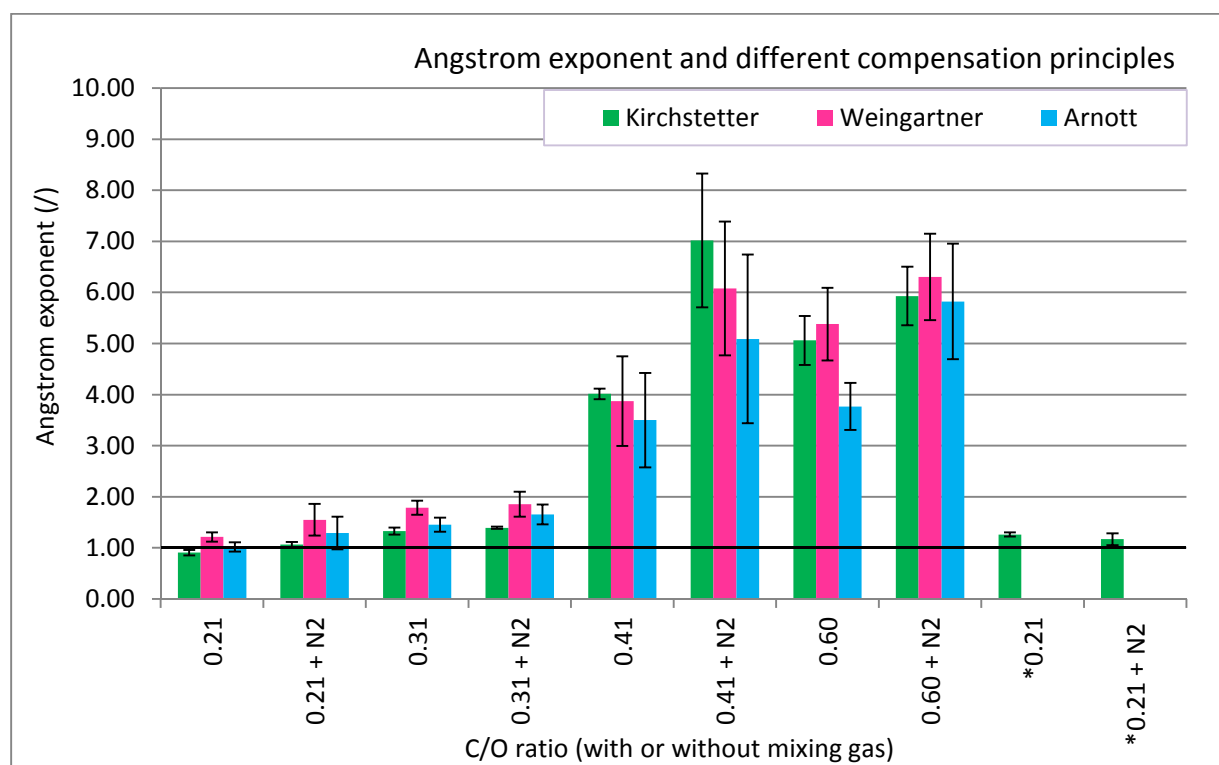


Figure 23: Absorption Angstrom exponents of different compensation principles: the Kirchstetter principle (green), the Weingartner principle (pink), and the Arnott principle (blue) for all operating conditions (C/O ratio = 0.21, 0.31, 0.41, and 0.60) where "0.21" is a sample with the C/O ratio 0.21 without the mixing gas and "0.21 + N₂" is a sample with the C/O ratio of 0.21 with the mixing gas (Error bars are standard deviations). * Repeated condition with the C/O ratio of 0.21.

In the following graph (**Figure 24**), the difference between absorption Angstrom exponents (α) for the conditions with and without the mixing gas using the Weingartner compensation principle is shown.

Angstrom exponent in conditions with the mixing gas is much higher at higher C/O ratios (C/O = 0.41 and 0.60). The added mixing gas (N₂) could be a logical explanation for the high absorption Angstrom exponent due to absorption of nitrogen compounds at low wavelengths from 410 nm to 600 nm (U.S. Pat. No. 3,970,430 issued on Jul. 20, 1976, to John R. Reader, Jr. et al.).

In **Figure 24**, the behavior of black carbon measured with Aethalometer is also shown. Aethalometer raw data were compensated with the Weingartner principle.

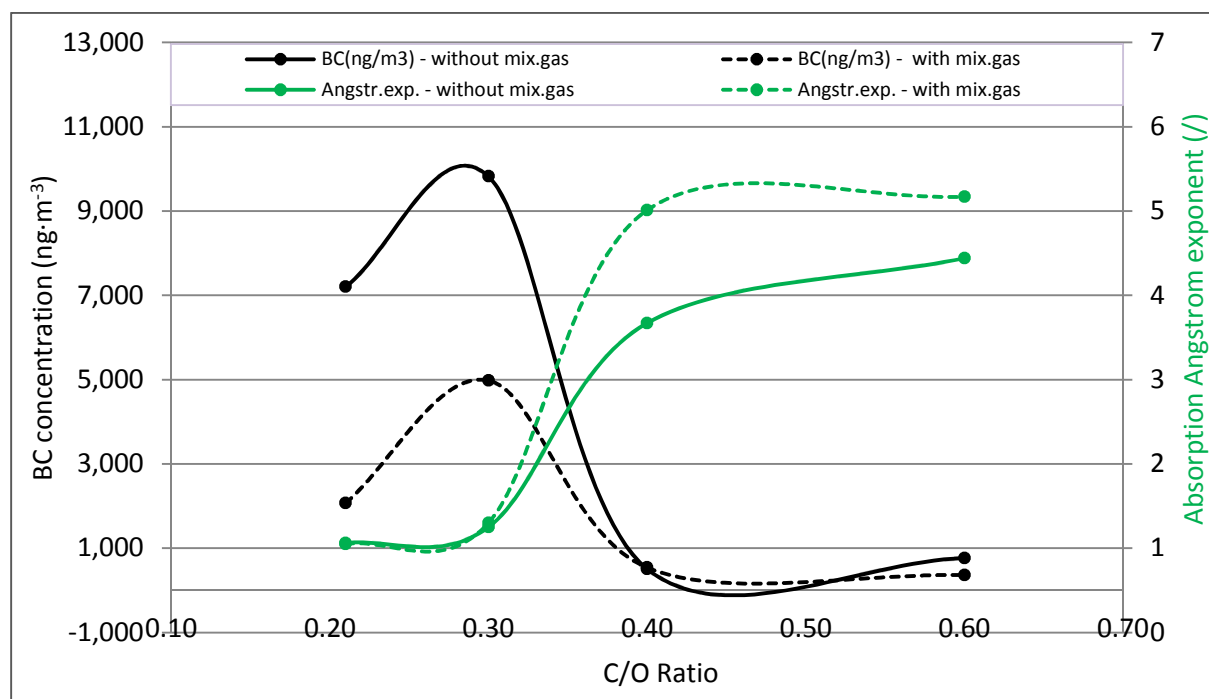


Figure 24: Black carbon concentration measured with Aethalometer and absorption Angstrom exponent dependence of the C/O ratio in operating conditions of combustion with (solid line) and without (dotted line) the added mixing gas (N_2).

With the increase of the C/O ratio, the absorption Angstrom exponent increased up to 5 and more as well. This situation is typical for conditions with the decrease of oxygen and subsequent incomplete combustion.

The concentration of BC, as opposed to the Angstrom exponent, decreases with the increasing C/O ratio; with higher C/O ratios less BC or EC and more organic carbon is produced, which is reflected in the high Angstrom exponent.

3.2.3. Analysis made by two-component Aethalometer model (absorption vs. wavelength) to determine two carbonaceous components: BC and BrC

Several studies pointed out that BrC could significantly absorb light at around 400–500 nm (e.g. Kirchstetter et al., 2004; Sandradewi et al., 2008); therefore Aethalometer data measured at 470 nm wavelength were used for the analysis, although data were also collected at 370 nm.

An Aethalometer model developed by Sandradewi et al. (2008) was implemented. Several studies use the following Angstrom exponent $\alpha_{BC} = 1.00 \pm 0.20$ (Kirchstetter et al., 2004; Schnaiter et al., 2003, 2005). In this model, we assumed the Angstrom exponent of pure BC as $\alpha_{BC} = 1.00$, while $\alpha_{BrC} = 5.4$ (**Figure 25**) and 6.2 (**Figure 26**) were determined from the experiment data, assuming that in the experiment with the C/O = 0.60, only BrC was generated (see **Figure 14**). Values for $b_{abs,BrC}(470 \text{ nm})$, $b_{abs,BrC}(880 \text{ nm})$, $b_{abs,BC}(470 \text{ nm})$, and $b_{abs,BC}(880 \text{ nm})$ were computed with the following equations:

$$b_{abs,BC}(470 \text{ nm}) = \left(\frac{\lambda_1}{\lambda_2}\right)^{-\alpha_{BC}} \cdot b_{abs,BC}(880 \text{ nm}), \quad (24)$$

$$b_{abs,BrC}(470 \text{ nm}) = \left(\frac{\lambda_1}{\lambda_2}\right)^{-\alpha_{BrC}} b_{abs,BrC}(880 \text{ nm}), \quad (25)$$

using experiment data of α_{BrC} .

As already mentioned, it is assumed that the combustion process at the C/O ratio of 0.60 produced pure BrC (Equation 1), whereas the combustion process at the C/O ratio produced pure BC (Equation 2). Considering that, our calculation can be simplified in the following way:

$$b_{100\%BrC}(470) = b_{C/O=0.6, BrC}(470\text{nm}) + b_{C/O=0.6, BC}(470\text{nm}) \quad (26)$$

$$b_{100\%BC}(880) = b_{C/O=0.21, BrC}(880\text{nm}) + b_{C/O=0.21, BC}(880\text{nm}) \quad (27)$$

Thus the following can be deduced: $b_{100\%BrC}(470\text{nm}) = b_{C/O=0.6, BrC}(470\text{nm})$ and $b_{100\%BC}(880\text{nm}) = b_{C/O=0.21, BC}(880\text{nm})$. Calculations given in equation 3 and 4 were also made for the rest of the wavelengths. b is a mark for absorption coefficients.

In **Figure 26**, the same procedure was followed as in **Figure 25**, the only difference being the operation conditions. In **Figure 26**, data with the mixing gas were used, while **Figure 25** features data gathered when no mixing gas was present. The absorption Angstrom exponent value of data gathered in the conditions with mixing gas and the C/O ratio of 0.60 is $\alpha_{BrC} = 6.30$; this is almost 1 unit higher than in the operation conditions without the mixing gas (C/O = 0.60).

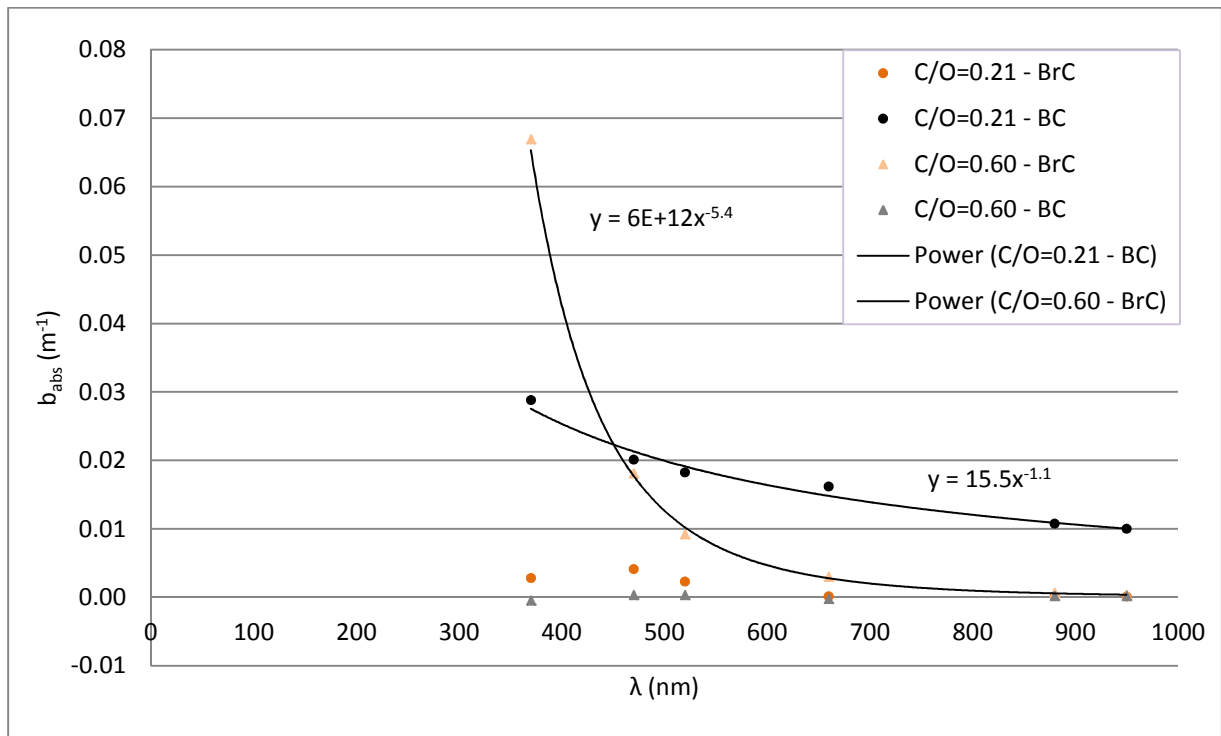


Figure 25: Dependence of absorption coefficient on wavelength: (o) $b_{abs,BrC}$ and $b_{abs,BC}$ at C/O ratio = 0.21, and (Δ) $b_{abs,BrC}$ and $b_{abs,BC}$ at C/O ratio = 0.60. ($\alpha_{BrC} = 5.38$, without the mixing gas (N_2)).

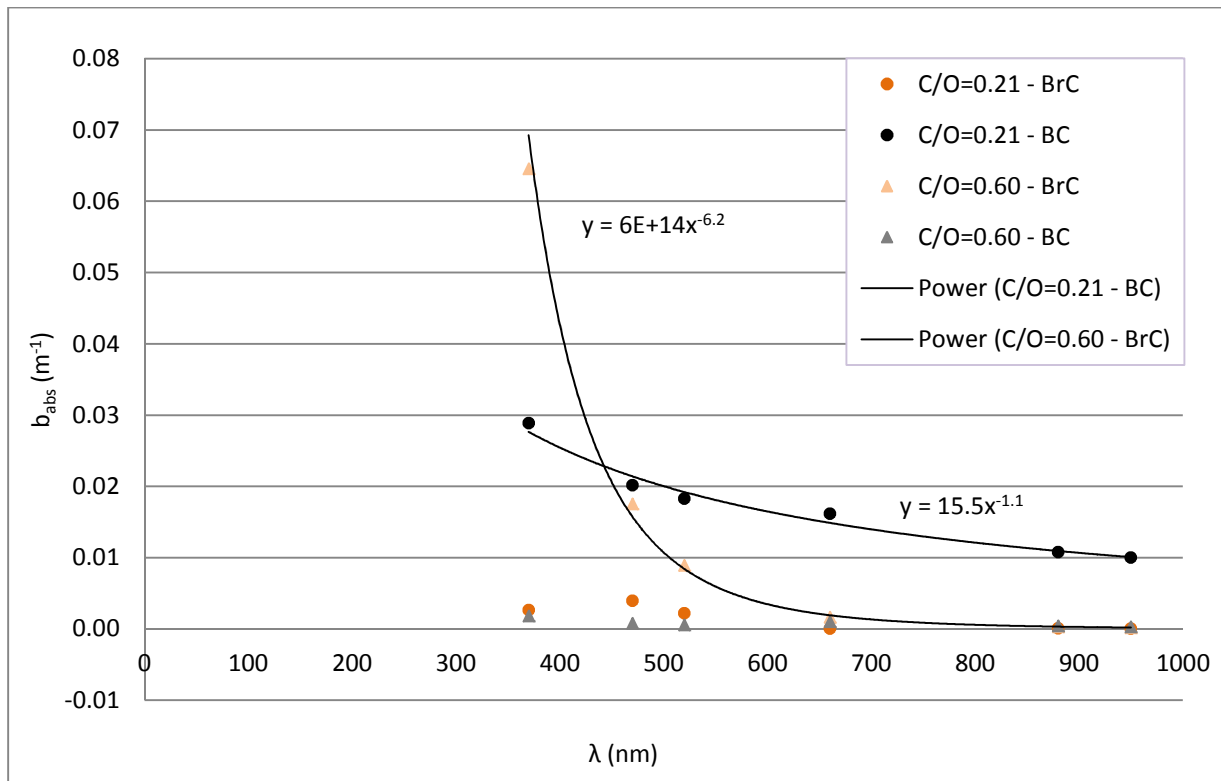


Figure 26: Dependence of absorption coefficient on wavelength: (o) $b_{abs,BrC}$ and $b_{abs,BC}$ at C/O ratio = 0.21, and (Δ) $b_{abs,BrC}$ and $b_{abs,BC}$ at C/O ratio = 0.60. ($\alpha_{BrC} = 6.20$, with the mixing gas (N_2)).

When observing **Figure 25** and **Figure 26**, we can see that the input of the mixing gas in the combustion process at the C/O ratio of 0.60 does not affect $b_{\text{abs,BC}}$, but it has a big influence on the absorption coefficient of BrC. Results can be seen as an increased slope ($\Delta - b_{\text{abs, BrC}}$, C/O = 0.60–BrC).

In the study, the two-component model of the Aethalometer was employed to identify BrC and BC contributions to absorption. High α -values, up to 6, were observed in conditions with the C/O ratio of 0.60, while in measurements with the C/O ratio of 0.21 α values between 1.2 and 1.8 were noticed. Contributions of BC and BrC for various values of the C/O ratio were determined, and two extreme examples, C/O = 0.21 and 0.60, are shown in **Figure 25**. It can be seen that for combustion conditions with high C/O the BrC absorption dominates and can even surpass the BC absorption at low C/O conditions.

In **Figure 27** and **Figure 28**, an overview of the absorption coefficient through the wavelengths is shown. In the histogram for brown carbon, there are high absorption values of BrC at low wavelengths (370 nm, 470 nm) and high C/O ratio (C/O = 0.41 and 0.60). It was assumed that at the C/O ratios of 0.41 and 0.60 mostly BrC was evolved, while the portion of BC was small. At high wavelengths (880 nm, 950 nm), the contribution of BrC is negligible.

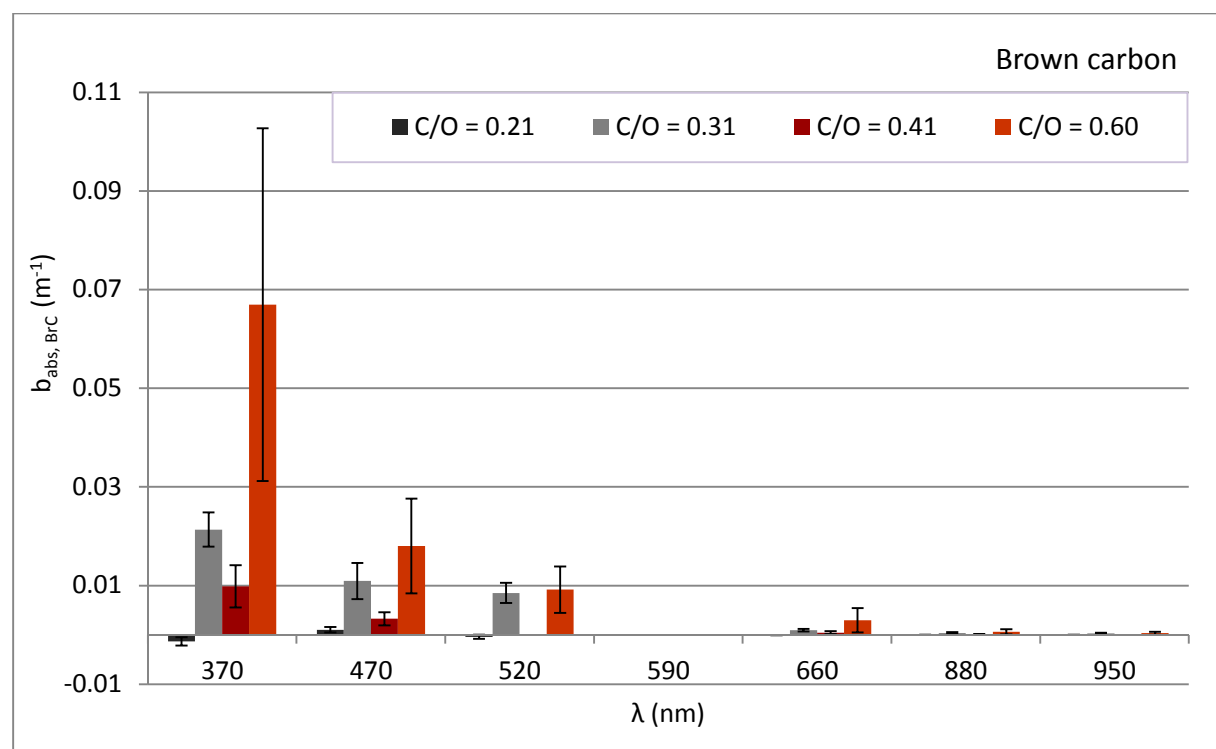


Figure 27: Histogram of BrC absorption coefficient ($b_{\text{abs, BrC}}$) dependence on various wavelengths (λ) and operation conditions (C/O ratio = 0.21, 0.31, 0.41 and 0.60). (Error bars are standard deviations).

It is known that lack of oxygen in combustion leads to formation of brown carbon and other organic matter. The applied source apportionment model enables a good result interpretation of combustion processes under various combustion conditions. From the results, important information relating to brown carbon can be deduced. The main source of brown carbon is biomass combustion; however, quite a lot of brown carbon may apparently also be emitted from fuel (propane) combustion at very low levels of oxygen present in the process.

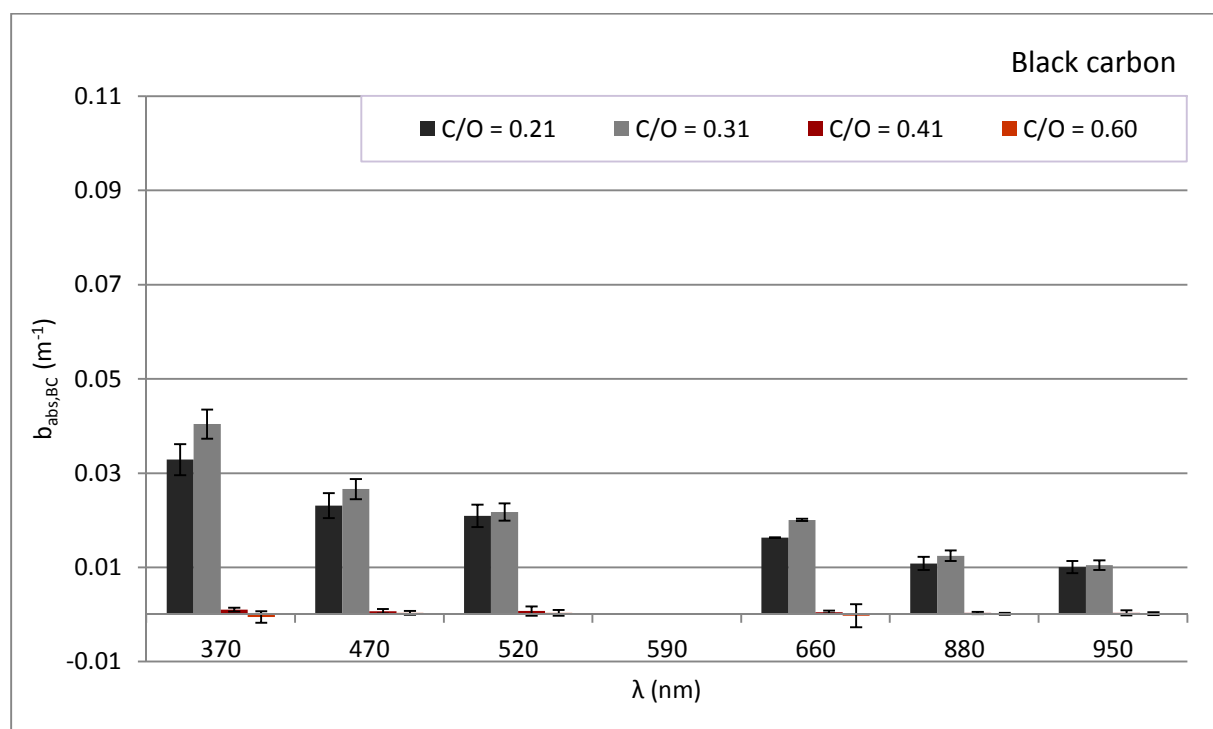


Figure 28: Histogram of BC absorption coefficient ($b_{obs, BC}$) dependence on various wavelengths (λ) and operation conditions (C/O ratio = 0.21, 0.31, 0.41 and 0.60). (Error bars are standard deviations).

In black carbon histogram, the values of BC are the highest at the C/O ratios of 0.21 and 0.31 (**Figure 28**). The amount of BC at short wavelengths is very high, which means that a portion of BC could be brown carbon.

To sum up, at combustion conditions with high C/O ratio, absorption from BrC dominates and can even surpass the BC absorption at low C/O conditions. Biomass combustion in simple stoves, open fireplaces and forest fires also takes place at unfavorable C/O values. With our model, we show that the absorption of BrC in such combustion processes needs to be taken into account when studying climate effects of biomass combustion.

CHAPTER 4

The wood-burning experiment

Contents

4.1. Emissions from household heating	55
4.1.1. Wood-burning sampling system.....	55
4.1.2. Combustion chamber – a wood-burning stove	59
4.1.1. Combustion procedures	60
4.2. Type of wood	63
4.3. Results	64
4.3.1. Organic carbon, elemental carbon, black carbon and brown carbon concentration dependence on various types of wood	67
4.3.2. Determination of the absorption Angstrom exponent.....	78
4.3.3. Anhydrosugar analysis – tracers of wood-burning emissions.....	82

Wood is a recommended energy source, because it is a renewable source of fuel and it is relatively easily obtained. Burning wood is very common in residential properties as well as in the cities, where wood-burning stoves have become popular household additions.

With this in mind, a wood-burning experiment was set up to observe combustion processes using different types of wood stoves (wood stove and self-igniting pellet stove) and different types of wood (softwood, hardwood and pellets). The carbonaceous material evolved during the wood-burning process of different wood types was analyzed using off-line methods to quantify its amount. On-line measurements were used to calculate the Angstrom exponent as an indicator for combustion efficiency and detection of specific carbonaceous compounds, such as brown carbon. In the next chapter, results of controlled combustion experiment will be compared to ambient measurements. However, the main goal of this chapter is to quantify all the carbonaceous species and anhydrosugar tracers in order to raise the awareness of wood-burning emissions and the importance of using an appropriate wood stove.

4.1. Emissions from household heating

The combustion of wood leads to emissions of carbon monoxides (CO), nitrogen oxides (NO_x) and a very heterogeneous mixture of particulate matter. The latter consist of a high amount of black carbon (BC), and other species of light absorbing carbonaceous aerosols. In addition, organic compounds, such as polycyclic aromatic hydrocarbons (PAH), are present in the emitted particulate matter (Hoffer et al., 2006, Kochbach et al., 2006). These emissions are brought in the atmosphere. In addition, secondary aerosols are formed from the gaseous emissions in the atmosphere and aerosols are aged – humic-like substances (HULIS) are generated.



Figure 29: Household heating.

The efficiency of biomass combustion is very variable. Combustion at low temperature can lead to extremely high emissions of PM including LACA.

4.1.1. Wood-burning sampling system

The measurements regarding the emitted particles forming when burning wood were carried out at a test stand at the Vienna University of Technology. The sampling port was positioned 3 m above the burning chamber (**Figure 30**). Emission samples were taken from the center of the chimney using a nozzle connected to a dilution apparatus.



Figure 30: Chimney of the wood-burning laboratory experiment.

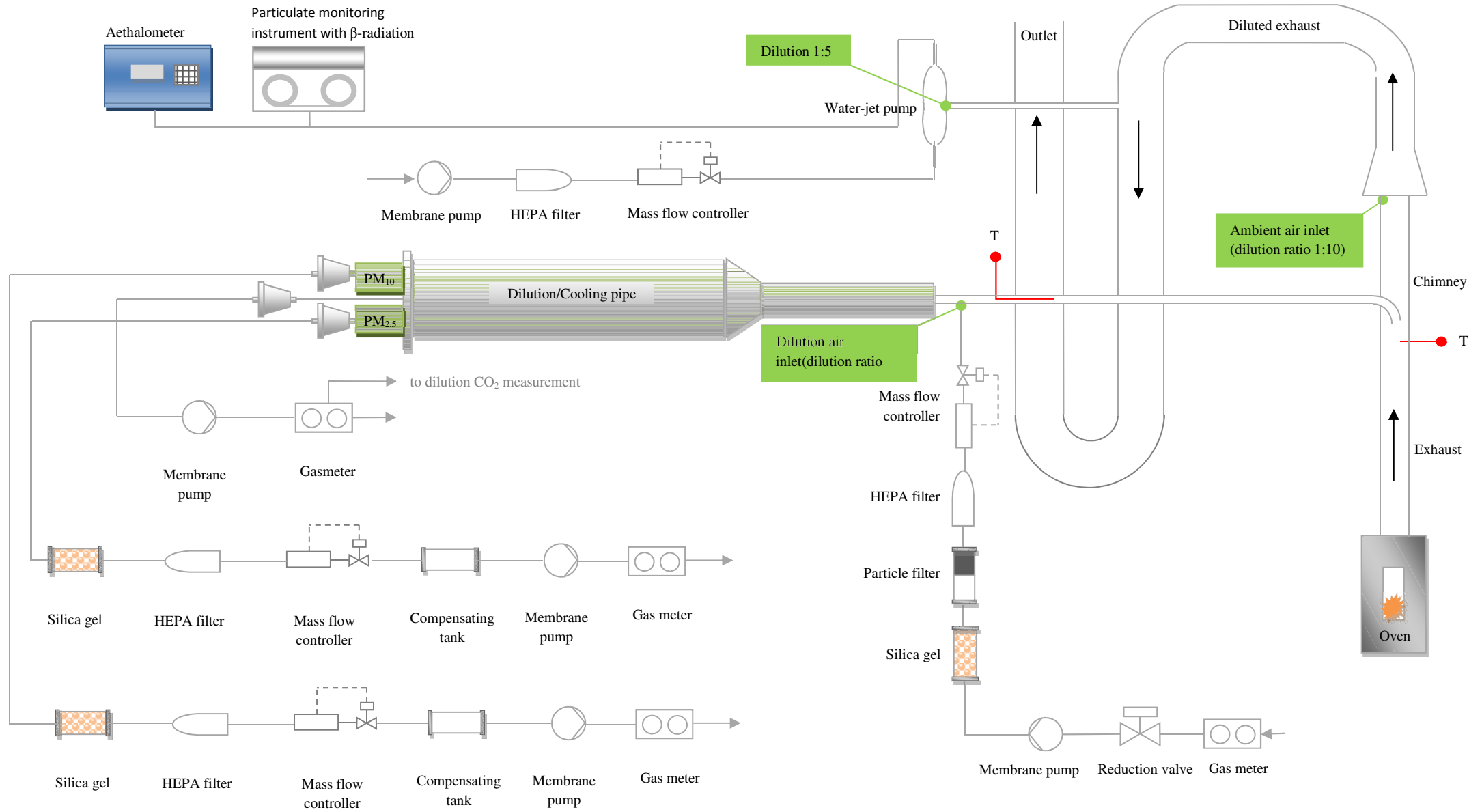
In the dilution apparatus, the exhaust gas was diluted (dilution 1:10) with clean air, which had been dried and purified by passage through activated silica, activated carbon and at the end through a HEPA filter, shown in **Scheme 2**. The emission gases were cooled down sufficiently in the dilution/cooling pipe (see also **Figure 31**) to let the organic compounds condense (Schmidl et al., 2008). After the dilution and cooling step, the exhaust gas was divided into two streams passing through Digital sampling heads for separation of the PM₁₀ and PM_{2.5} fractions, respectively. Both particle separators (PM₁₀ or PM_{2.5}) with tree parallel filter holders were subsequently installed to obtain enough material. Additionally, there was also one independent filter holder which measured total suspended particles (TSP) directly from the dilution/cooling pipe. All filter holders were loaded with *quartz filters* (47 mm diameter, Pallflex-Tissuequartz 2500QAT-UP, Pall Life Science) which were used for determination of carbon species, anhydrosugars and total particulate mass. The volume flows of the sampling lines were regulated by needle valves being placed behind the filter holders (Schmidl et al., 2008, Kistler et al., 2012). Absolute volumes of sampled air and dilution air were measured with gas meters.



Figure 31: Dilution/cooling pipe with two-particle separators (PM_{10} and $PM_{2.5}$) and filter holders.

On a parallel exhaust line, the on-line instruments were installed, as shown in **Scheme 2**. An Aethalometer (AE31-ER, Magee Scientific Corp.) was used to detect black carbon in the wood-burning exhaust; while a β -Attenuation Particulate Monitoring Instrument FH 621-R (Thermo ESM Andersen, ESM Andersen Instruments GmbH) determined the mass concentration. At this point, two dilution steps were already in effect. The first one (dilution ratio 1:10) was carried out at the end of the chimney, when the exhaust gases got diluted with ambient air. The second dilution step took place when part of the diluted exhaust was extracted. Here, the dilution ratio of 1:5 for on-line measurements was accomplished by installing a water-jet pump, using zero air as a main air flow. In overall, the exhaust air used for on-line measurements was diluted 1:50 and for off-line measurements (filters) 1:10. The whole set-up is graphically represented in **Scheme 2**.

Scheme 2: Wood-burning experiment system.



4.1.2. Combustion chamber – a wood-burning stove

Typical small scale stoves for household heating in Austrian and Slovenian regions were chosen for the experiment, since previous works (McDonald et al., 2000) pointed out that factors, like the type of stove and type of wood used, can have an important influence on particle emissions.

Wood stove (Wodtke)

A “Vision 7” KK 65 H model of a wood-burning stove was employed in the laboratory experiment for burning woods. These types of stoves are used mainly for heating homes during the winter period. Dimensions of the combustion chamber are described in **Figure 32**. The ambient air needed for combustion enters at the bottom of the chamber through a grating.



Figure 32: Wodtke wood stove and its dimensions (<http://www.wodtke.si/toplozracni-polena-vision7.html#ime>).

The heat output of the stove is 7.0 kW, if the input is 2.23 kg of wood, and its room heating capacity is 56–144 m². Wood and briquettes can be used for heating.

Pellets stove (Rika pellets stove MEMO)

The second test stove for pellet burning was Rika Memo stove (Rika Company, **Figure 33**). It is a self-igniting pellet stove with internal pellet storage.

The dimensions of the stove are 978 x 495 x 544 mm and its room heating capacity is 50–240 m². The heat output of this stove is 2.4–9 kW.



Figure 33: Rika pellet stove MEMO (www.rika.at).

Pellets were supplied to the combustion chamber using an “auger screw”. Combustion air supply was adjusted for the selected thermal output by a fan situated in the flue gas stream. Air entered through holes under the fuel bed. Both fuel (pellets) and fan speed were controlled automatically, only the percentage of the power output (30–100%) was set by hand (Kistler et al., 2012).

Cycles of pellet burning lasted for about 120 min. Ignition took place with an electrical resistance heater and air supply from a blower. The ignition phase was not included in the tests with pellets.

4.1.1. Combustion procedures

The procedure of wood combustion (beech and spruce)

In our case, the combustion of wood took place in two phases (**Figure 34**). The first phase was named phase 1 and the second phase was named phase 2. At phase 1, we loaded around 2.23 kg of wood (beech or spruce) into the cold stove according to the manufacturer's instructions. Wood logs were arranged one to another and one lighter (Wodtke fire cube)

was placed on the top of the wood load to start the fire. We turned on the entire sampling system a few seconds before we started the fire. The burning lasted for about one hour (with the power of 7 kW), and when the emitted CO₂ decreased below 3% the measurement system was stopped.

A new load of wood was prepared immediately, again around 2.23 kg, and put into the hot stove to start the second stage of burning (phase 2). With the start of the phase 2 and the fire ignition, all instruments were turned on. The wood again burned for about 1 hour (with the power of 7 kW) until the emitted CO₂ decreased below 3%.

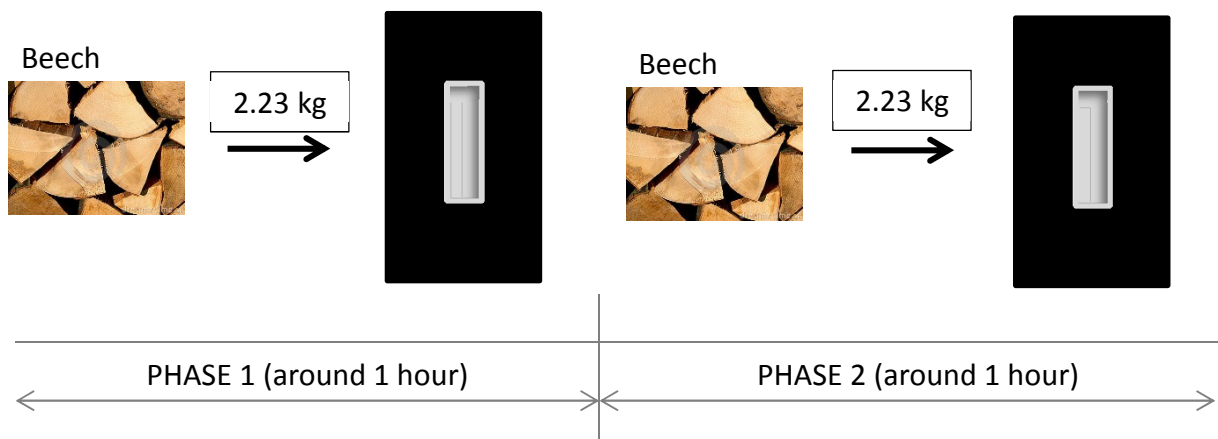


Figure 34: Description of the combustion procedure in wood-burning tests: the phase 1 and phase 2.

The description of the two burning phases is important for on-line analyses (Aethalometer measurements), at which the Angstrom exponent was observed at different burning phases: For filter sampling, the distinction between the phases is not possible, because the same filter sampling comprised phase 1 and phase 2.

The procedure of pellet combustion

In **Figure 35**, the procedure of pellet combustion is presented. Before the experiment, a 6-kg load of pellets was placed in the storage tank. The stove is a self-igniting burner and we only had to set the percentage of the power output (30–100%) to determine the intake of the pellets by the stove.

After the experiment, the remaining material was removed from the storage tank with a vacuum cleaner. Approximately 3 kg of pellets remained in the tank.

Three experiments were performed using the pellet stove. Each cycle of pellet burning consisted of a full load run lasting for about 120 min. The first experiment featured a 30% stove capacity, the second a 100% stove capacity, and the last a 30% stove capacity for 60 min and a 100% capacity for 60 min.

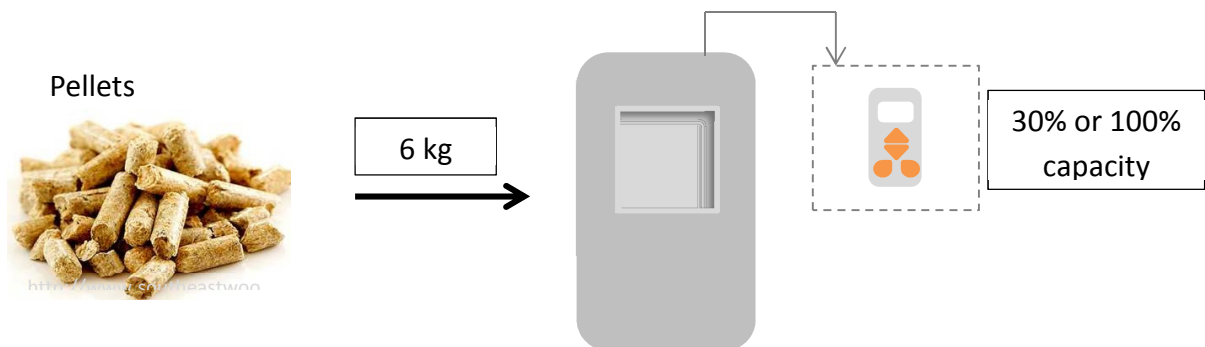


Figure 35: Description of the combustion procedure of pellet-burning.

4.2. Type of wood

Type of wood (hardwood or softwood) chosen for combustion processes is important for its production of heat and energy efficiency. Wood combustion leads to emissions of gases and aerosolized particulate matter (PM) and has a negative influence on the environment. Jordan and Seen (2005) showed clearly that in combustion processes the type of wood is even more important than the given air flow income.

For our wood-burning experiment, we took two of the most frequently used wood types for household heating in Austrian and Slovenian regions: beech (hardwood) and spruce (softwood); and pellets as an example of an alternative (**Table 9**).

Table 9: Stock average moisture content and number of tests with different wood types (* tests containing spruce with 16% moisture – spruce IV).

Wood type	Scientific name	Moisture content % w/w	No. of tests
Beech	<i>Fagus sylvatica</i>	8	4
Spruce	<i>Picea abies</i>	8 (16*)	4
Pellets	100% softwood	-	2

All wood types were burned as around 30–50 cm long split logs with a 10 cm diameter.

In our experiment, two types of spruce were used. Their genus was in fact the same, but their moisture was different. The first three tests featured wood with 8% moisture, whereas the moisture of the wood in the last one was 16%.

The experiment involving pellet burning was conducted using the FireStixx Premium Pellets (www.firestixx.com – 05/02/13). FireStixx Premium pellets are produced from 100% softwood. Pellets can be produced from peat, wood waste and agricultural waste. The process of pellet production is divided into two stages, the first being the preparation of the wood raw materials (drying and disintegration), and the second granulating.

4.3. Results

The aim of the experiment was to observe the values of the Angstrom exponent which was calculated with the help of Aethalometer data. Aethalometer data were post-processed with the Weingartner principle to get the Angstrom exponent values for different tests. The experiment tried to answer questions regarding the wood types and the effect they have on the values of the Angstrom exponent, the relevance of softwood or hardwood burning, and the influence of the phase 1 or phase 2 on the Angstrom exponent, which are both described in the section about the combustion procedure. Moreover, the influence of the pellet stove type (wood vs. pellet stove) and pellet stove capacity on the values of the Angstrom exponent was also examined.

The particles were sampled with filters, Aethalometer (AE31-ER) and β -Attenuation Particulate Monitoring instrument (Model FH 62I-R). The exhaust air was diluted 1:10 for collecting aerosols on quartz filters, and 1:50 for on-line measurements. After analyzing the filters and raw data of on-line instruments, the observation of PM_{10} and $PM_{2.5}$ concentrations aroused our interest, accompanied with the question about the effect various wood types have on air pollution and the influence of different temperature protocols (NIOSH 5040 and EUSAAR 2). Attention was also put on anhydrosugars that are known as tracers of wood smoke in the air pollution. Focus was put on their proportion and incidence in the wood-burning exhaust.

Filters were prepared for analysis by being punched in 8 or 10 mm diameter, depending on the needs of the analyzers. Filter "beech III" for PM_{10} was lost so the results of its analyses are not presented in the graphs. The measurement conditions were different for some tests. Tests involving beech and spruce burning were divided in the phase 1 and phase 2 as mentioned before, while tests of pellet burning had a different combustion efficiency (30% or 100%) of the stove (30% or 100%).

Below in **Table 10**, the results of on-line and off-line measurements for each test and for all analyses are presented.

All flow measurements refer to standard temperature and pressure (STP) (0 °C and 1013 mbar). No corrections for O_2 content and relative humidity were carried out.

Table 10: PM_{10} , $PM_{2.5}$ and TSP results of on-line and off-line analyses for all types of wood (beech, spruce, pellets) and burning stages. Aethalometer data are presented in a slightly different way in the table; (p1) are average BC concentrations in phase 1, and (p2) are average BC concentrations in phase 2.

Type of wood	Particle size	Δm (mg)	Sampling time (min)	ΔV (m^3)	Mass-flow controller Flow (L(STP)/min)	Total V (L(STP))	SUNSET NIOSH EC/TC %	OC (mg/m^3)	EC (mg/m^3)	TC (mg)	SUNSET EUSAAR2 EC/TC %	OC (mg/m^3)	EC (mg/m^3)	TC (mg)	TLT EC/TC (%)	BC-IS (mg/m^3)	BrC (mg/m^3)	BC (mg/m^3)	Ång. exp. α_{abs} (/)	Levogl. (mg)	Mann. (mg)	Galact. (mg)
beech I	PM10	6.61	114	2.06	14.95	1775.7	0.447	17.97	14.55	6.69	0.284	23.06	9.14	66.27	70.3	0.42	2.38		0.90	0.032	0.002	0.001
	PM2.5	6.26		1.84	14.95	1613.8	0.576	11.71	15.88	5.08	0.490	14.21	13.65	51.26	78.3	0.54	1.69		2.04	0.027	0.002	
	TSP	5.79		0.51			0.558				0.281				78.1			5.917 (p1), 0.058 (p2)	0.020	0.001		
beech II	PM10	8.91	113	1.80	14.95	1565.8	0.000	37.82	0.00	6.81	0.211	31.38	8.41	71.62	78.8	0.59	1.87		1.60		0.013	0.006
	PM2.5	7.47		1.76	14.95	1561.6	0.490	15.35	14.75	5.31	0.321	22.21	10.52	57.72	75.9	0.62	1.25		0.00	0.118	0.000	0.005
	TSP	7.67		0.47			0.428				0.453				78.0			3.207 (p1), 0.000 (p2)	0.122	0.011	0.005	
beech III	PM10		109	1.86	14.79	1600.0	-	-	-	-	-	-	-	-	-	-	-		1.52			
	PM2.5	1.83		1.82	14.79	1594.5	0.646	2.52	4.60	1.30	0.622	2.70	4.43	13.00	94.8	0.68	0.56		1.38		0.001	0.001
	TSP	1.82		0.53			0.640				0.562				93.5			6.157 (p1), 1.778 (p2)	0.024	0.002	0.001	
beech IV	PM10	3.17	130	2.23	14.86	1923.8	0.495	6.07	5.96	2.69	0.315	8.63	3.97	28.12	93.7	0.63	0.63		1.28	0.068	0.003	0.002
	PM2.5	2.82		2.18	14.86	1917.7	0.625	4.05	6.73	2.35	0.345	7.23	3.81	24.10	93.2	0.68	0.49		1.41	0.057	0.002	0.002
	TSP	2.72		0.63			0.638				0.305				92.7			14.168 (p1), 3.690 (p2)	0.056	0.002	0.001	
spruce I	PM10	10.98	145	2.50	14.88	2145.7	0.205	27.72	7.13	8.72	0.088	32.04	3.08	87.87	71.0	0.33	2.06	21.561 (p1)	1.51		0.145	0.034
	PM2.5	9.11		2.45	14.88	2139.6	0.247	20.75	6.81	6.77	0.109	25.95	3.18	71.52	70.5	0.36	1.74	4.179 (p2)	1.27	0.314	0.125	0.029
	TSP	9.78		0.71			0.207				0.080				73.9				0.308	0.122	0.029	
spruce II	PM10	3.93	141	2.42	14.68	2060.2	0.258	9.87	3.42	3.22	0.148	10.84	1.89	30.80	74.8	0.50	0.84	4.401 (p1)	2.23	0.118	0.042	0.009
	PM2.5	3.21		2.38	14.68	2054.1	0.238	8.16	2.54	2.55	0.198	8.89	2.20	26.38	77.0	0.64	0.97	1.345 (p2)	1.19	0.101	0.035	0.008
	TSP	3.50		0.69			0.274				0.183				76.6				0.100	0.035	0.008	
spruce III	PM10	3.77	114	2.05	14.83	1754.7	0.592	6.36	9.22	3.19	0.606	6.49	9.96	33.69	93.1	0.99	0.33	3.027 (p1)	1.99	0.098	0.031	0.003
	PM2.5	3.02		2.00	14.83	1749.1	0.676	3.95	8.23	2.44	0.652	4.53	8.48	26.04	92.7	0.91	0.68	6.200 (p2)	1.21	0.074	0.024	0.003
	TSP	3.78		0.57			0.600				0.558				93.4				0.085	0.027	0.003	

Type of wood	Particle size	Δm (mg)	Sampling time (min)	ΔV (m ³)	Mass-flow controller Flow (L(STP)/min)	Total V (L(STP))	SUNSET NIOSH EC/TC %	OC (mg/m ³)	EC (mg/m ³)	TC (mg)	SUNSET EUSAAR2 EC/TC %	OC (mg/m ³)	EC (mg/m ³)	TC (mg)	TLT EC/TC (%)	BC-IS (mg/m ³)	BrC (mg/m ³)	BC (mg/m ³)	α_{abs} exp. (/)	Levogl. (mg)	Mann. (mg)	Galact. (mg)	
spruce IV	PM10	3.96	132	2.28	14.72	1950.3	0.312	7.74	3.50	2.57	0.287	8.73	3.51	27.95	81.4	0.58	0.66	15.173 (p1)	1.04	0.084	0.039	0.007	
	PM2.5	4.07		2.23		14.72	1944.0	0.257	10.30	3.56	3.09	0.214	12.50	3.41	35.50	77.6	0.51	0.85	0.674 (p2)	1.69	0.112	0.048	0.008
	TSP	4.88		0.78					0.269				0.404				77.4					0.140	0.062
pellets I	PM10	1.55	95	3.24	14.95		0.731	0.60	1.63	0.72	0.775	0.51	1.75	7.32	94.9	0.43	0.07	3.673 (p1)	1.06	0.004	0.001	0.000	
	PM2.5	0.87		3.18		14.95		0.669	0.53	1.08	0.51	0.690	0.48	1.06	4.90	91.8	0.42	0.08		0.00	0.003	0.001	
	TSP	0.94		0.93					0.705				0.759				95.3					0.003	0.001
pellets II	PM10		120	2.10	15.15	1838.1	0.782	0.83	2.99	0.80	0.757	0.94	2.93	8.15	96.2	0.71	0.07		0.00	0.008	0.004	0.001	
	PM2.5			2.06		15.15	1832.1	0.768	0.72	2.38	0.64	0.772	0.72	2.42	6.47		0.79	0.14		0.00	0.007	0.003	0.001
	TSP			0.59					0.770				0.785									0.007	0.003
pellets III	PM10		123	2.09	14.95	1804.6	0.542	0.51	0.61	0.23	0.619	0.41	0.66	2.23		0.35	0.14		0.00	0.003	0.001		
	PM2.5			2.04		14.95	1798.9	0.526	0.45	0.50	0.19	0.600	0.35	0.52	1.77		0.33	0.18		0.00	0.002	0.001	
	TSP			0.60					0.550				0.586									0.003	0.001

4.3.1. Organic carbon, elemental carbon, black carbon and brown carbon concentration dependence on various types of wood

In **Figure 36** and **Figure 38**, average concentrations of EC and BC determined with various methods are presented for various types of wood. Results of thermal-optical methods are shown for both temperature protocols (NIOSH 5040 and EUSAAR 2). IS-BC refers to the BC concentration measured with the integrating sphere, while Aeth-BC is the BC concentration measured with the Aethalometer.

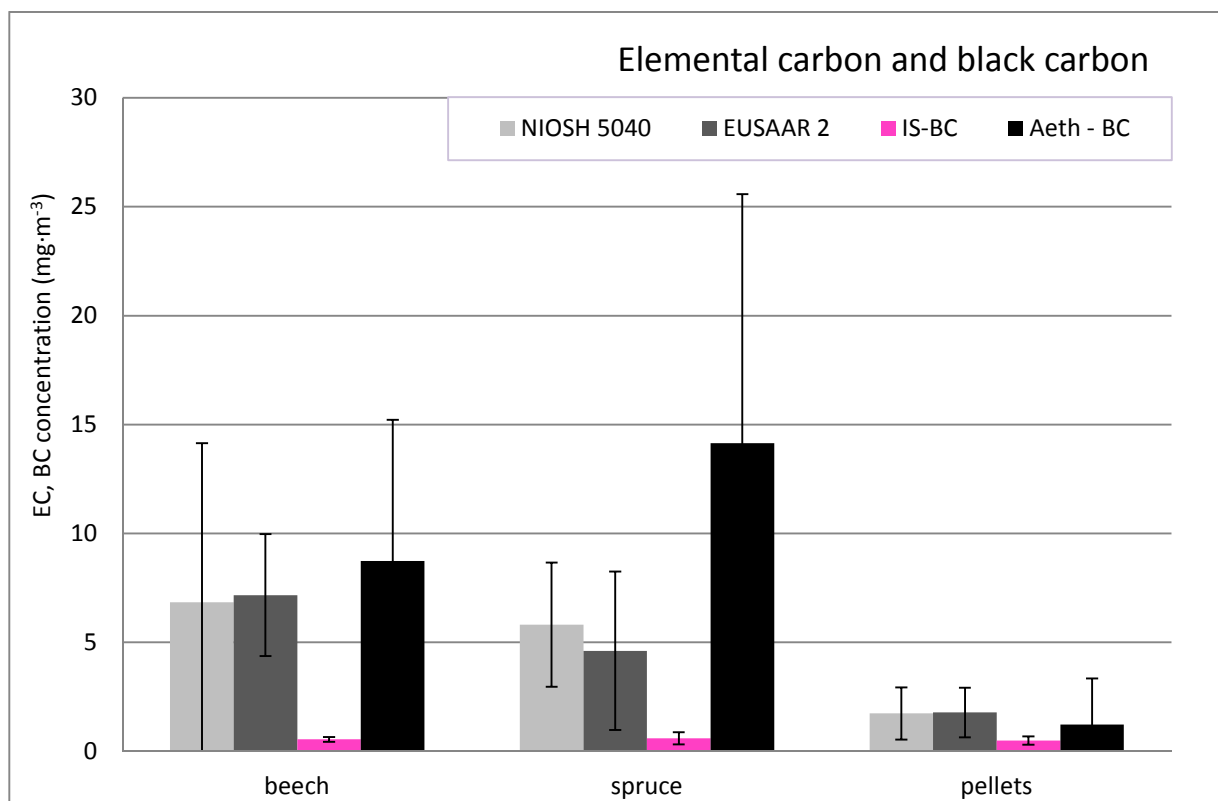


Figure 36: Average PM_{10} values of EC concentration for different types of wood that were measured with the OC-EC dual-optical instrument using NIOSH 5040 (light grey) and EUSAAR 2 (grey) temperature protocols. Average values of BC concentration using optical methods: Integrating sphere (IS-BC) and TSP values of Aethalometer (Aeth-BC). Error bars reflect the standard deviations of the variations occurring in four experiments conducted for beech and spruce and the three experiments involving pellets.

The average EC concentrations (PM_{10}) in the above graph (**Figure 36**) show that no significant difference in results was obtained during the analyses of beech and pellet burning using different temperature protocols (NIOSH 5040 and EUSAAR 2). A slightly bigger deviation can be recognized in the amount of spruce samples, where more EC evolved during the NIOSH temperature protocol. Optical methods provide BC concentration which is

much higher if compared to the EC concentration data provided by the Aethalometer. One of the reasons for this could be the underestimation of EC concentration of thermal-optical analyses. Below (**Figure 37**) is a thermogram of a beech sample with, obviously, highly loaded and consequently very dark filters. It is difficult to set the split point because the laser line is almost flat and a significant part of the EC peak area is represented as OC.

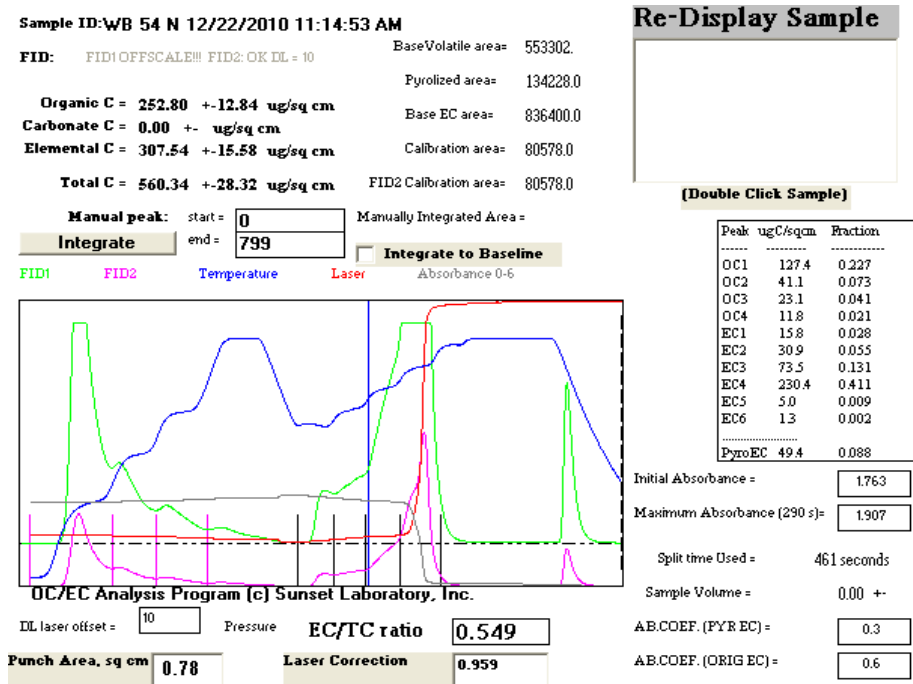


Figure 37: Thermogram of PM₁₀ filter sample (beech) using the NIOSH temperature protocol and automatic setting of split point.

The BC concentration measured with Aethalometer during the beech and spruce combustion is higher than the comparable EC concentration. Concerning the PM₁₀ results, the BC concentration produced while burning pellet samples is lower than the adequate EC concentration. Pellets give less exhaust when burning and, consequently, less deposit on the filters, which means less chance of an under- or overestimated EC concentration.

The BC concentration calculated by measuring absorption coefficient with integrating sphere is always much lower than that obtained by other methods. It may be that optical methods underestimate the concentration of BC. This is most certainly due to different calibration of the respective methods. The IS was calibrated with Carbon Black (Elftex 125 by Cabot Corp).

A comparison of the results for PM₁₀ and PM_{2.5} shows that in the case of beech the concentration values of PM_{2.5} are higher than the values of PM₁₀, regardless of the method

employed. It is possible that an error occurred in analyses or that the average results may show a different picture when there is a high level of fluctuation between the results of the individual tests.

In **Figure 38**, average $PM_{2.5}$ values using different methods and wood types are presented.

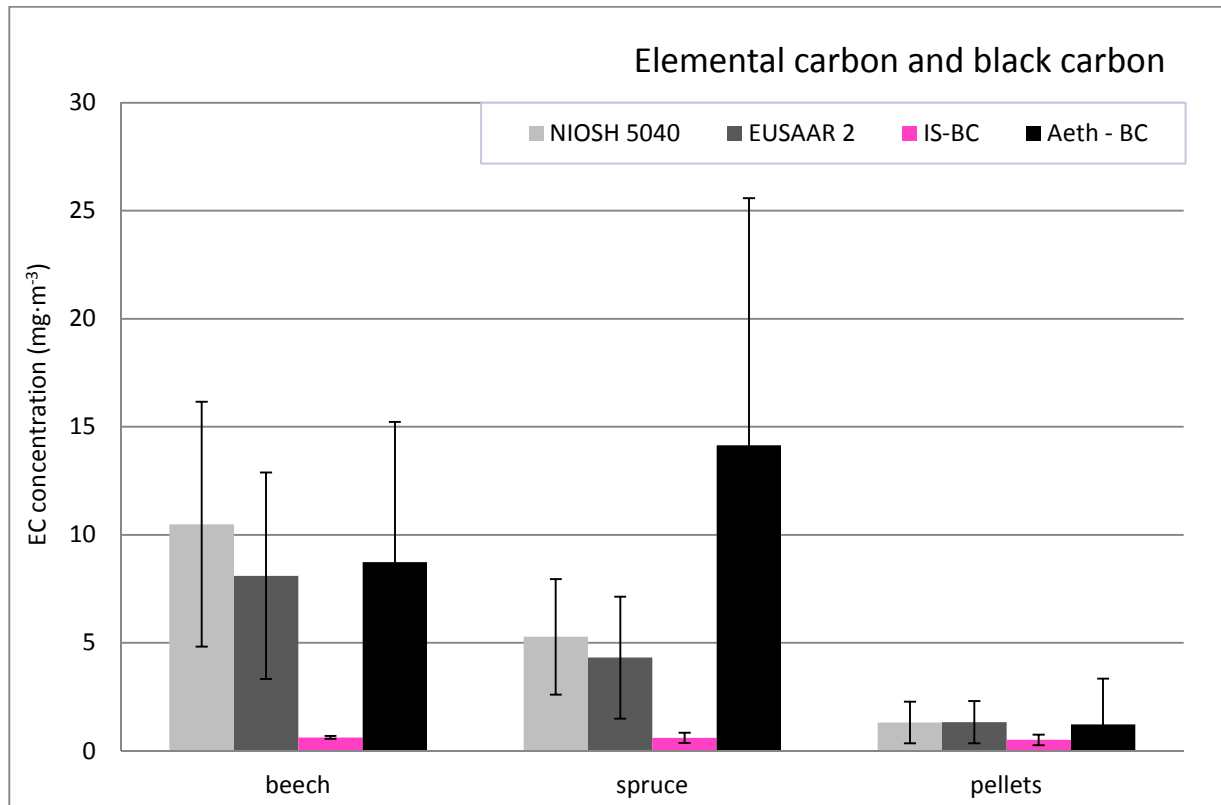


Figure 38: Average $PM_{2.5}$ values of EC concentration for different types of wood that were measured with the OC-EC dual-optical instrument using NIOSH 5040 (light grey) and EUSAAR 2 (grey) temperature protocols. Average values of BC concentration using optical methods: Integrating sphere (IS-BC) and TSP values of Aethalometer (Aeth-BC). Error bars reflect the standard deviations of the variations occurring in four experiments conducted for beech and spruce and the three experiments involving pellets.

The graph of $PM_{2.5}$ concentrations (**Figure 38**) shows slightly different results than that in **Figure 36**. The influence of both temperature protocols in the case of beech and spruce combustion can be noticed. When the NIOSH temperature protocol is used, more EC evolves during analyses. The BC concentration of beech sample measured with Aethalometer in fact matches the EC concentration, while the amount of BC in spruce emissions is higher for almost a factor of 3. The reason for this may be the resin contained in spruce. As for pellets, the same trend as in **Figure 36** can be observed.

To sum up, a result comparison of PM₁₀ (**Figure 36**) and PM_{2.5} (**Figure 38**) sample analyses shows that EC concentration of beech in PM_{2.5} samples is higher than in PM₁₀ samples – the error may be due to large discrepancies between the concentrations of the individual beech tests. From **Figure 39** to **Figure 44** it will be examined what happened with concentrations of different carbonaceous compounds (OC, EC, BC and BrC) in each test.

Figures from **Figure 39** to **Figure 44** depict particle comparisons of carbonaceous aerosols which differ regarding the type of analysis made and the particle separators used (PM₁₀ and PM_{2.5}). OC and EC result from thermal-optical analysis (the NIOSH 5040 temperature protocol), whereas BC and BrC are the products of optical analysis (integrating sphere).

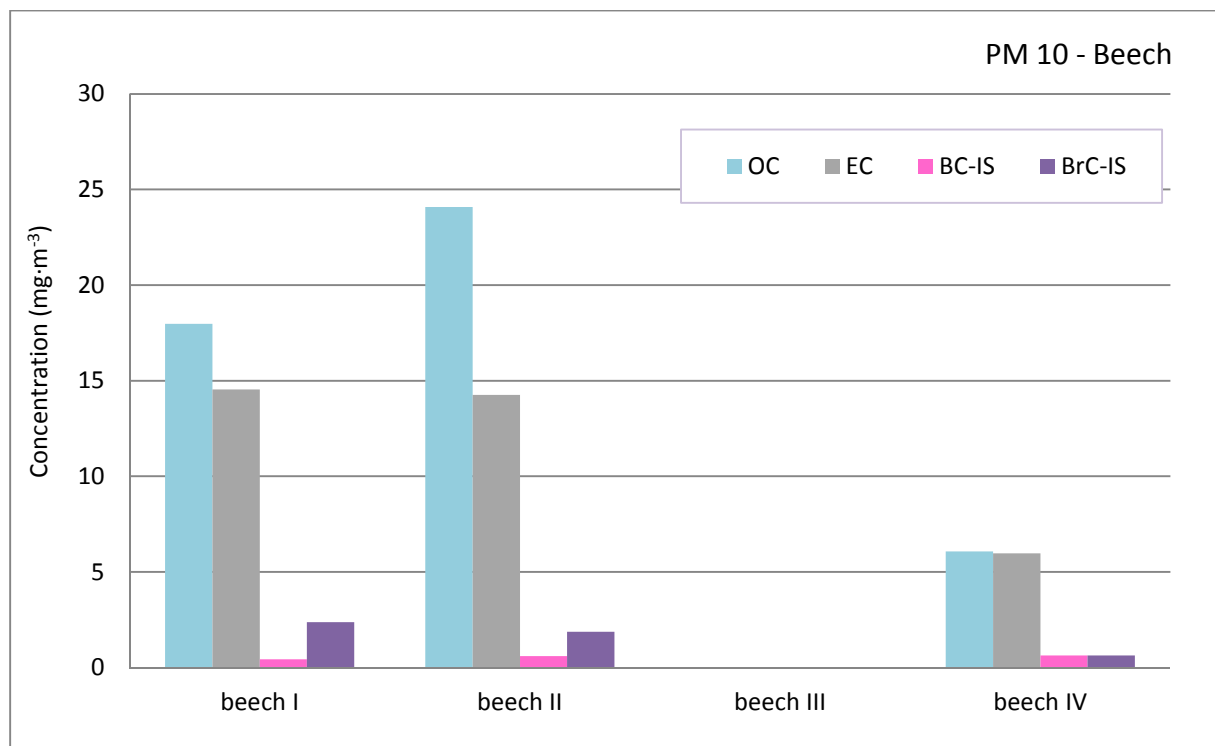


Figure 39: PM₁₀ concentrations of organic carbon (OC) and elemental carbon (EC) measured with the OC-EC dual-optical instrument, and black carbon (BC-IS) and brown carbon (BrC-IS) concentrations measured with integrating sphere in various wood-burning tests using beech wood.

When comparing data from the analyses involving PM₁₀ particles (**Figure 39**), significant differences between the results can be noticed. The values of EC and BC differ by as much as a factor of 15, and also high concentrations of OC are detected (24.02 mg·m⁻³), which differ between the burning cycles for a factor of 4. The BrC concentration is, on average, almost the same in all four tests.

All tests, with the exception of one (beech III), were carried out in a completely cooled stove at different days. If we compare the morning measurements (beech I and beech II) at different days, a big difference in concentrations is noticed, especially regarding OC and EC. This implies that the time of the day, at which the burning is carried out, has little bearing on the amount of generated particles. Moreover, even humidity does not have an impact, as the humidity of all wood logs was 8%.

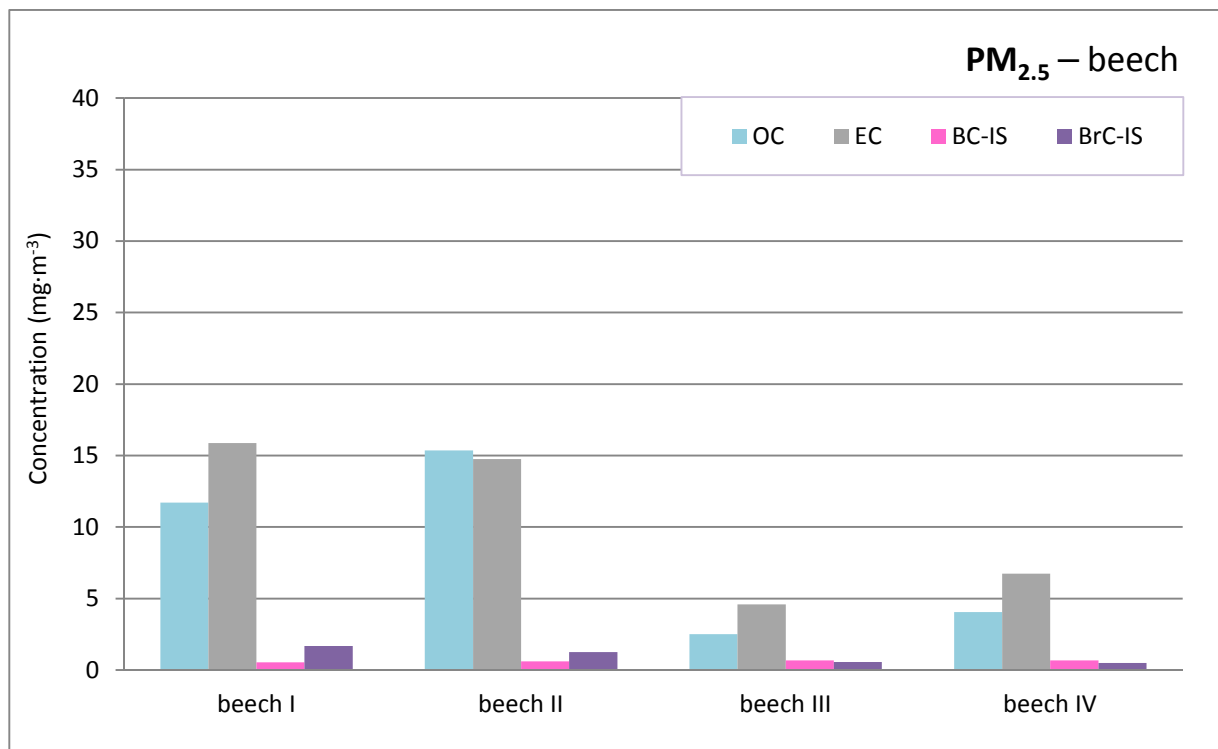


Figure 40: PM_{2.5} concentrations of organic carbon (OC) and elemental carbon (EC) measured with the OC-EC dual-optical instrument, and black carbon (BC-IS) and brown carbon (BrC-IS) concentrations measured with integrating sphere in various wood-burning tests using beech wood.

When reviewing the results of the PM_{2.5} particle concentrations (**Figure 40**), it can be seen that the EC concentration is, on average, about 20% higher than that of OC. Perceived values of BrC in each test are more or less the same as values in »PM₁₀ – beech« graph (**Figure 39**). Therefore, the graphs show clearly that the EC, BC and BrC diameter is about 2.5 μm or less, while the organic carbon also contains larger particles.

In the following two graphs (**Figure 41** and **Figure 42**), the results of spruce combustion emissions are presented. All tests involved spruce wood with moisture content of 8%, with the exception of the last test (spruce IV*), at which the moisture content was 16%.

Similar findings as in the experiments with beech can also be found here, in the experiments with spruce. As evident from the graphs, the values of OC and EC are very different in each experiment. In addition, in one test the value of OC dominates, and only once the value of EC prevails. A similar situation occurs with optical methods (BC-IS). The amount of resin in wood logs is likely to contribute significantly to this effect. The high values of OC concentration compared to EC concentration may be due to resin contained in the spruce logs.

One of the aims of the experiment was to discover how wood moisture affects the wood emissions. Therefore, the spruce tests featured a »PM₁₀-spruce IV*« (**Figure 41**) with 16% moisture and a »PM₁₀-spruce II« with 8% moisture. It can be concluded that a higher value of moisture content (up to 16%) does not affect the EC and BC concentrations significantly; however, it does have some effect on the OC and BrC concentrations.

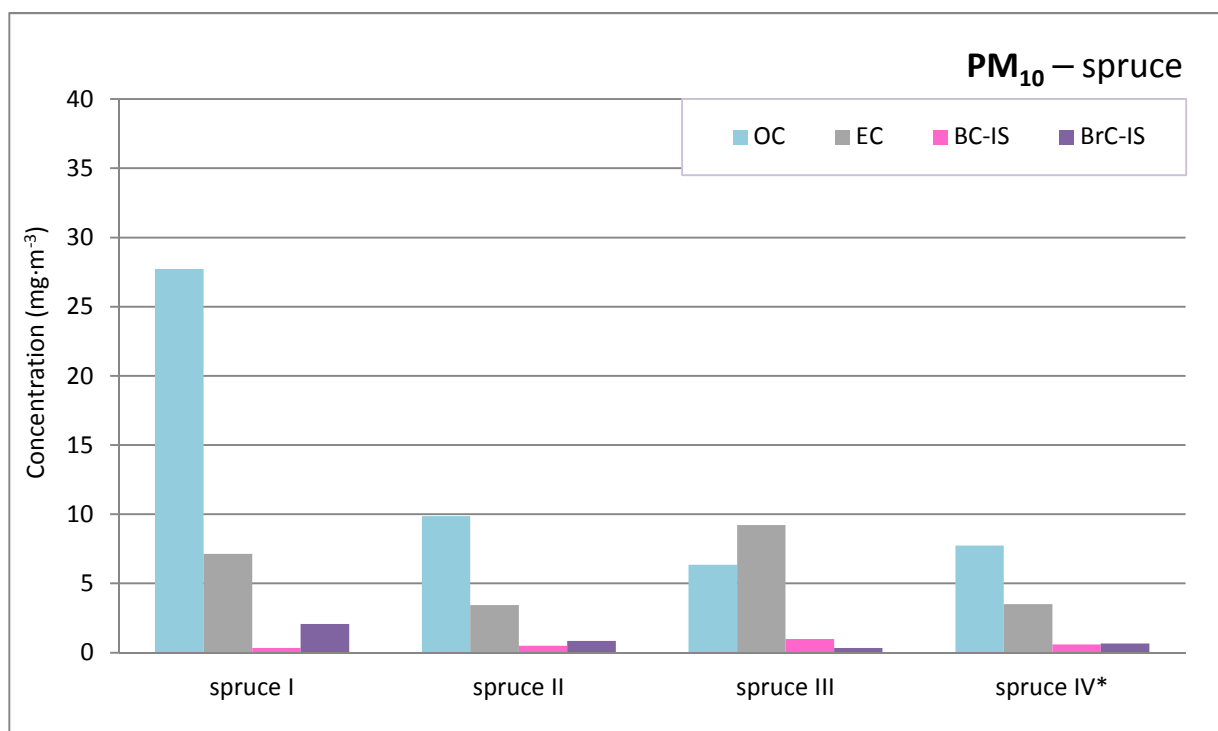


Figure 41: PM₁₀ concentrations of organic carbon (OC) and elemental carbon (EC) measured with the OC-EC dual-optical instrument, and black carbon (BC-IS) and brown carbon (BrC-IS) measured with integrating sphere in different wood-burning tests using spruce wood. The Spruce IV* sample has a moisture content of 16%.

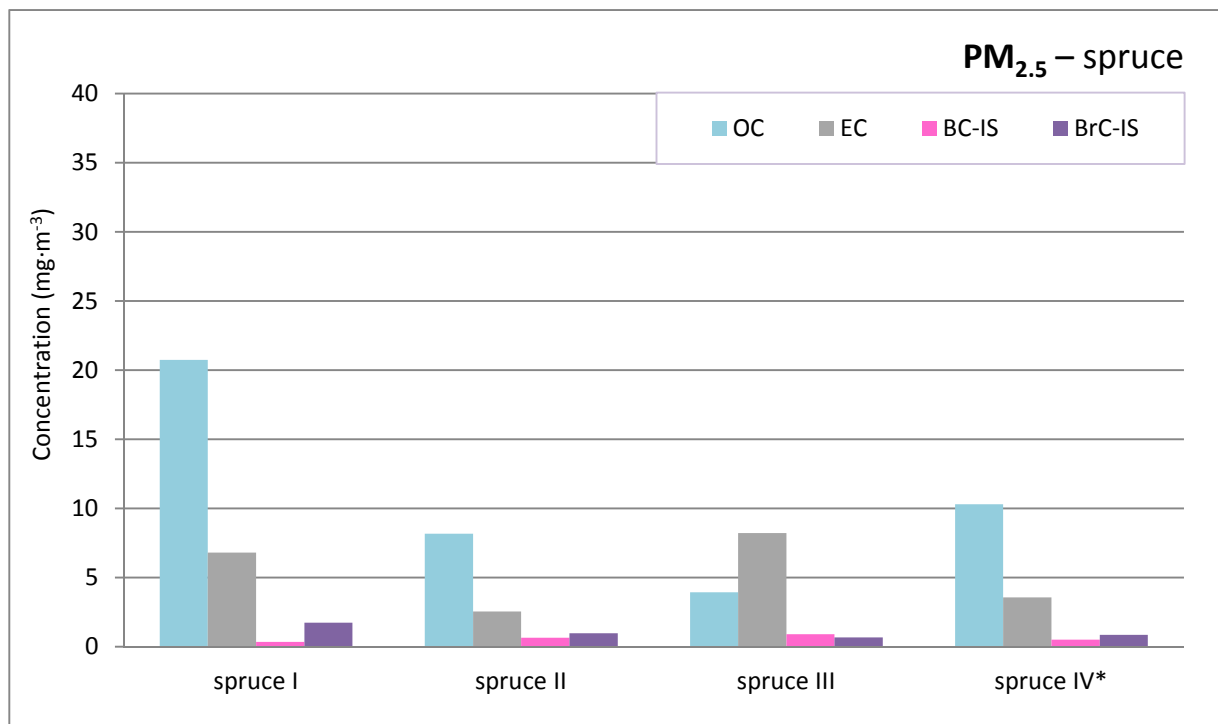


Figure 42: PM_{2.5} concentrations of organic carbon (OC) and elemental carbon (EC) measured with the OC-EC dual-optical instrument, and black carbon (BC-IS) and brown carbon (BrC-IS) measured with integrating sphere in different wood-burning tests using spruce wood. The Spruce IV* sample has a moisture content of 16%.

Pellet experiments have a different categorization. They are classified according to the power output of the stove (30% or 100%). The pellets I sample burned in the stove with 100% power output for one hour, and then for the next hour its output was lowered down to 30%. The pellets II sample burned in the stove with 100% power output the entire time, whereas the pellets III sample's stove power output was 30%.

Experiments with the stove using pellets are an example of a technologically advanced system. In general, it can be said that the results for PM₁₀ (Figure 43) and PM_{2.5} (Figure 44) particles are identical. The concentrations of EC and BC are mostly present; nonetheless, very low values of OC concentration can be observed. It is interesting that choosing the appropriate stove capacity (30%) actually reduces the already low emissions.

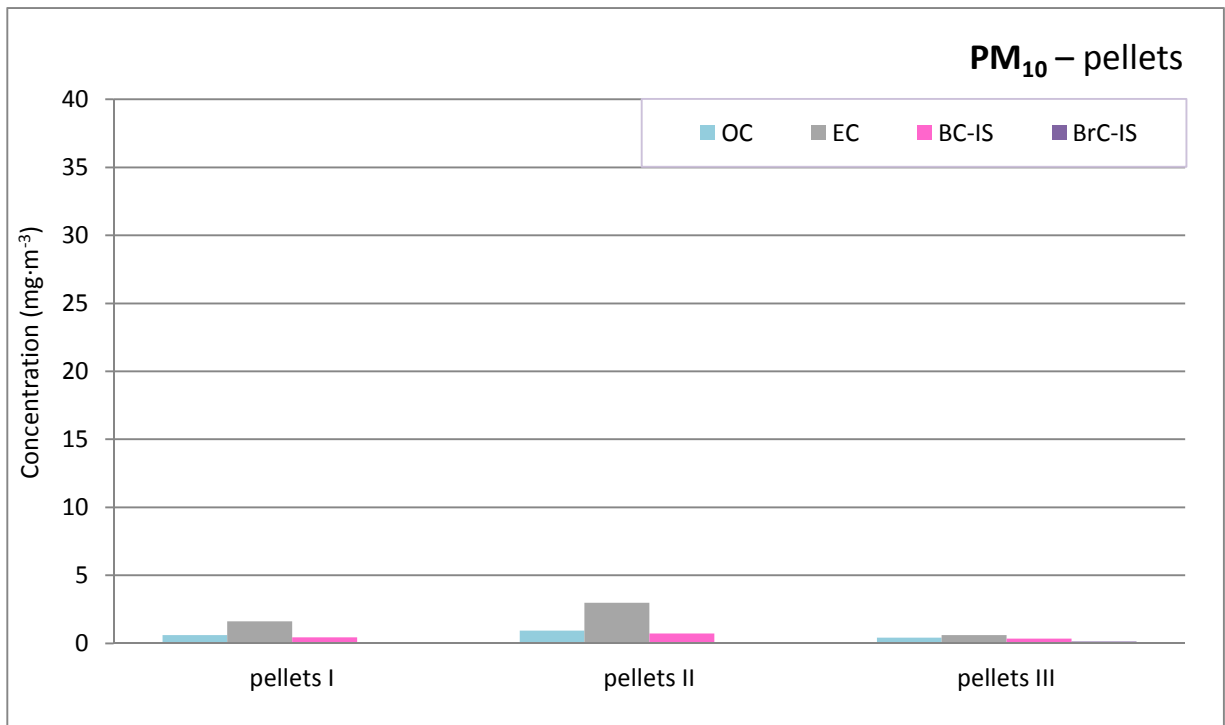


Figure 43: PM₁₀ concentrations of organic carbon (OC) and elemental carbon (EC) measured with the OC-EC dual-optical instrument, and black carbon (BC-IS) and brown carbon (BrC-IS) measured with integrating sphere in different stove capacity tests using pellets.

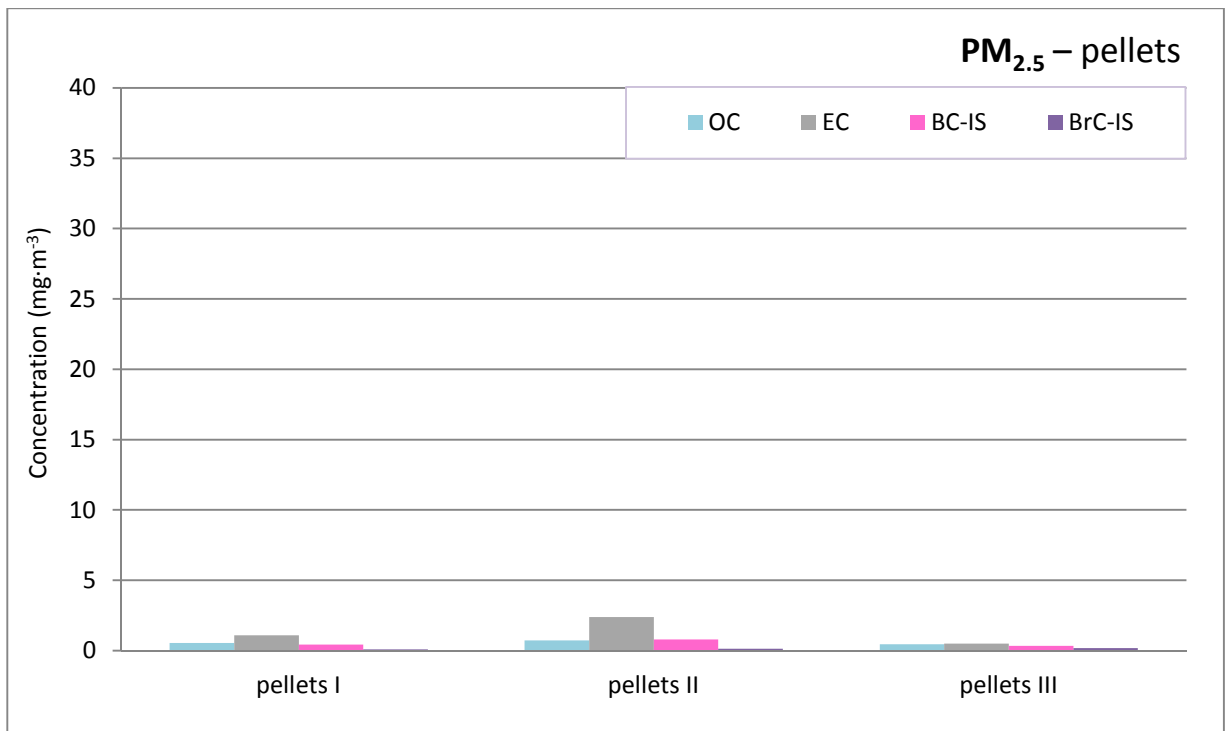


Figure 44: PM_{2.5} concentrations of organic carbon (OC) and elemental carbon (EC) measured with the OC-EC dual-optical instrument, and black carbon (BC-IS) and brown carbon (BrC-IS) measured with integrating sphere in different capacity tests using pellets.

To sum up, our experiment shows that wood smoke pollutes the environment heavily, while "controlled" pellet-burning system greatly reduces the amount of emitted particles, especially organics. The most polluting type of wood in terms of the thermal-optical analysis identification is beech, at which the OC and EC concentrations, in general, share very similar values. What is more, spruce produces more organic carbon compared to EC, which is most probably due to the effect of resin content. When burning spruce, two values of wood moisture (8% and 16%) were employed. The results show that low humidity of wood does not play a major or important role in the particle concentrations.

One of the raised issues of the experiment was how various temperature protocols influenced the measurements, i.e. if using the NIOSH 5040 or EUSAAR 2 protocols significantly affected the outcome of the individual tests. In the following two charts (**Figure 45** and **Figure 46**), the average values of OC and EC concentrations when using the two temperature protocols are presented.

If we first examine the concentration of organic carbon in **Figure 45**, we can see that more organic carbon evolves when using the EUSAAR 2 temperature protocol, and this is evident for both types of wood (beech – around 25%, spruce – around 20%). As for pellets, the temperature difference effect of the protocols is negligible.

When observing the concentration of EC in **Figure 46**, the opposite situation can be noticed. More elemental carbon evolves when using the NIOSH 5040 temperature protocol. Regarding the pellet combustion, again no differences between temperature protocols can be found.

These results suggest that the NIOSH 5040 protocol detects higher concentrations of EC, while the EUSAAR 2 protocol shows higher OC values. For systems, such as the pellet-burning, the choice of the temperature protocol is irrelevant because there are no differences in the experiment outcome. The concentrations on pellet filter samples are rather low and are therefore also easy to sample, because there is no problem with filter overloading that can interfere with thermal-optical methods.

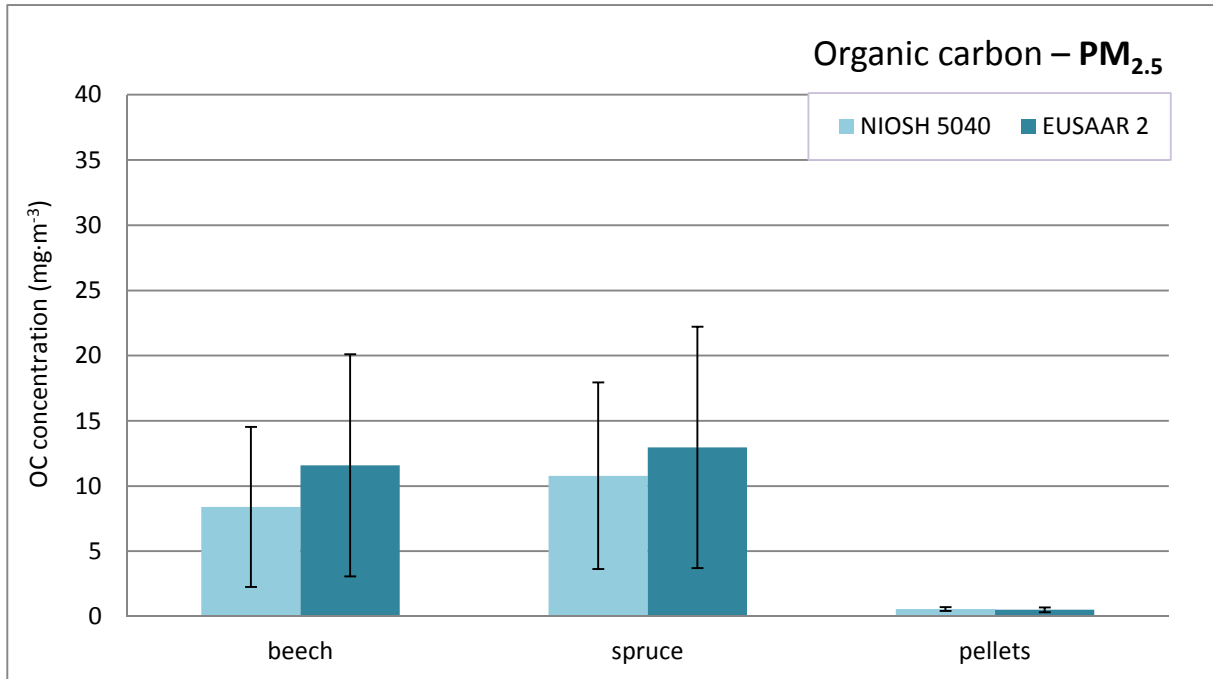


Figure 45: Average OC values of various wood types when using the two temperature protocols (NIOSH 5040 and EUSAAR 2) – PM_{2.5} (Error bars are standard deviations).

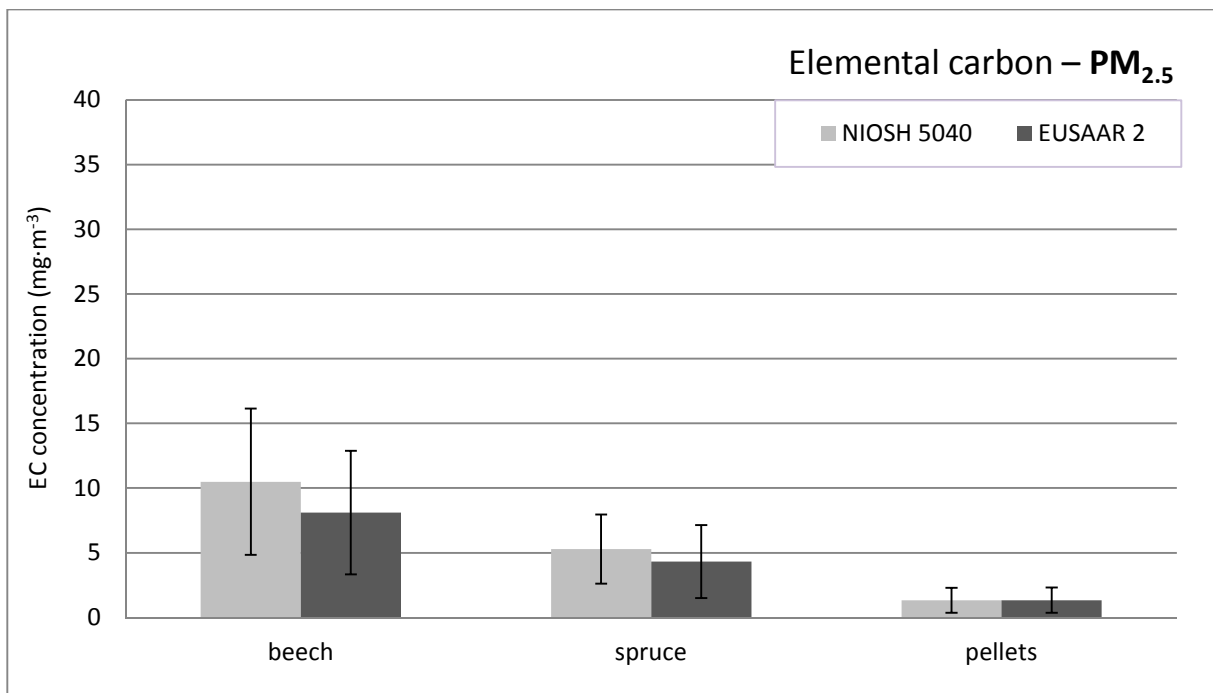


Figure 46: Average EC values of various wood types when using the two temperature protocols (NIOSH 5040 and EUSAAR 2) – PM_{2.5} (Error bars are standard deviations).

Figure 45 and **Figure 46** again clearly show that beech combustion contributes significantly to the pollution caused by elemental carbon and organic carbon, while burning spruce contributes mainly to an increase in OC concentration in the air. However, its contribution to the concentration of EC in the atmosphere certainly cannot be ignored, even if it is almost half lower than that of beech.

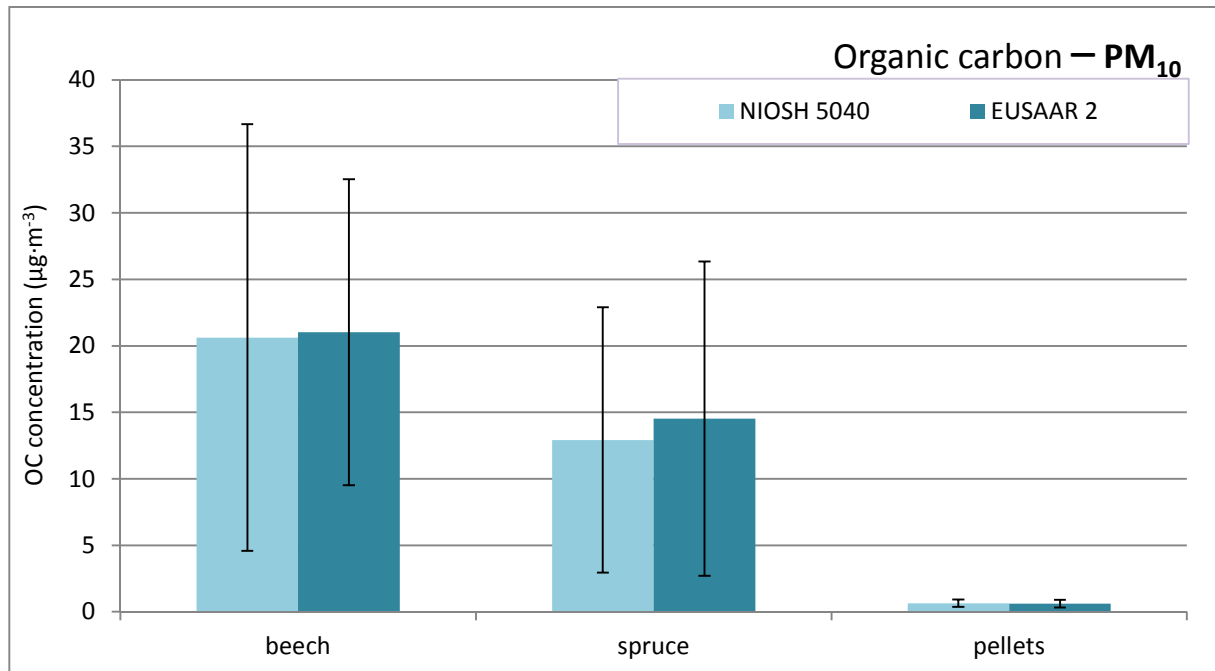


Figure 47: Average OC values of various wood types using the two temperature protocols (NIOSH 5040 and EUSAAR 2) – PM_{10} (Error bars are standard deviations).

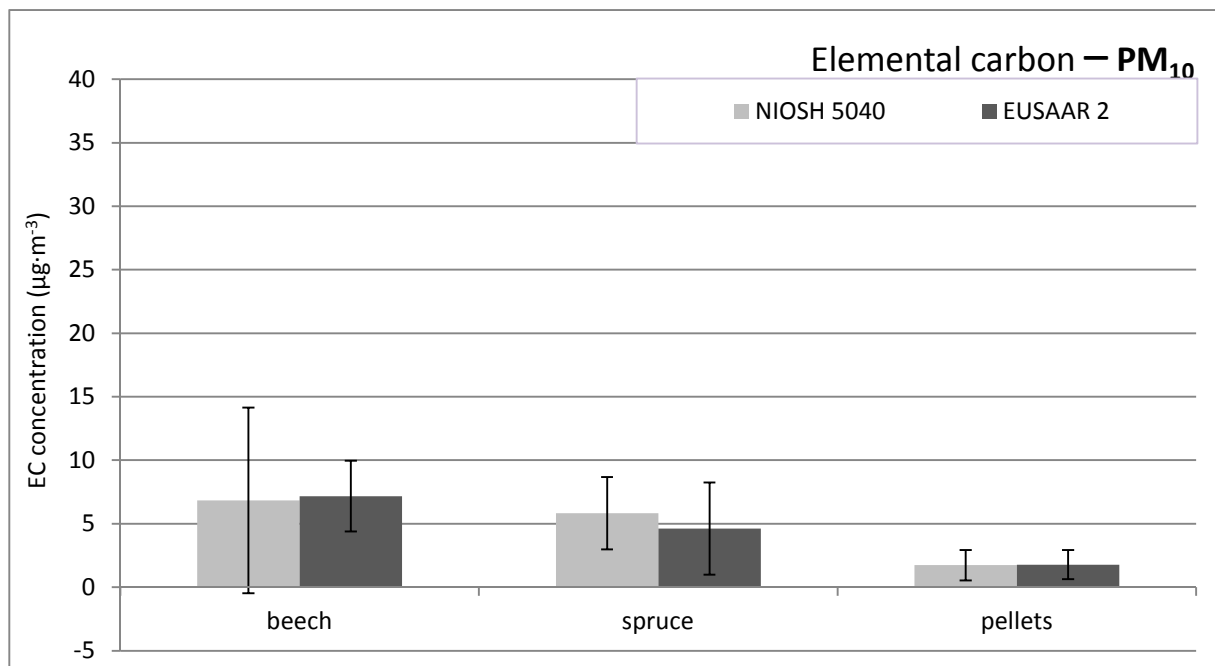


Figure 48: Average EC values of various wood types using two the temperature protocols (NIOSH 5040 and EUSAAR 2) – PM_{10} (Error bars are standard deviations).

In **Figure 47** and **Figure 48**, average PM_{10} values of various wood types using the NIOSH 5040 or EUSAAR 2 temperature protocols are depicted. Graphs show that the PM_{10} concentration of the samples does not depend on the temperature protocols employed because no significant difference in the concentrations resulting from the usage of the NIOSH and EUSAAR protocols can be recognized.

When comparing the PM_{10} (**Figure 47**) and $\text{PM}_{2.5}$ (**Figure 45**) concentrations, it becomes clear that the majority of evolved organic particles is big because the PM_{10} concentration (**Figure 47**), is almost twice as high as that of the $\text{PM}_{2.5}$ (**Figure 48**). The diameter of the elemental carbon is mainly around $2.5 \mu\text{m}$ (or less) – except in the case of beech samples. Here, the EC concentrations in the PM_{10} graph are also almost twice as high.

4.3.2. Determination of the absorption Angstrom exponent

When studying the results obtained with optical methods, attention was put also on the absorption Angstrom exponent values for different types of fuel/wood. While the spectral dependence of BC light absorption is low ($\alpha \sim 1$; Bond and Bergstrom, 2006), brown carbon exhibits a much higher absorption Angstrom exponent (up to 7; see, e.g. Hoffer et al., 2006); the CAST experiment leads us to the same estimations.

In the following histogram (**Figure 49**), the absorption Angstrom exponent values are depicted for each wood type and both phases (phase 1 and phase 2). At the pellet experiment, only one bar in the histogram can be seen since the criterion of combustion emissions was the capacity of the stove (100% or 30% capacity).

The analysis shows that the average Angstrom exponent values for spruce emissions are high and could even exceed the value of 2, which tells us that the content of organic matter emitted when burning spruce is very high in the starting phase, while the highest individual value from burning beech reaches only ~ 1.6 . The high values we witness when burning spruce can probably be explained with the presence of resin in spruce.

If comparing phases in the results of beech combustion, the phase 1 shows a greater production of BC ($\alpha_{BC} \sim 1$, Kirchstetter et al., 2007), while in the phase 2 the content of OC increases. Burning pellets mainly produced BC emissions ($\alpha \cong 1$) in small quantities, as it is shown in the thermal-optical analysis in the previous section.

The results obtained from Aethalometer, which were compensated by using the Weingartner principle, distinguish emissions of diesel exhaust and wood smoke in the environment that can be seen in the value of the Angstrom exponent of the wood smoke which rises to ~ 1.4 or more.

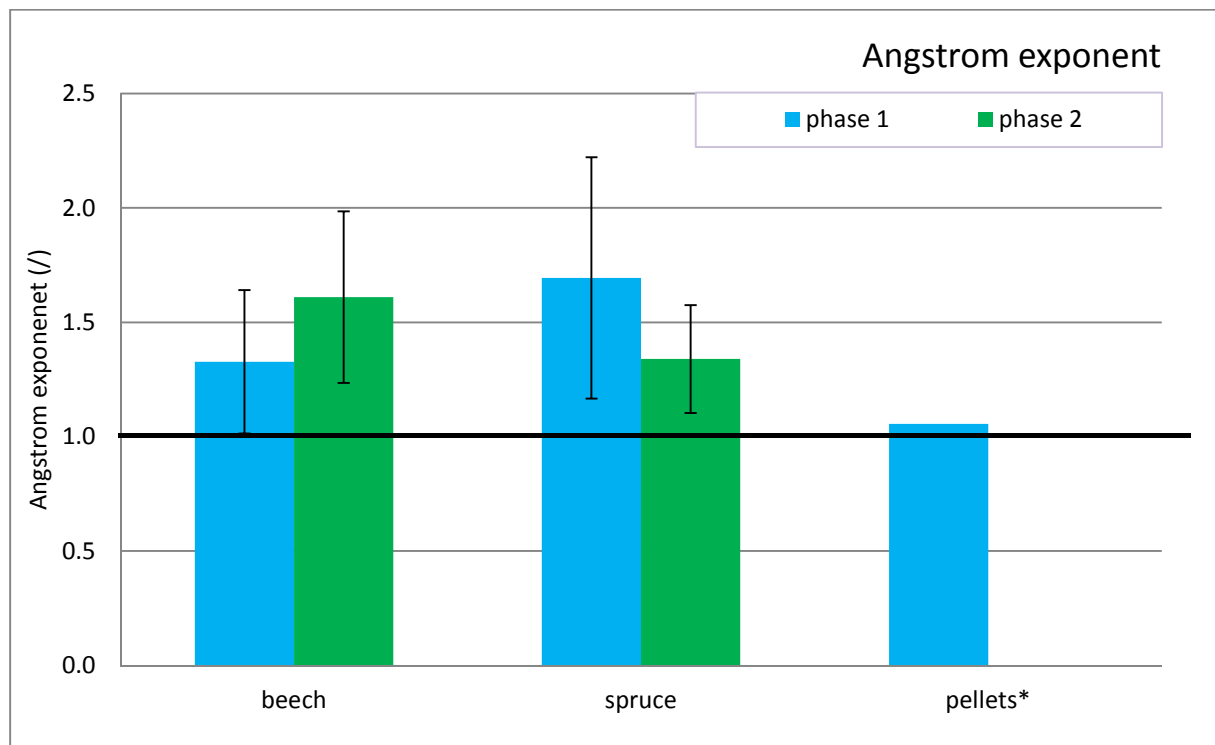


Figure 49: The Angstrom exponent dependence on various burning phases: phase 1 (blue) and phase 2 (green). *Pellet results are presented with only one bar because they were analyzed according to the stove capacity. Error bars are standard deviations of averaged Aethalometer data of 5-minute time base.

In the following figures (**Figure 50–Figure 52**), the Angstrom exponent dependence on time for each burning cycle is presented.

Figure 50 shows that comparing Angstrom exponent for each cycle of beech burning might explain the significant difference in EC and OC concentrations measured with thermal-optical methods. In the filter samples of beech I (**Figure 40**), higher OC concentration than EC concentration is detected and the Angstrom exponent values were in general also above 1.5 which is already the detection limit for organic material present in the sample or the atmosphere.

In the beech II burning cycle (**Figure 50**), only data for phase 1 were available. A higher Angstrom exponent (up to 2.7) was detected already in phase 1 where amount of black carbon or elemental carbon was expected to be higher (lower Angstrom exponent). In phase 2 of beech III (**Figure 50**) burning cycle, where ignition started in the hot stove, lower values of Angstrom exponent ($\alpha \sim 1$) were observed at the beginning of ignition, but they increased up to 3.5 afterwards. The same trend was observed also in phase 2 of beech IV burning cycle.

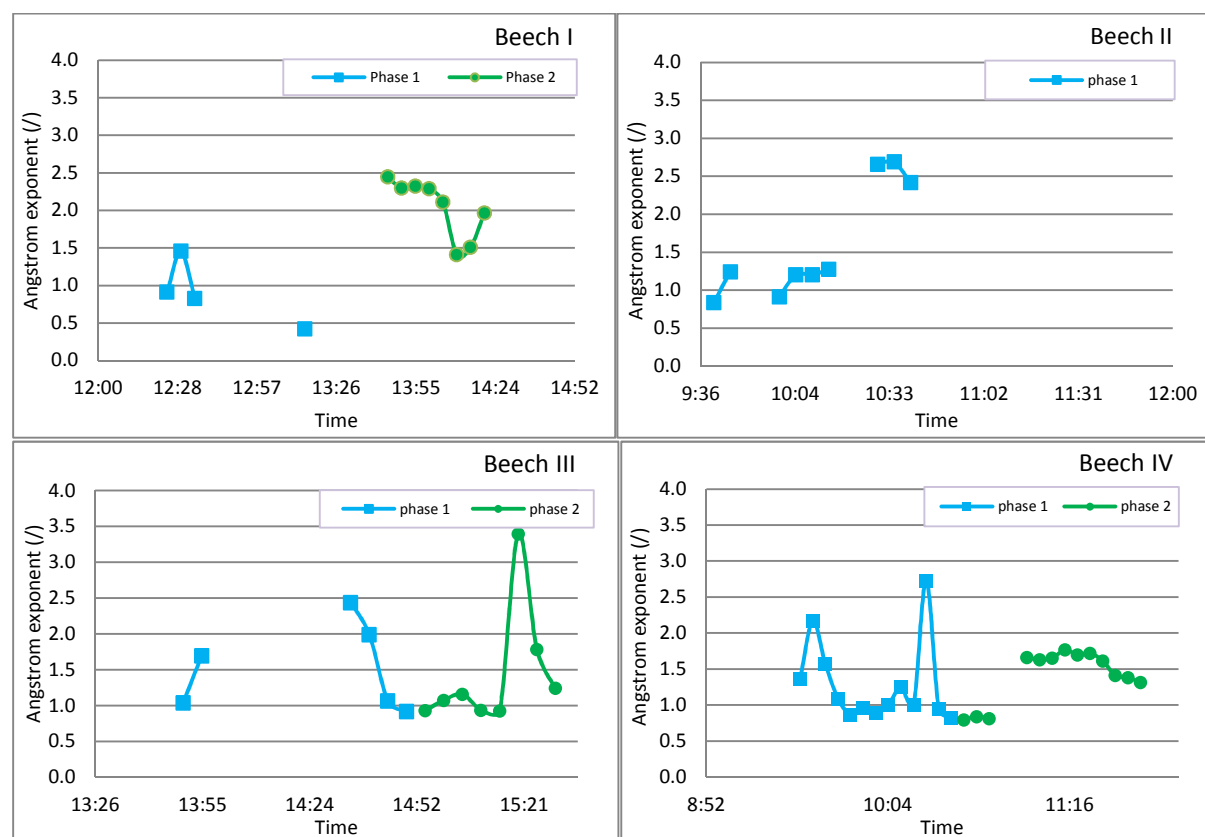


Figure 50: The Angstrom exponent dependence on time for each cycle of beech burning; blue (□) is burning phase 1 and green (○) is burning phase 2.

In **Figure 51**, the comparison of the Angstrom exponent dependence on time for each spruce burning cycle is presented. The situation in the spruce burning cycles is even more variable than in the beech burning cycles; especially in the Spruce II burning cycle (**Figure 51**). This cycle shows high range of Angstrom exponent values ($\alpha \approx 1.0 - 3.4$) in phase 1. The high α values give information about a large amount of organic content evaluated during the burning in the phase when ignition starts in the cold stove. In phase 2, Angstrom exponent of ~ 1.0 was observed with some high α peaks ($\alpha \sim 2.5$). **Figure 41** also shows that much more OC evolved during the spruce I, II and IV burning cycle than EC and, as mentioned, OC content in the sample leads to high Angstrom exponent values.

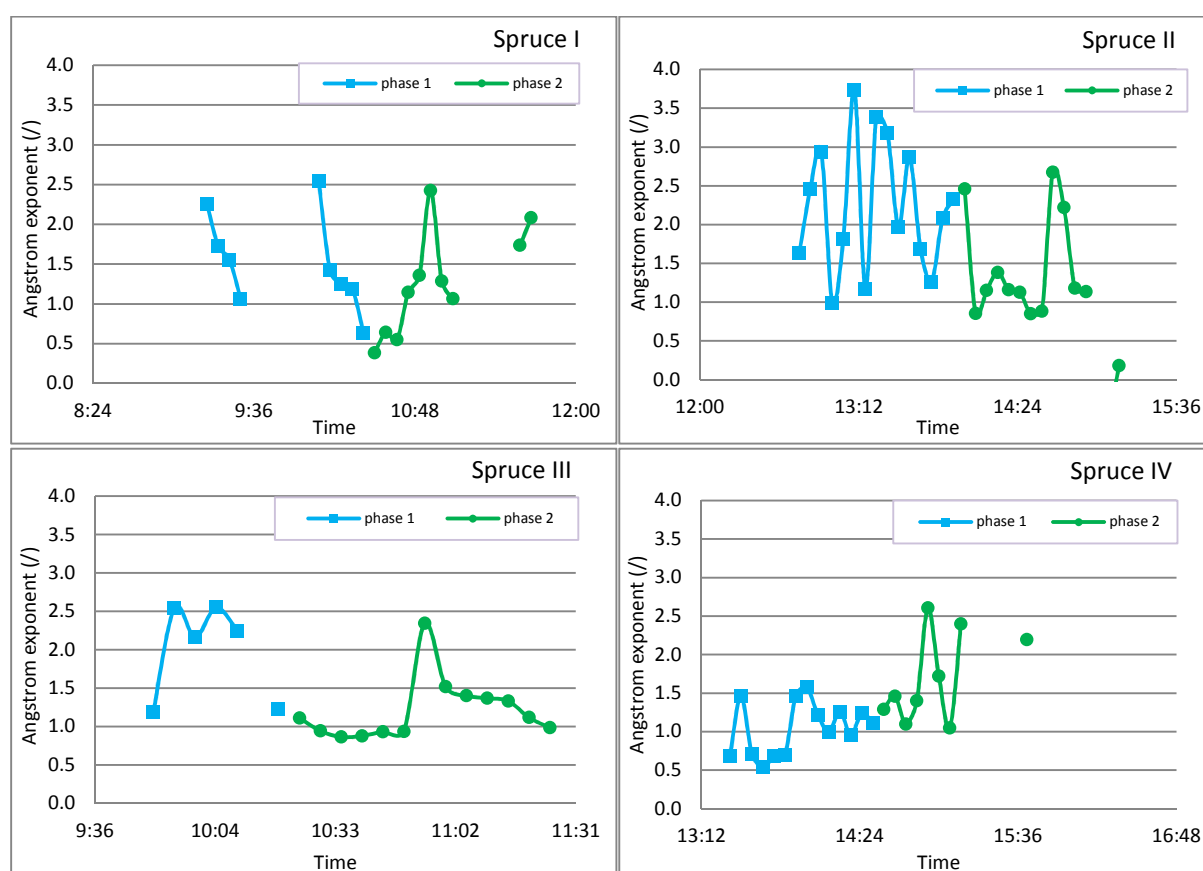


Figure 51: The Angstrom exponent dependence on time for each cycle of spruce burning: blue (\square) is burning phase 1 and green (\circ) is burning phase 2.

In general, a higher Angstrom exponent of spruce combustion emissions was observed during phase 1 than during phase 2 (see spruce III burning cycle, where the trend is evident). The spruce IV burning cycle is an exception. It might be due to higher moisture of spruce wood; instead of logs with 8% moisture, logs with 16% moisture were burned. In this cycle

(spruce IV), lower Angstrom values around $\alpha \sim 1.0$ were observed in phase 1 and in phase 2 α increased after ignition up to 2.6.

Figure 52 shows the Angstrom dependence on time for pellet burning cycles with 100% and 30% burning efficiency.

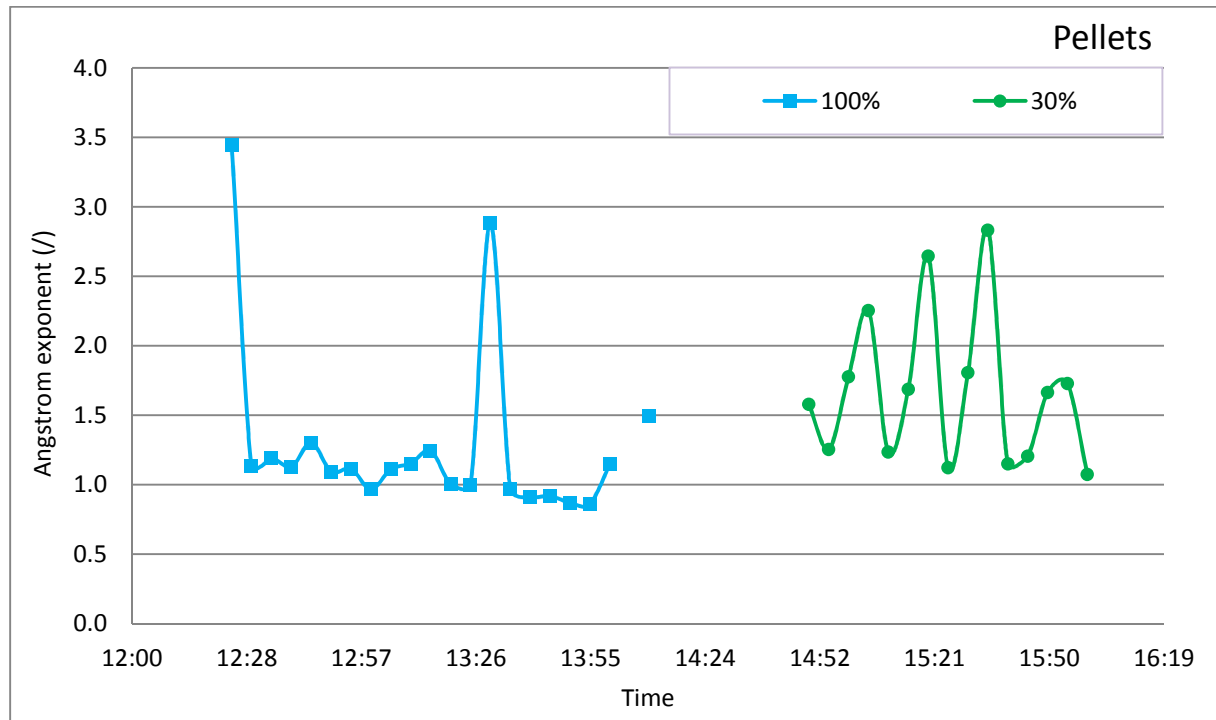


Figure 52: The Angstrom exponent dependence on time for each cycle of pellet burning: blue (□) is a 100% burning efficiency and green (○) is a 30% burning efficiency.

In the cycle where burning efficiency was 100%, lower Angstrom exponent values were observed than in the 30% burning efficiency cycle. These results may suggest that lower Angstrom exponent could mean better burning efficiency in the case of pellets.

4.3.3. Anhydrosugar analysis – tracers of wood-burning emissions

Wood consists of cellulose which is mainly responsible for the structural strength. During the wood burning process, the wood constituents start to hydrolyze, oxidize, dehydrate, and pyrolyse due to the increase of the temperature. The combustible volatiles are formed and charring of highly reactive carbonaceous occurs (Alger, 1972; Roberts, 1970; Sergejewa, 1959; Shafizadeh, 1983).

The decomposition of cellulose is happening in two stages. The first stage, at temperatures below 300 °C, involves depolymerization, water elimination, fragmentation and oxidation and ends with charring. In the second stage, at temperatures higher than 300 °C, formation of transglycosylation, fission and disproportionation reactions yielding anhydrosugars (levoglucosan, mannosan, etc.) and volatile products occur (Simoneit et al., 1999).

In the wood burning experiment, and later ambient measurements, the attention was also put on the anhydrosugars, since levoglucosan has been detected in residential wood smoke and ambient air. Levoglucosan was reported to be totally in the fine particle phase of smoke (Horing et al., 1985; Locker, 1988).

The samples of wood-burning experiment were analyzed with a liquid chromatography. The results are presented in the following figures.

In **Figure 53** and **Figure 54**, average values of measured deposition mass of anhydrosugars (levoglucosan, mannosan, galactosan) on the filter samples for various types of wood (beech, spruce, pellets) are presented.

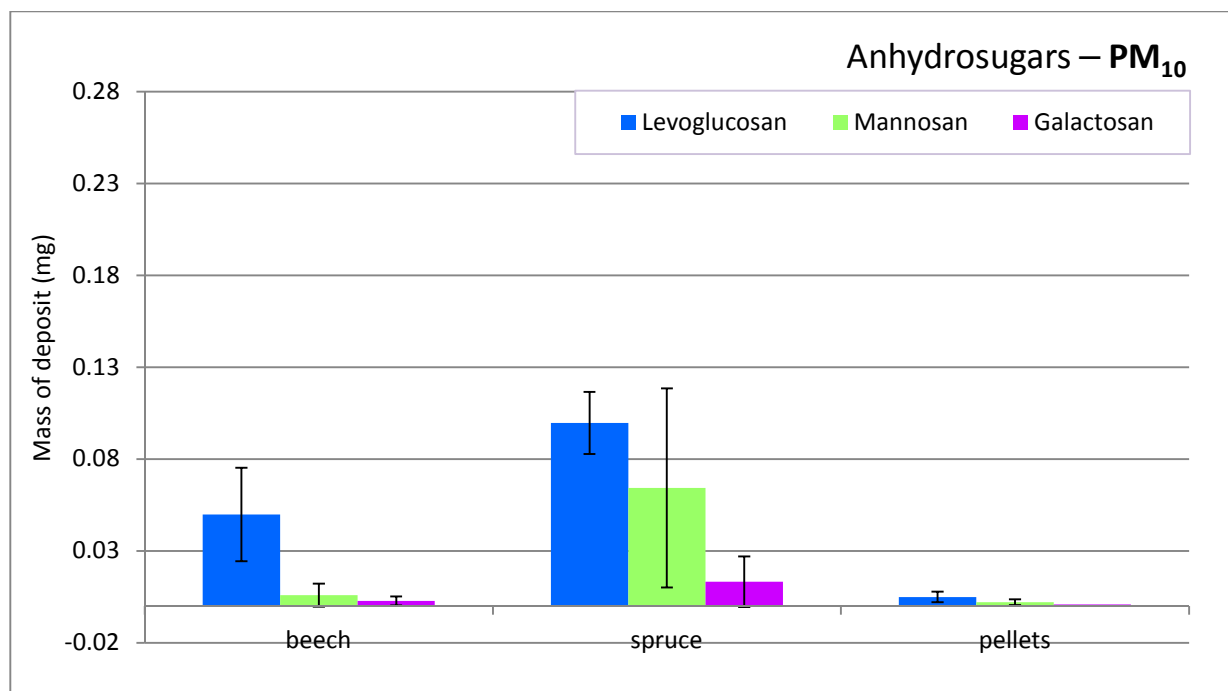


Figure 53: Average deposition mass of anhydrosugars (levoglucosan, mannosan, galactosan) for various types of wood (beech, spruce, pellets) – PM_{10} . Error bars are standard deviations.

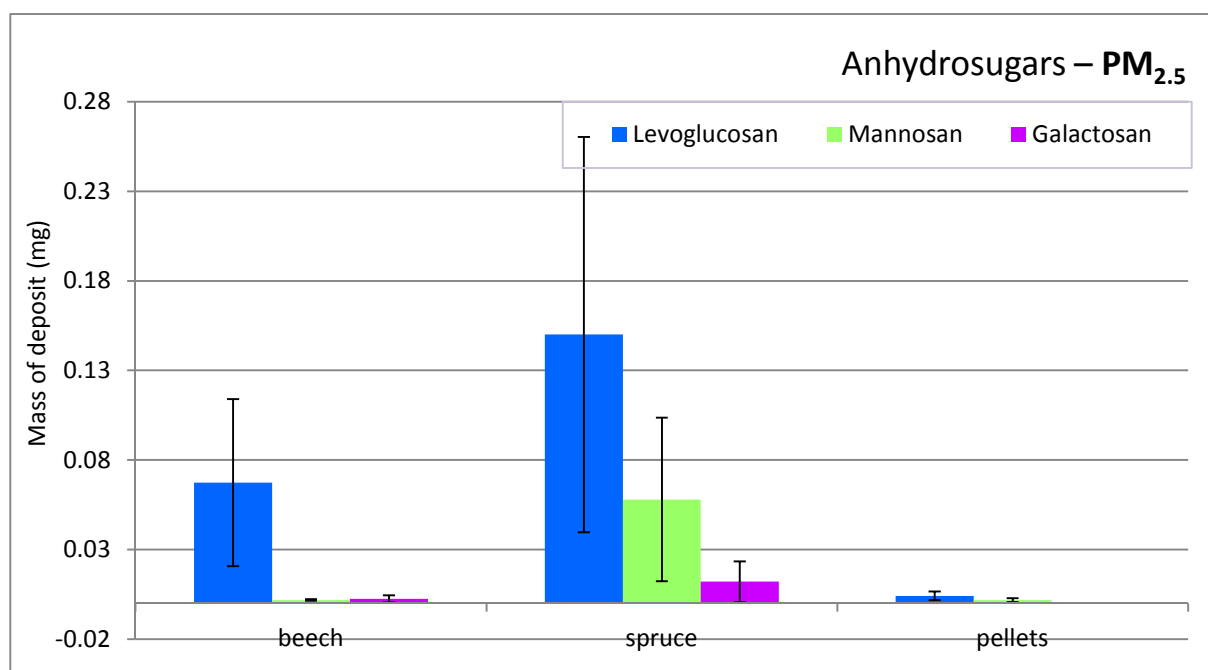


Figure 54: Average deposition mass of anhydrosugars (levoglucosan, mannosan, galactosan) for various types of wood (beech, spruce, pellets) – $PM_{2.5}$. Error bars are standard deviations.

Both figures show that levoglucosan is a major organic component in fine smoke particulate matter (PM_{10} and $PM_{2.5}$) emitted from wood-burning. It is accompanied by other monosaccharide derivatives (mannosan and galactose), however, those are present in much smaller quantities.

In **Table 11**, average values of anhydrosugar mass on the filter samples of various wood types are presented.

Table 11: Average deposition mass of anhydrosugars (levoglucosan, mannosan, galactosan) loaded on the filter samples of various wood types (beech, spruce, pellets); with the ratio between levoglucosan and mannosan.

Type of wood	Particle size	Levoglucosan (mg)	Mannosan (mg)	Galactosan (mg)	Levog./Mann. Ratio (/)
beech	PM_{10}	0.050	0.006	0.003	8.4
spruce		0.100	0.064	0.013	1.6
pellets		0.005	0.002	0.001	2.3
beech	$PM_{2.5}$	0.067	0.002	0.002	37.8
spruce		0.150	0.058	0.012	2.6
pellets		0.004	0.002	0.001	2.4

Mannosan, a pyrolyse product from hemicelluloses, is the second most abundant anhydrosugar in the wood smoke samples. Considering the ratio of levoglucosan to mannosan, the difference between hard- and softwood types becomes more marked. Hardwoods give high ratios, around 14–15 and softwood exhibit a ratio of 2.5 (Schmidl et al., 2008).

In **Table 11**, the ratios of levoglucosan to mannosan for all used wood types are calculated. Similar to the aforementioned research (Schmidl et al., 2008), the ratio of softwood is around 2.5, which goes for pellets as well. The reason why pellets have the same ratio as spruce lies in the composition of the pellets, which is 100% softwood.

In beech samples, there is a considerable deviation between the ratio of levoglucosan and mannosan for both PM_{10} and $PM_{2.5}$. The ratio of levoglucosan to mannosan for PM_{10} amounts to 8.4 and is almost twice as low as that in the results from the aforementioned research (Schmidl et al., 2008), whereas the same ratio for $PM_{2.5}$ is more than twice as high (37.8).

In summary, levoglucosan and the related monosaccharaides can be utilized as indicator compounds for the presence of emissions of fine atmospheric particulate matter from wood-burning. Ratio of levoglucosan to mannosan is a good marker for soft- and hardwood.

CHAPTER 5

Ambient measurements

Contents

5.1. Measurement stations	87
5.2. Sources of energy and emissions.....	90
5.3. Results	93
5.3.1. Urban and rural emissions – black carbon measurements	93
5.3.2. Source apportionment – residential combustion and traffic	97
5.3.3. Anhydrosugars – tracers of wood-burning.....	102
5.3.4. Sensitivity of the Aethalometer model when changing the absorption Angstrom exponent of wood-burning (α_{wb}) and fossil fuels (α_{ff}) for 10%	103

In view of the observations that wood smoke is one of major contributors to atmospheric pollution during winter, we decided to specifically examine its sources and composition in the field (Puxbaum et al., 2007). To carry out the measurements, we choose the Austrian city Klagenfurt, which is situated in a basin, and the rural village Zell near Klagenfurt, where no industry and, consequently, very little traffic is present.

In our research, we were also interested in the actual contribution of wood to pollution and tried to answer the following questions: what is the structure of wood-burning particles in the atmosphere and how widely spread the burning of wood is in areas which are rural.

5.1. Measurement stations

PMinter is an interregional project which is focused on interregional interaction of residential heating and traffic related measures of PM-levels in the Slovenian-Austrian border region. Aethalometer measurements were part of this project as well. The project lasts from July 1, 2010 until December 31, 2013. The overall objective formulated in proposal of the PMinter project is a significant improvement in air quality by focusing on PM (particulate matter/fine dust) in Klagenfurt (Lower Carinthia, Southern Styria) and Maribor (northern Slovenia) in order to lower the risk of exposure for the inhabitants of the regions mentioned. Our work was focused on BC concentrations at Klagenfurt – Lower Carinthia region, Klagenfurt – Völkermarkter Strasse measurement station (hereinafter Klagenfurt) and Zell – Ebenthal measurement station (hereinafter Zell).

Basins always represent pollution problems. Exhaust gases and aerosol particles remain in the basin and have a strong impact on the quality of life. This happens especially in winter when temperature inversion occurs.

Particulate matter measurements were done at two stations in the south of Austria – Klagenfurt and Zell (*Figure 55*).

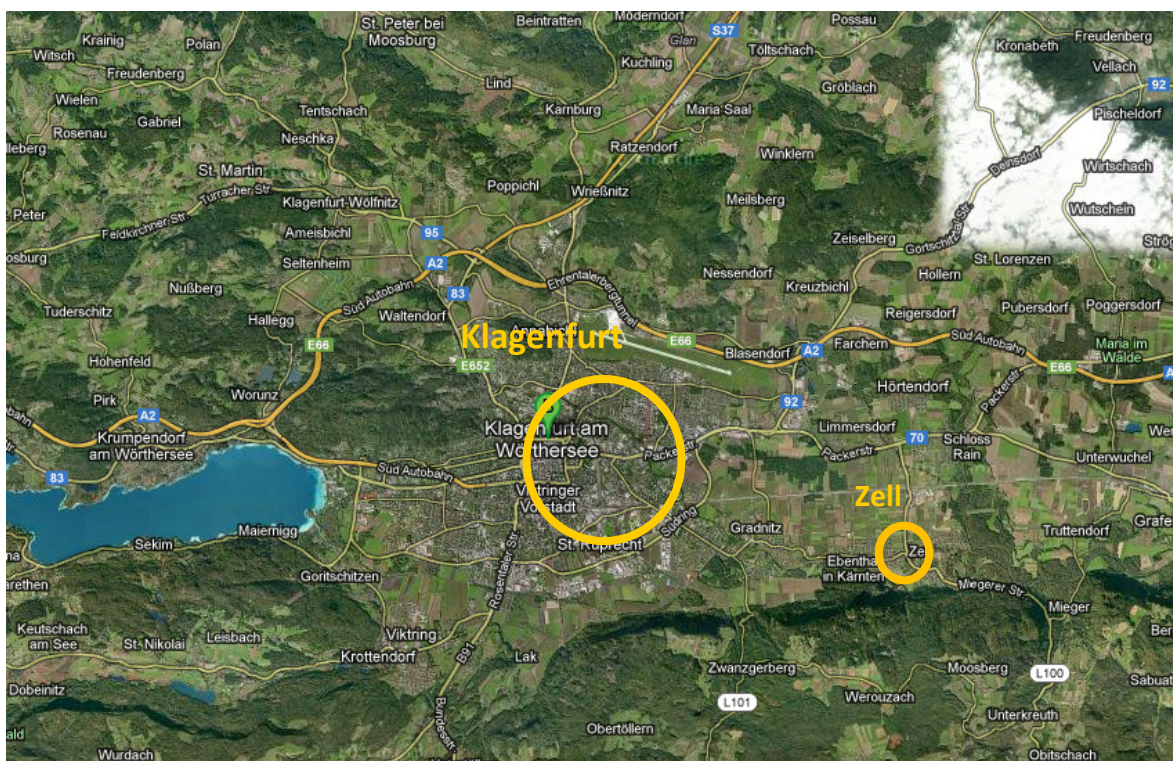


Figure 55: Southern part of Austria with the locations of measurement stations – Klagenfurt and Zell (Google maps).

Klagenfurt is located in a basin 446 m above sea level and is surrounded by hills covered with forest; the hills range up to 1000 m above sea level and more. Zell is a small town less than 10 km away from Klagenfurt to the southwest. It is located at the foot of the hills (Karawanks mountain range).

Klagenfurt is the sixth largest city in Austria and has approximately 90,000 inhabitants. It has a typical continental climate (four seasons) with average daytime winter temperature from 4 to 1.7 °C. The urbanized area covers approximately 120.07 square kilometers (Source: Wikipedia – 05/22/13).

Use of land is roughly shown in the following chart (**Figure 56**), where we can see that 32.8% of the city area is covered with forest; the same portion goes to agriculture and just 19.7% to constructed area (Source: Year Book, Klagenfurt 2012 – 04/06/13).

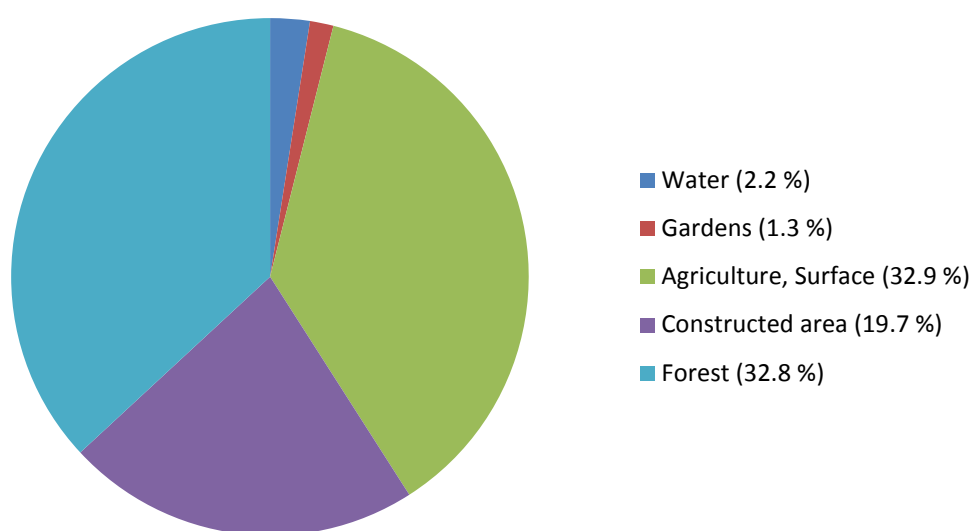


Figure 56: Land covered with waters, buildings or forests, or used for gardens and agriculture/surface (Source: Year Book, Klagenfurt 2012).

In **Figure 57** and **Figure 58**, the sampling sites of measurements in Klagenfurt and Zell are presented. The sampling site in Klagenfurt was located at the measuring station of the Environment Department of the Regional Government of Carinthia, Völkermarkter Strasse (**Figure 57**). This location is directly impacted by local traffic. At the measuring station, daily measurements of SO₂, PM₁₀, NO₂, CO, and HC are carried out. To existing measurements the measurements of BC were added, with the Aethalometer on both measurement stations. In the Klagenfurt town center a lot of trucks, vans and other vehicles burning diesel and gasoline fuel can be expected.

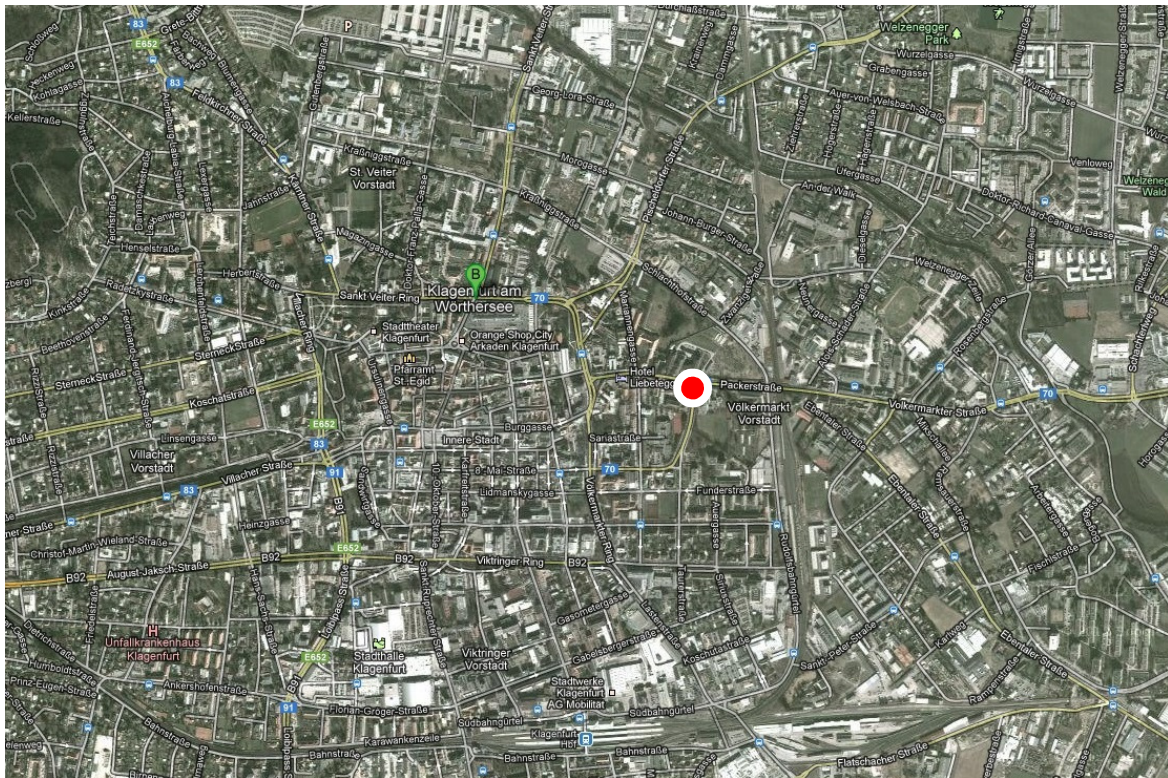


Figure 57: Urban measurement station in the Klagenfurt city center, Völkermarkter Strasse – marked with the red dot (Source: Google maps – 05/22/13).

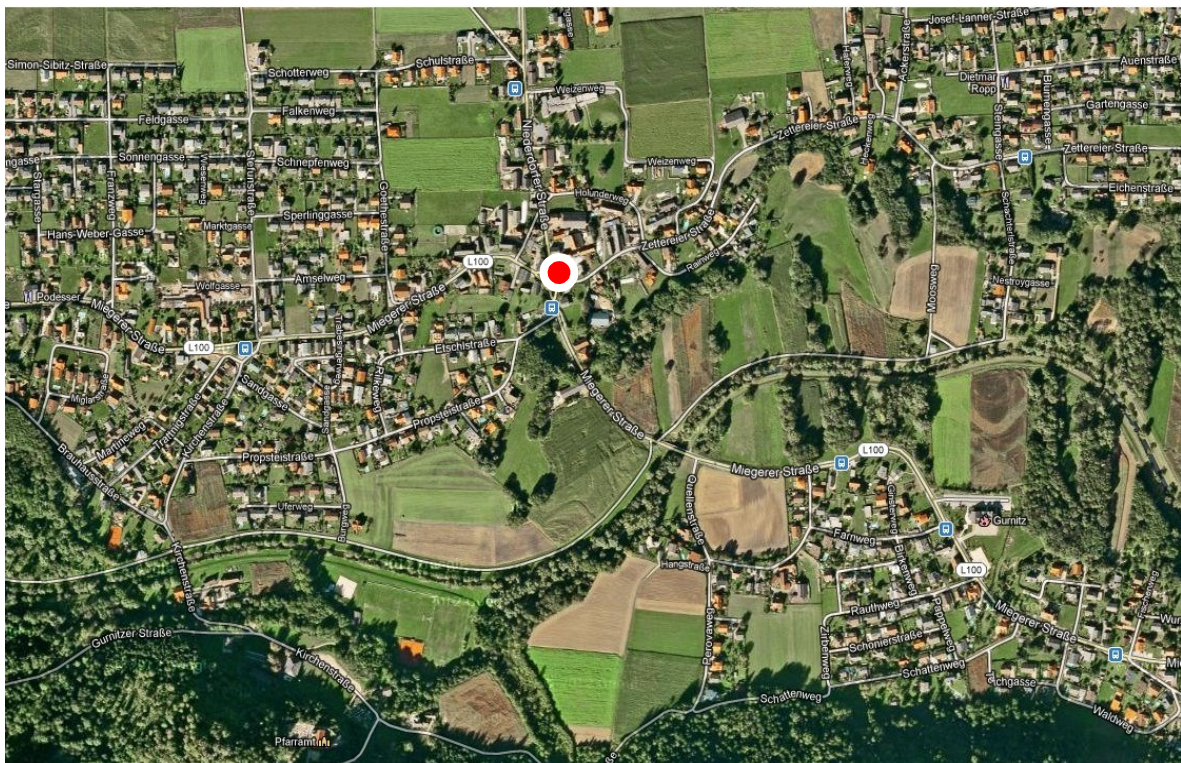


Figure 58: Rural measurement station in the village of Zell – marked with the red dot (Source: Google maps – 05/22/13).

In **Figure 58**, the position of the second measuring station in Zell is depicted. The measuring station in Zell is also located near a street; however, traffic there is not as heavy as in Klagenfurt. In Zell, mostly motorbikes and tractors are present. As for cars, those burning diesel fuel prevail, because using diesel fuel is less expensive especially for long distance driving.

5.2. Sources of energy and emissions

Data on sources of energy and emissions that follow are valid for the whole Carinthia region. **Figure 59** shows the use of different sources of energy for the years 2005 and 2010. Klagenfurt is the biggest city in Carinthia. The highest growth rates of an energy source were achieved in the use heat pumps and district heating, so the share of renewable energy sources increased from 39% to 48%.

The highest total effective impact in terms of energy efficiency and renewable sources of energy is achieved through the installation of solar thermal systems. Ranked next is the use of biomass heating systems or connection to biomass district heating.

The following pies (**Figure 59**) show the change in the fuel mix used for Carinthia for the years 2005 and 2010.

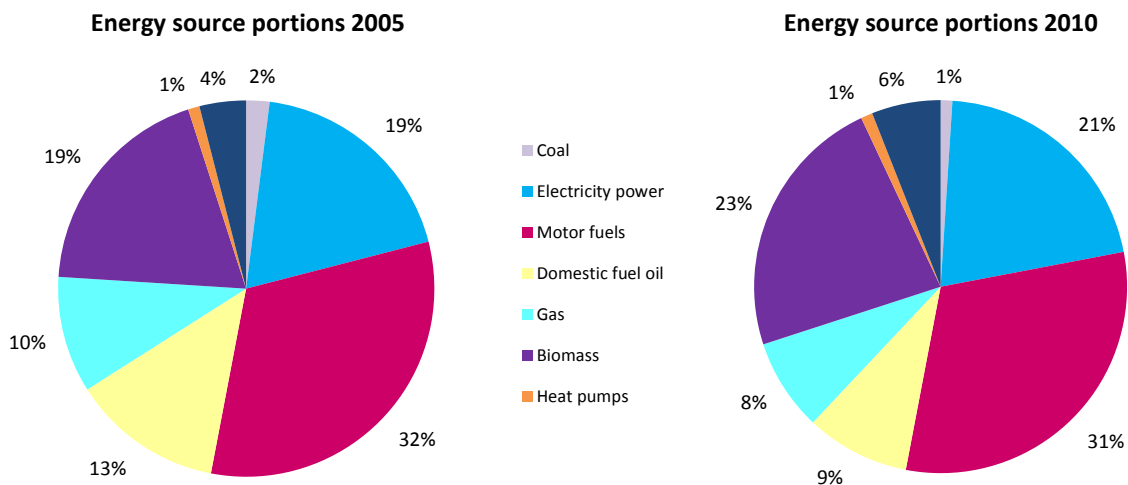


Figure 59: Sources of energy in Carinthia for the years 2005 and 2010 (Source: Environmental Report Carinthia 2012 – 4/6/13).

As obvious from the pie charts, the share of biomass as a source of energy increased from 19% to 23%, the share of district heating from 4% to 6%, and the share of electricity power from 18% to 21%. Simultaneously, heating oil's share dropped from 13% to 9% as well as that of gas, namely from 10% to 8%.

The statistics show that pollutants in the countryside mainly come from combustion processes and re-suspension of dust into the atmosphere. The emissions stem largely from the region and traffic, the production of energy from industrial processes and household heating (domestic). The sources of air pollutant emissions to the atmosphere are usually divided into groups of emitters, including industry (including power plants), transport and small consumers.

Using a computer model based on emission data from enterprises and on statistical data and emission factors for these main groups of emitters, an emission inventory calculation of the existing emissions from industrial, commercial and heating plants as well as traffic and domestic heating was created (Source: Environmental Report Carinthia 2012). These data are represented in **Figure 60**.

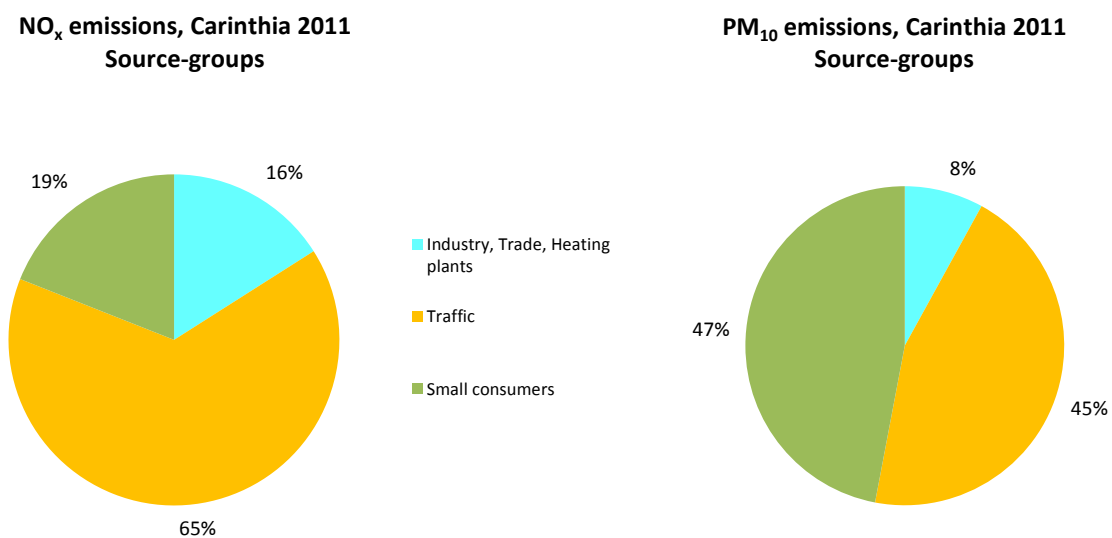


Figure 60: NO_x and PM₁₀ emissions from industry/trade/heating plants, traffic and small consumers in Carinthia (Source: Environmental Report Carinthia 2012).

The most important emitter of NO_x is traffic, which is confirmed by data presented in the left pie chart of **Figure 60**. If we observe the overall contribution of transport, we can see that transport accounts for 65% of NO_x, while its share of PM₁₀ contribution is 20 percentage points lower. The situation is opposite in the case of small users, since their impact on PM₁₀

particle production is the highest, i.e. 47%. In the case of NO_x , their influence accounts for 19%, which is 26% less compared to PM_{10} .

It is evident from the pie charts that emissions of PM_{10} particles are strongly influenced by small-scale users, which include furnaces, central plants, etc. (Source: Environmental Report Carinthia 2012).

In **Table 12**, numbers of PM_{10} exceedances (daily values) per month and year are shown for both stations (Ebenthal – Zell and Völkermarkter Strasse – Klagenfurt). Data were supplied by PMinter project partners.

European limit values for PM_{10} (annual mean value $40 \mu\text{g}\cdot\text{m}^{-3}$, daily mean value $50 \mu\text{g}\cdot\text{m}^{-3}$; Air Quality Directive EC/50/2008) cannot be met in most Austrian, Slovenian and European cities. Road traffic is the main cause of this, followed by residential heating. At least 50% of the PM_{10} exposure cannot be specifically defined, which means that this background exposure cannot be directly influenced through local measures (<http://pminter.eu> – 05/05/13).

Table 12: Number of PM_{10} exceedances ($\text{TMW} > 50 \mu\text{g}\cdot\text{m}^{-3}$) per month and year.

Station	Winter 2011/12				Winter 2012/13			
	Dec 11	Jan 12	Feb 12	$\Sigma_{\text{observations}}$	Dec 12	Jan 13	Feb 13	$\Sigma_{\text{observations}}$
Zell – Ebenthal	2	6	4	12	8	7	1	16
Klagenfurt – Völkermarkter Strasse	5	10	9	24	7	9	5	21

From **Table 12**, strong pollution in the city (Klagenfurt) can be inferred, where the excess of PM_{10} values is about twice as high in all months (Dec 2011–Feb 2012) of winter 2011/12 as in Zell.

Winter 2012/13 shows a completely different picture. Rural and urban areas witnessed almost the same number of PM_{10} exceedances in the first two winter months, while in February the number of PM_{10} exceedances in Zell fell to 1 and in Klagenfurt to 5. By comparing the two winters, it can be concluded that winter 2012/13 was "cleaner" in Klagenfurt and much more polluted in Zell. The reason may lie in much harder winter 2012/13 conditions than experienced in the winter of 2011/12.

5.3. Results

The results include the analysis of samples gathered at two monitoring sites: Klagenfurt as an urban site and Zell as a rural site. In the last chapter, the main focus is put on the Angstrom exponent and the question about its value and impact in the real environment.

For further analyses, we have used the values of the absorption Angstrom exponent (α) (see **Table 14**), where α of diesel exhaust (α_{ff}) is 1.0 and α of wood smoke (α_{wb}) is 2.0. These are standard values used in various present studies: Sandradewi et al., 2008, Favez et al., 2010, Kirchstetter et al., 2004. In the chapter of wood-burning (4.4.2. Determination of the absorption Angstrom exponent) is shown that primary sources of wood smoke give an α around 2.0 during different burning phases (phase 1 or phase 2).

5.3.1. Urban and rural emissions – black carbon measurements

Using the Aethalometer optical method, the black carbon concentration was measured for two consecutive winter periods, from November 2011 until February 2012 and from November 2012 until February 2013. The long-time periods of black carbon measurements are shown in **Figure 61** for 2011/12 winter period and in **Figure 62** for 2012/13 winter period.

Graphs in **Figure 61** and **Figure 62** depict the time evolution of BC concentration in Klagenfurt and Zell. In the city of Klagenfurt, concentrations of BC are high because of different emission sources. Traffic contributes a major impact on the air pollution in the city, however, a substantial portion can also be ascribed to wood-burning and power plants. With the Aethalometer (AE31-ER), we detect the light absorbing part of the particulate matter; our concern here is the carbonaceous fraction of it.

Zell is located in the countryside where mostly local traffic is present with addition to some trucks or tractors a few times per day. In the summer time, the air pollution should not pose a big problem, but in the winter time, the problem with wood smoke arises. Many domestic heating systems depend on wood because it is cheap and convenient.

In **Figure 61** or **Figure 62**, it can be seen that on specific days pollution in the village is as high as in the city. This could be due to the impact of surroundings (local or regional pollution). However, with the real-time measurement of the Aethalometer, a time resolution of 5 minute periods or less can be achieved and thus the actual sources of pollution could be identified. The dilution distance of the source must also be of importance. One would think that the longer the distance from the source the lower is the BC concentration; nevertheless,

this is not true for PM and also for BC emissions, because the relative amount can stay constant at the end. PM is the "sum" of primary and secondary aerosols, so the PM concentration may vary less spatially due to the formation of secondary aerosols (Hallquist et al., 2009). Prolonged periods of higher contamination were detected during the months of December 2011/12 and 2012/13 (**Figure 61** and **Figure 62**), and January 2011/12 (**Figure 61**).

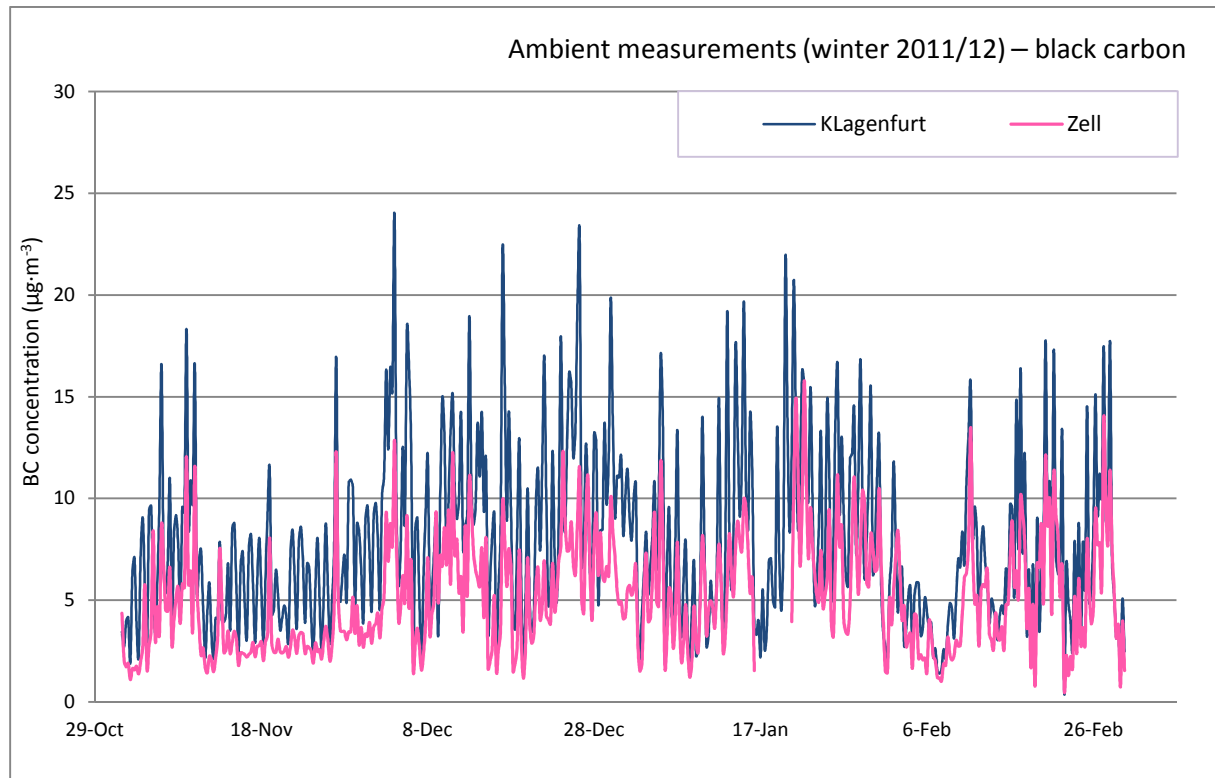


Figure 61: Black carbon concentration measured in urban (Klagenfurt) and rural (Zell) areas with Aethalometer during 2011/12 winter period.

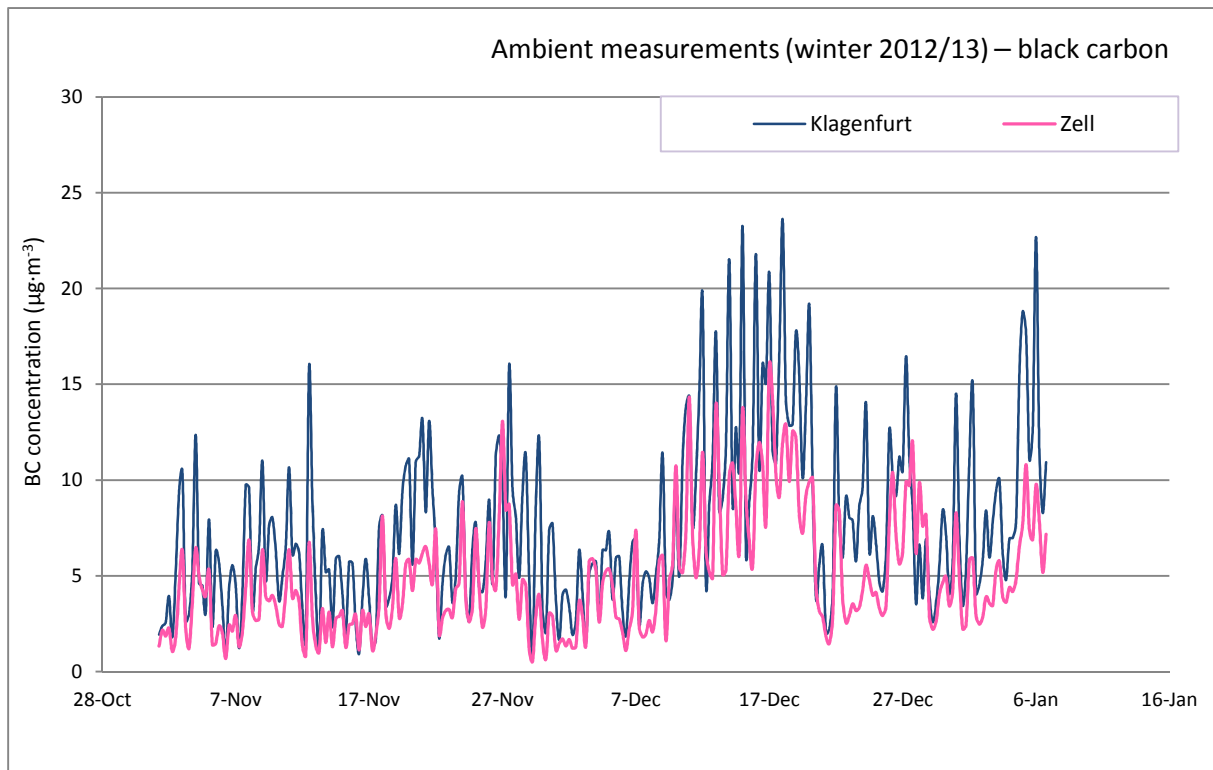


Figure 62: Black carbon concentration measured in urban (Klagenfurt) and rural (Zell) areas with Aethalometer during 2012/13 winter period.

In **Figure 63**, it can be seen that the use of the Aethalometer model allows us to distinguish between BC_{ff} and BC_{wb} because the instrument is capable of detecting the absorption at seven wavelengths (370 nm–950 nm). BC_{wb} is BC originating from wood smoke emissions and BC_{ff} is BC emitted by burning diesel and gasoline, heating oil and coal, which is neglected because of its minor source of 1% (see **Figure 59**).

With the use of the Aethalometer model, source apportionment can be attributed to traffic (diesel emissions) or wood-burning (wood-burning emissions).

Histogram in **Figure 63** shows the BC concentrations and BC fractions for both measurement stations. The BC concentrations originating from traffic (BC_{ff}) in Klagenfurt are twice as high as traffic related BC concentrations in Zell. This can be expected (Dobovicnik, 2008), considering the size of the city and daily commuters that drive in the city to work and back from surrounding towns; Klagenfurt is the center of Carinthia and therefore a big “source” of pollution.

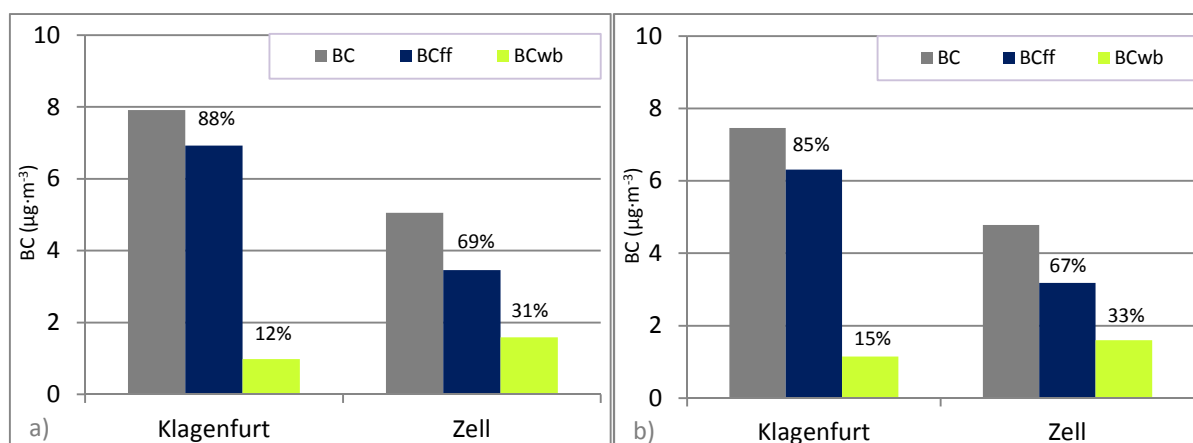


Figure 63: BC fractions of wood-burning (BC_{wb}) and fossil fuel (BC_{ff}) in Klagenfurt and Zell for a) winter 2011/12, and b) winter 2012/13.

As expected, wood-burning emissions in winter 2011/12 (BC_{wb}) are higher in Zell than in Klagenfurt (for 19 percentage points). The same trend was recognized in the 2012/13 winter period (from 15 % to 33%). Both winter campaigns (2011/12 and 2012/13) present almost the same portions of source. This is not evident only from **Figure 63**, but also from the following table (**Table 13**) where average results of absorption Angstrom exponent (α) and average BC concentrations are given.

The α value for Klagenfurt is almost 1.2 which tells us that traffic emissions and organic substances that result largely from the combustion of wood smoke prevail. The average value of α in Zell is approximately 1.4 which means that an impact of wood-burning emissions in the town is present. Usually, the α values for wood-burning emissions start from 1.3 onwards (see Chapter 3). In winter 2012/13, the same situation was observed, despite of the fact that the concentrations were slightly lower and the Angstrom exponent values were higher.

Table 13: The average values of the Angstrom exponent (α) and black carbon concentration (BC) during winter periods of 2011/12 and 2012/13 with standard deviations and median values.

	Winter 2011/12						Winter 2012/13					
	α	St. dev.	Median	BC ($\mu\text{g}\cdot\text{m}^{-3}$)	St. dev.	Median	α	St. dev.	Median	BC ($\mu\text{g}\cdot\text{m}^{-3}$)	St. dev.	Median
Klagenfurt	1.19	0.11	1.18	7.91	5.27	6.68	1.21	0.09	1.22	7.46	5.11	6.16
Zell	1.38	0.12	1.38	5.05	3.30	3.97	1.40	0.10	1.41	4.79	3.38	3.84

As for α values, there are small standard deviations, and median values are therefore equal to the average values. The variations (st. dev.) of BC concentrations are much higher, so the

median values are lower than the average values; we get log- instead of Gaussian-distribution.

Zell has the highest BC_{wb} concentration and Klagenfurt the highest BC_{ff} concentration. An even more detailed analysis featuring contributions of BC_{wb} and BC_{ff} on an hourly basis can be seen in the next section about apportionment.

5.3.2. Source apportionment – residential combustion and traffic

The method used for source apportionment was the Aethalometer model (Sandradewi et al., 2008, Section 2.2.3.2) but extended to the seven wavelengths. The graphs below (**Figure 64** and **Figure 65**) show the daily BC concentration in 2012/13 winter season. A similar phenomenon also occurred in the 2011/12 winter.

First, concentrations sampled in Klagenfurt between Monday and Thursday, which are normal working days, are compared. During these periods, it is interesting to observe the peaks as the result of rush hours in the city. These happen in the morning between 7:00 am and 9:00 am, when people go to work, and between 4:00 pm and 6:00 pm when they return back home. At these times, we witness to an almost identical increase of morning and evening concentrations of BC_{ff} on all four days (from Monday until Thursday). BC concentrations in rush hour periods are high – between 10 and 13 $\mu\text{g}\cdot\text{m}^{-3}$. Fridays are different; morning concentration increases up to 8 $\mu\text{g}\cdot\text{m}^{-3}$ and stays on almost the same level from 7:00 am to 3:00 pm. In the evening, it increases again up to $\sim 11 \mu\text{g}\cdot\text{m}^{-3}$. A general explanation for this occurrence is that people leave the city on Fridays to return home or come visit their homes in Klagenfurt for the weekend. Similarly, high concentration on Sunday evenings can be observed. Saturday does in fact count to working days, but this day was excluded from the measurements and only average working days and Sundays (weekends) were compared. On Saturdays, much fewer people commute to work in the morning, but nevertheless a slight increase in the BC concentrations of morning traffic can be noticed, probably due to heavy duty trucks, which have driving permission until 1 pm. On weekends (Sundays), the BC concentration increases in the afternoon and evening due to household heating, commuters and weekend traffic. BC_{wb} concentrations are about the same on workdays and weekends, which suggest that the emissions of household heating might be constant in the city.

Diurnal BC plots – Klagenfurt, winter 2012/13

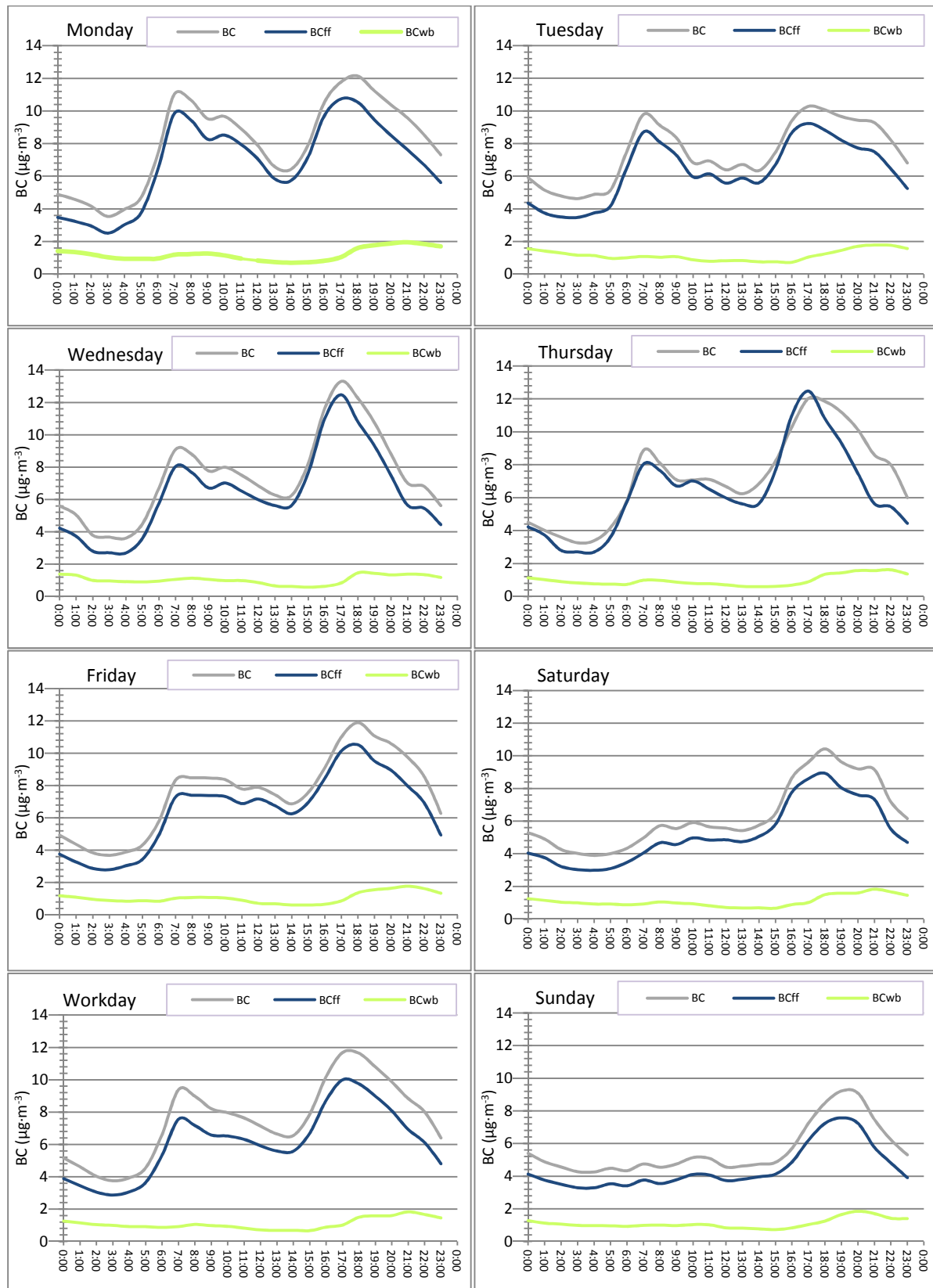


Figure 64: Diurnal plots of BC concentrations/fractions for workdays and weekends in Klagenfurt –2012/13 winter period.

Diurnal BC plots – Zell, winter 2012/13

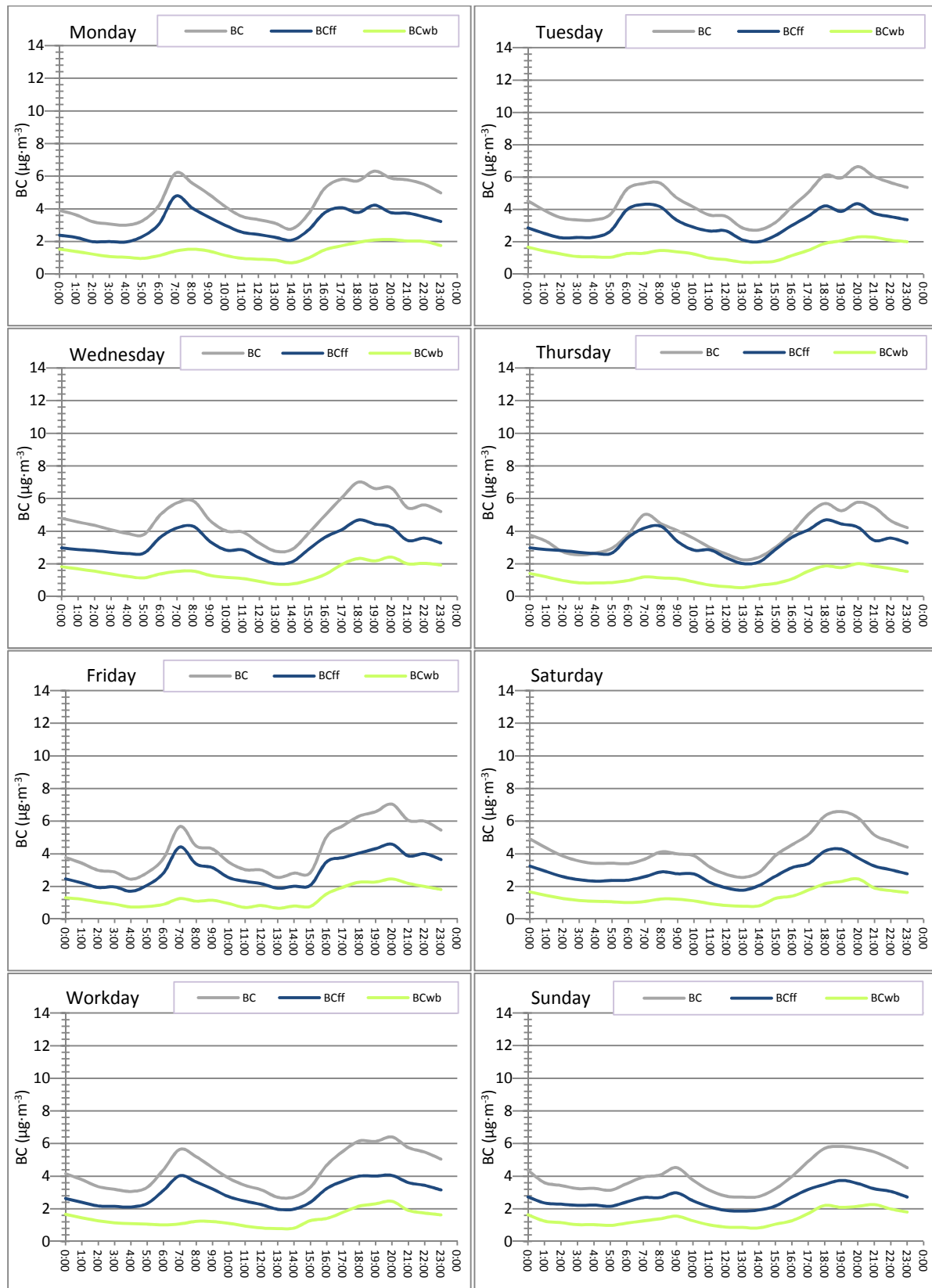


Figure 65: Diurnal plots of BC concentrations/fractions for workdays and weekends in Zell – 2012/13 winter period.

Workdays in Zell show the same situation during rush hours as presented in Klagenfurt, i.e. the BC concentration increase in the morning and in the afternoon. BC concentrations in the afternoon (on some days) remain high not just during “rush hour” but even longer, until late in the evening. On weekends, increase of BC concentration in the morning can be observed due to home heating. BC_{wb} fractions are higher in Zell than in Klagenfurt.

In the next two figures, the diurnal plots of the absorption Angstrom exponent (α) behavior during working days and weekends (Sunday) are shown for 2011/12 winter period (**Figure 66**) and 2012/13 winter period (**Figure 67**).

When comparing both winter seasons (2011/12 and 2012/13), almost no difference can be recognized, but a comparison of both measurement locations (Klagenfurt and Zell) shows some deviations in the values of α .

The values of α (**Figure 66**) in Klagenfurt range between 1.1 and 1.3, which indicates the presence of traffic emissions, while the values around 1.3 can already be attributed to the traces of wood smoke in the ambient air. In Zell, the situation is a little bit different. There, the values of α are mostly above 1.3, and on Sundays they even almost constantly range around 1.45 ± 0.05 .

The values of α in **Figure 67** where data for 2012/13 winter period are presented are the same as the ones in **Figure 66**. The α values increase during evening and afternoon on workdays and decrease during the day when there is no rush hours. During the weekend, the α values are more constant, especially in Zell, while in Klagenfurt, a slight decrease during the day can be observed.

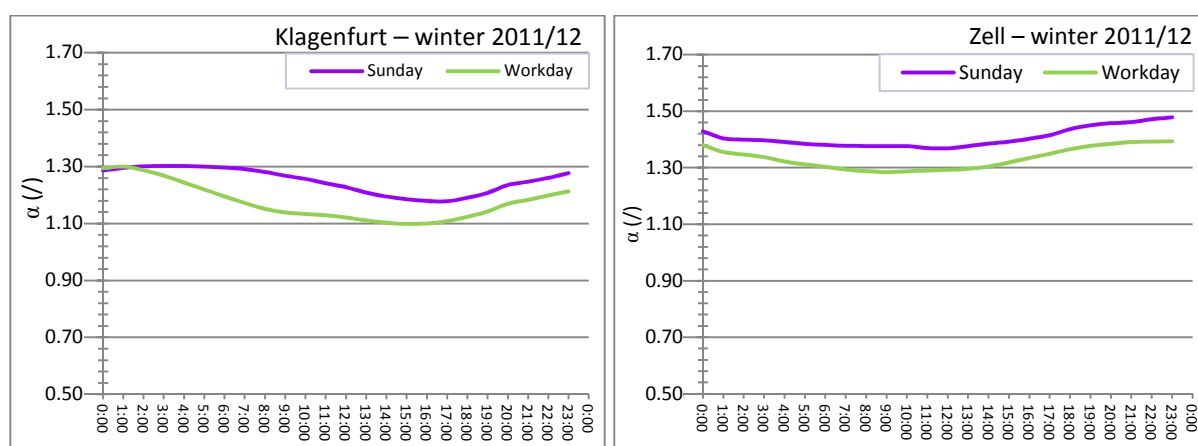


Figure 66: Diurnal plots of the absorption Angstrom exponent values for Klagenfurt and Zell in the 2011/12 winter period.

Figures also show how high the contribution of wood smoke to contamination during the weekend is. Both in Klagenfurt and in Zell, the values of α are higher than the predicted value of the α for traffic emissions; i.e. higher than 1.2.

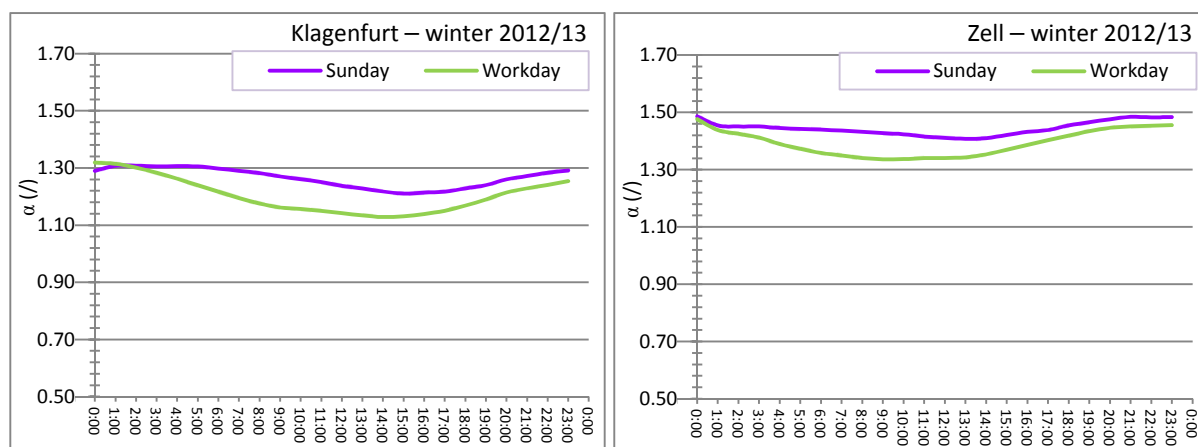


Figure 67: Diurnal plots of absorption Angstrom exponent (AAE) values for Klagenfurt and Zell in the 2011/12 winter period.

When comparing the results from both measurement stations, we come to the conclusion that Klagenfurt is more exposed to the influence of traffic ($\alpha \approx 1.0 \pm 0.1$), while in Zell more wood smoke (α above 1.2) is present in the atmosphere. However, the relative contribution of wood smoke and traffic varies slightly when the two winter periods are compared, as illustrated in **Figure 68**.

Figure 68 shows the relative contributions of CM_{ff} and CM_{wb} at both stations during the two winter periods. CM fractions are the ones that tell us, which source contributes to PM_{10} the most (a mixture of primary and secondary aerosols). Primary particles are directly emitted to the atmosphere, while secondary particles are formed in the atmosphere by condensation (nucleation and growth) after chemical transformation (Hallquist et al., 2009). In winter 2011/12, the wood-burning emissions in Zell were around $10 \mu\text{g}\cdot\text{m}^{-3}$ higher than in winter 2012/13; one of the reasons can surely be attributed to very low temperatures in winter 2011/12.

In winter 2012/13, a decrease in traffic emissions can be observed. The reason for this is hard to explain. Maybe increased use of public transport due to rises in fuel prices could be a reasonable cause.

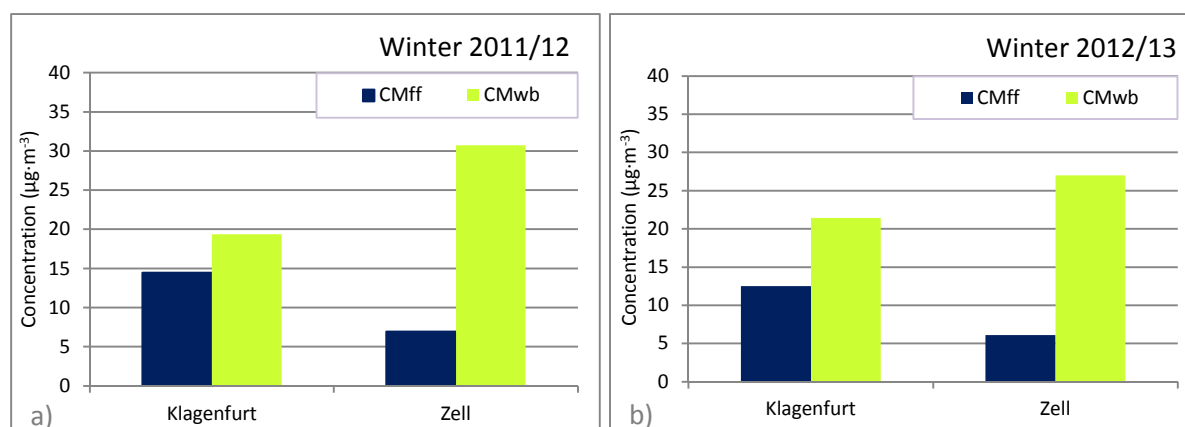


Figure 68: Source apportionment for Klagenfurt and Zell in a) winter 2011/12, and b) winter 2012/13.

The BC concentration in **Figure 63** represents the primary pollutants, while the concentration of CM in **Figure 68** also represents the secondary pollutants and a big portion of PM emissions. The benefit of using the two-component Aethalometer model is that the model does not distinguish between primary and secondary pollutants and therefore it is easier to evaluate the source. BC tells us more about source apportionment and CM more about the contribution to PM.

In summary, Klagenfurt is more affected by traffic, while in Zell more wood smoke is present in the atmosphere.

5.3.3. Anhydrosugars – tracers of wood-burning

As expected, the levoglucosan anhydrosugar was the most organic (Schmidl et al., 2008), and was found in all analyzed wood smoke samples. In a previous study concerning the stability of levoglucosan, Simoneit et al., 2004, found no degradation due to acid-catalyzed hydrolysis which took place under conditions simulating the aqueous chemistry of atmospheric droplets for over 15 days.

Since open-air burning of agricultural waste is not allowed in Austria, and is indeed rarely seen, we can conclude that the presence of levoglucosan in ambient PM in Austria must indicate the burning of wood for domestic heating (Schmidl et al., 2008).

In **Figure 69**, a comparison between BC_{wb} and levoglucosan data for both measurement stations (Klagenfurt and Zell) is presented. The anhydrosugar analyses were carried out at the Institute of chemical analyses and technologies, TU Vienna as part of the PMinter project.

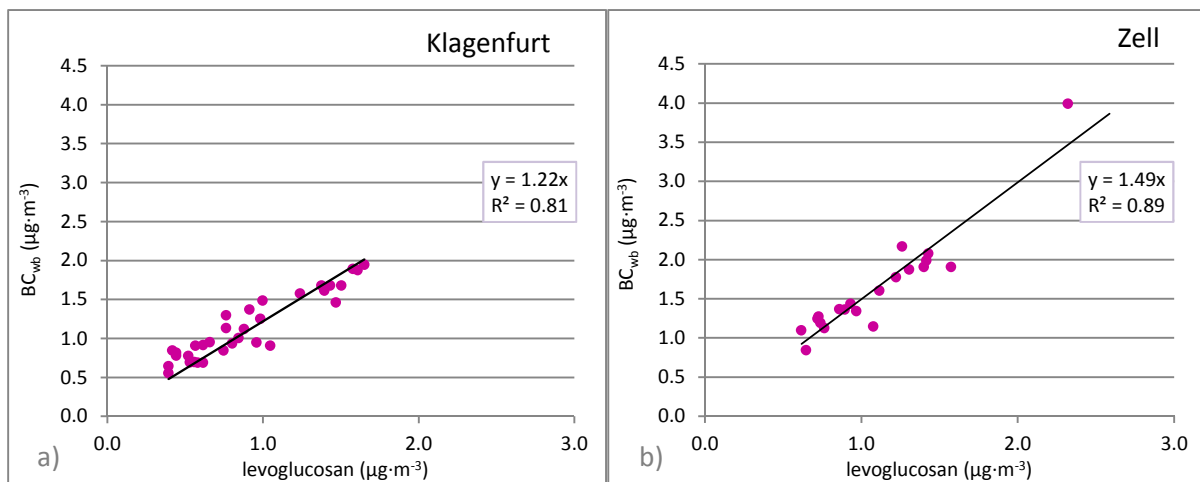


Figure 69: Sugar analyses: BC concentration dependence of wood-burning emissions (BC_{wb}) from levoglucosan measured with Aethalometer, and analyzed with HPLC method: a) Klagenfurt – Völkermarkter Strasse, and b) Zell – Ebenthal.

The comparison of BC_{wb} data calculated from the Aethalometer model and levoglucosan concentrations of the winter campaign (January 28–March 2, 2011) gives a linear dependence. The well correlated slope ($R^2 = 0.81$ and $R^2 = 0.86$, **Figure 69**) of BC_{wb} /levoglucosan ratio confirms the presence of wood smoke in the samples, as both BC_{wb} and levoglucosan are parameters (tracers) of wood smoke. BC_{wb} /levoglucosan ratio, according to other results, tells us that both methods correlate very well together, while the results from the sites do not confirm that and have to be discussed further. In the scatter plot (**Figure 69, b**) of Zell measurement, we observe a few high concentrations which may be the result of an almost direct entry of wood smoke in the sampling system due to a nearby source. Concentrations of levoglucosan in this case do not exceed the value of $3 \mu\text{g}\cdot\text{m}^{-3}$.

5.3.4. Sensitivity of the Aethalometer model when changing the absorption Angstrom exponent of wood-burning (α_{wb}) and fossil fuels (α_{ff}) for 10%

To examine the sensitivity of the Aethalometer model, different values were set for the Angstrom exponent of wood smoke (α_{wb}) and fossil fuel (α_{ff}). Sensitivity was investigated by setting the α_{ff} and α_{wb} values $\pm 10\%$ (**Table 14**). In the following tables (**Table 15** and **Table 16**), the data of BC_{wb} are presented according to the described change in α . The variations of the calculated BC_{wb} concentrations and the resulting relative contributions are most important, as wood smoke emissions form a major contribution to PM concentrations in the regions (Klagenfurt or Zell).

Table 14: Five different calculations resulting from a change in the absorption Angstrom exponent of fossil fuel (α_{ff}) and the absorption Angstrom exponent of wood-burning (α_{wb}) for $\pm 10\%$.

	α_{ff}	α_{wb}
I	1.0	2.0
II	0.9	2.0
III	1.1	2.0
IV	1.0	1.8
V	1.0	2.2

When examining the results obtained for winter 2011/12 (**Table 15**), the impact of a changed α_{ff} for Klagenfurt is found to be around 3 times greater when decreasing the α_{ff} for 10%, rather than increasing it; α_{wb} remains unchanged and is 2.0. In Klagenfurt, the contribution of traffic emissions to pollution is about 80%, while in Zell it ranges between 60 and 70%. In Zell, the decrease of α_{ff} also has a greater impact than the increase of α_{ff} . In this case, the contribution of wood-burning emissions increased for 27%.

In Klagenfurt, the decrease of α_{wb} also has a greater impact on the results than the increase; decreasing of α_{wb} leads to a 43% contribution of wood-burning to ambient emissions.

An observation of sensibility by setting the right α in the winter 2012/13 (**Table 16**) brings similar results. Change of α_{wb} for $\pm 10\%$, especially an increase of α_{wb} , contributes to the same deviations as in the winter 2011/12. These deviations are more significant in the case of Zell, as here more wood-burning emissions are present.

Table 15: The wood-burning contribution to ambient emissions in the 2011/12 winter period when using the source apportionment model.

		Winter 2011/12			
				Klagenfurt	Zell
	α_{ff}	α_{wb}	BC _{wb} (%)		
I	1.0	2.0	12.4	31.5	
II	0.9	2.0	17.9	35.8	
III	1.1	2.0	5.7	26.2	
IV	1.0	1.8	16.8	42.5	
V	1.0	2.2	9.6	24.2	

Table 16: Wood-burning contribution to ambient emissions in the 2012/13 winter period when using the source apportionment model.

Winter 2012/13					
		Klagenfurt	Zell		
	α_{ff}	α_{wb}	BC _{wb} (%)		
I	1.0	2.0	15.4	33.4	
II	0.9	2.0	20.6	37.6	
III	1.1	2.0	8.8	28.3	
IV	1.0	1.8	20.7	45.2	
V	1.0	2.2	11.8	25.7	

The model shows great sensibility when changing the α_{wb} value. The selection of the right α_{wb} value has a big impact on the source apportionment of wood-burning, especially in Zell. In Klagenfurt, where traffic is the main emitter, the deviation in α_{ff} is very important and it influences the portion of BC_{wb} by up to 70%. For the Aethalometer model, it is therefore very important, which value of α_{ff} and α_{wb} is chosen. Too low or too high values of α_{ff} and α_{wb} can lead to false conclusions of the source apportionment. However, the values of the Angstrom exponents for traffic emissions are very well determined and lie close to the value of 1.0 for wood-burning, the values are less well known but also not expected to vary greatly. In this context, stable results from the Aethalometer model can be expected.

CHAPTER 6

Summary and conclusions

The study is composed of three separate experiments in which optical properties of carbonaceous aerosols were measured. The following was investigated in the study:

1. Determination of the dependence of the optical absorption of the emitted aerosol on the combustion efficiency in a CAST propane burner;
2. Analysis of primary emissions from wood stoves when using different wood types (beech, spruce and pellets); again with special focus put on the determination of the aerosol optical absorption;
3. The field measurement campaign in which the results obtained during experiments 1 and 2 were used to quantify the influence of emissions from traffic and wood combustion on ambient concentrations of particulate matter.

The CAST experiment

The CAST burner was used to produce aerosols at various fuel-to-air ratios (C/O ratio) to form a wide range of various carbonaceous aerosols. Each condition (i.e. fuel-to-air ratio) included two parts. The first part involved measurements without mixing gas (N₂) added to the combustion process. In the second part, nitrogen as mixing gas was present in the combustion process.

In our research, we generated aerosols with four different C/O ratios (0.21, 0.31, 0.41, and 0.60). At low C/O ratios (0.21 and 0.31), black and dark brown aerosols were produced, while at higher C/O ratios (0.41 and 0.60) brown and orange aerosols were deposited on the filters – the colors were easily visible. According to their color, the filters have completely different absorption characteristics. Absorption coefficient is decreasing with increasing wavelength: from $6.64 \cdot 10^{-2} \text{ m}^{-1}$ (at 370 nm) to $5.24 \cdot 10^{-4} \text{ m}^{-1}$ (at 950 nm). The colored filters (brown and orange) give a steeper slope in a log-log plot of that dependence than the black filters, where the slope is smaller. Dark filters contain black carbon (BC) and a mixture of BC and brown carbon (BrC), while colored filters contain more organic material and BrC and just some traces of BC along with other substances.

Thermal-optical methods are useful for analyzing the portion of elemental carbon (EC) and organic carbon (OC) in each sample. The results of the OC-EC measurements using a dual-

optical instrument (Sunset Analyzer) show that with the increase of the C/O ratio OC increases and EC decreases – the EC/TC ratio decreases from $\sim 80\%$ at the C/O ratio of 0.21 to $\sim 5\%$ at the C/O ratio of 0.60.

In the experiment, two temperature protocols were used: NIOSH 5040 and EUSAAR 2. We discovered that in our case no significant difference can be recognized when using one or the other protocol, as it could have been expected if considering Cavalli et al., 2010. However, the automatic or manual setting of the split point did show significant differences in the detection of EC concentration for a number of samples. In the filter sample with C/O ratio of 0.31, the manual setting of the split point reduced the EC concentration by a factor of 3. According to the other analytical methods used, the automatic setting of the split point would have given an over-estimation of EC concentrations due to heavily loaded filters.

Optical analyses conducted with an integrating sphere photometer (IS) gave results regarding BC and BrC deposited on the filter samples. Here, the same trend as with thermal-optical methods was recognized: with increasing C/O ratio, BC decreases and BrC increases. The BC concentrations analyzed with integrating sphere match the results obtained with the Aethalometer optical method. Optical methods are not influenced by pyrolysis, whereas thermal-optical methods can be, which may explain the difference in results that occurs between optical and thermal-optical methods and the overestimation of EC concentrations. Differences between integrating sphere and Aethalometer occur due to instrumentation differences and differences in calibration.

Due to methodology used within the Aethalometer, data are affected by multiple scattering and shadowing effects. In order to compensate these deviations, the procedure introduced by Weingartner et al. (2003) was applied. If we calculate the absorption Angstrom exponent α using different compensation algorithms (Weingartner et al., 2003, Arnott et al., 2005, Kirchstetter et al., 2007), we get to fairly similar results each time. The Angstrom exponent increases with an increasing C/O ratio – the more OC content we have, the higher the Angstrom exponent is. With the Aethalometer model, we can identify BrC and BC contributions to absorption. High α -values, up to 5.5 were observed in conditions with the C/O ratio of 0.60 without the mixing gas, while in measurements with the C/O ratio of 0.21 α values ranging between 1.2 and 1.8 were identified. When observing the Angstrom exponent of the samples with mixing gas added in the process, one can notice that the values of the Angstrom exponent are higher ($\alpha = 7$).

The wood-burning laboratory experiment

A special wood-burning system was built for the experiment in which primary emissions of wood combustion were measured. Beech and spruce logs and pellets were used as a wood-burning material in two types of stoves.

To account for the heterogeneity which had to be expected for single experiments, four burnings were carried out for each log type. Results of tests show that it is impossible to repeat a burning to get the same results even if both burnings have the same preparation, ingredients and sampling time. Emissions from pellet stoves were different: PM emissions of pellet burning tests were more stable and emissions were much lower than those of log wood burning.

Average values of beech and spruce emissions in the PM₁₀ and PM_{2.5} samples show that burning of beech produces less OC and more EC compared to spruce. In the case of pellets, the results for PM₁₀ and PM_{2.5} match. This means that PM₁₀ emissions are actually PM_{2.5} emissions.

When comparing different analytical methods (the Aethalometer optical method and thermo-optical method), the analyses of spruce smoke samples show markedly higher BC concentrations than EC concentrations. Dark filters are making it difficult to set the split point in the OC-EC dual-optical instrument software because the laser line is flat and a significant portion of EC may be represented as OC or vice versa. BC concentration matches the EC concentration values regarding the beech and pellet samples. The BC concentration of pellet smoke samples is lower than the EC concentration on the filters of both particle separators (PM₁₀ and PM_{2.5}).

The influence of using two different temperature protocols (NIOSH 5040 and EUSAAR 2) on the OC/EC split was investigated. The results show that by using the NIOSH 5040 protocol a higher EC concentration is detected, while with the EUSAAR 2 protocol higher OC concentrations are obtained. For analyses of pellet smoke samples, the choice of the temperature protocol is irrelevant.

The absorption Angstrom exponent (α) values were calculated from the Aethalometer data for each wood type. The burning cycle was divided into two phases: phase 1 was the one with a load of wood in the cold stove, and phase 2 was the one with a new load of wood in the hot stove. As the Aethalometer is an on-line instrument, it was possible to investigate the burnings with higher temporal resolution. Spruce smoke emissions in phase 1 (including a cold start) increase values of the Angstrom exponent up to 2 or more, which tells us that the content of organic matter from spruce combustion is very high in phase 1 and lower in phase 2 (mostly around α of 1.0, but some values also reach α of 2.5). Resin in spruce wood

can play an important part in the increase of α . α values of beech emissions in phase 2 reach only α of 1.6, while in phase 1 the values are even lower.

Anhydrosugars, products of burning cellulose, can be utilized as indicator compounds for presence of emissions from wood-burning of atmospheric fine particulate matter. Calculated ratios of levoglucosan to mannosan are around 2.5 for spruce (softwood), which is in agreement with Schmidl et al. (2008). The same value was calculated for pellet composition; pellets are in fact produced of softwood (100%). The results confirm that levoglucosan is a major organic component emitted as fine smoke PM from wood-burning and it is accompanied by other monosaccharaides (mannosan and galactosan).

Ambient measurements

Ambient measurements were performed during two winter periods (2011/12 and 2012/13) in the Klagenfurt basin in Carinthia. They were carried out at the Carinthia's roadside air quality station in Klagenfurt, which served as an urban site, and in Zell, located in the same basin, which served as a rural site. Klagenfurt (capital of Carinthia, approx. 94000 inhabitants) is impacted by traffic and wood-burning emissions, while Zell is a small village (approx. 600 inhabitants) at the edge of the basin and close to forests and surrounding hills. To measure the air pollution at these two sites, two Aethalometers were employed. Particles were also collected on High Volume filters in the 2011 winter campaign (January 28–March 2, 2011). The Aethalometer data were processed with the Aethalometer model and filters were analyzed with liquid chromatography to measure the amount of anhydrosugars, which are tracers of wood-burning.

The overall value of the absorption Angstrom exponent for Klagenfurt is almost 1.2, which signifies a major presence of traffic emissions and some organic substances which predominantly originate from wood combustion. The average value of α in Zell is approximately 1.4, which points to an impact of wood-burning emissions in this region. The use of the Aethalometer model enables us to distinguish between BC concentration from traffic (BC_{ff}) and BC concentration from wood smoke emissions (BC_{wb}). In Klagenfurt, the pollution originating from traffic (BC_{ff}) is twice as high as in Zell. Wood-burning (BC_{wb}) contributions to PM are higher in Zell than in Klagenfurt. To obtain these results α values for fossil fuel emissions ($\alpha_{ff} = 1.0$) and wood burning emissions ($\alpha_{wb} = 2.0$) determined within (or deduced from) the CAST and wood-burning experiments were used.

BC concentration represents primary pollutants, while the concentration of carbonaceous matter (CM – considered as a sum of all carbon-containing aerosols) also includes secondary pollutants. The benefit of using the Aethalometer model is that the model does not distinguish between primary and secondary pollutants and therefore source identification is

easier. BC concentration tells us more about source apportionment, while CM concentration carries more information about contribution to PM.

When comparing the two winter seasons, in winter 2012/13 we can observe a decrease in BC_{ff} concentration (contribution of traffic) at both measurement stations and an increase of BC_{wb} concentration (contribution of wood-burning) at both measurement stations.

Filter analyses with liquid chromatography yield the amount of anhydrosugars in deposited material. BC_{wb} data calculated from the Aethalometer model and levoglucosan are compared. The well correlated relationships ($R^2 = 0.81$ and $R^2 = 0.86$) of the BC_{wb} /levoglucosan ratios confirm the content of wood smoke in the samples, as both BC_{wb} and levoglucosan are parameters (tracers) of wood smoke. However, the slopes are different at the two sampling sites.

Aethalometer model provides us with a wide range of Angstrom exponent values in the CAST experiment; with increasing C/O ratio α values increased from $\alpha \sim 1.0$ (for black particles) to $\alpha \sim 7.0$ (for brownish/orange particles). The model was also used in wood burning and ambient measurements, where α values were smaller (1.2–2.2). These α values were compared to conditions with the C/O ratios of 0.21 and 0.31 in the CAST experiment, where the filters were dark with some brown material. The less oxygen is present in the process the higher the Angstrom exponent is and less black are the particles. In the ambient measurements, previous experiments and existing literature (Kirchstetter et al., 2004) were taken into consideration. It was thus decided to use α for BC (fossil fuel emissions) equaling 1.0 and α for brownish particles (wood-burning emissions) equaling 2.0. Sensitivity test shows that $\pm 10\%$ deviation of α values may have a significant influence on the source apportionment.

The Aethalometer model to determine the contribution of biomass burning to BC has been implemented in the new Aethalometer AE33. The new instrument now outputs the percentage of BC_{wb} in real time with a time resolution of 1 min.

Bibliography

- [1] Alger, R., 1972. Pyrolysis and combustion of cellulosic materials. In: *The Mechanisms of Pyrolysis, Oxidation, and Burning of Organic Materials*. National Bureau of Standards Special Publ. 357, Gaithersburg, pp. 171-183.
- [2] Andreae, M. O. and Gelencser, A. Black carbon or brown carbon? The nature of light-absorbing carbonaceous aerosols. *Atmos. Chem. Phys. Discuss.*, 2006, 6, 3419–3463.
- [3] Arnott, W. P.; Hamasha, K.; Moosmüller, H.; Sheridan, P. J.; Ogren, J. A. Towards aerosol light-absorption measurements with a 7-wavelength Aethalometer: Evaluation with a photoacoustic instrument and 3-wavelength nephelometer. 2005, 39, 17-29.
- [4] Babich, P.; Davey, M.; Allen, G.; Koutrakis, P. Method comparison for particulate nitrate, elemental carbon, and PM_{2.5} mass in seven U.S. Cities. *J. Air&Waste Manage.*, 2000, 50, 1095-1105.
- [5] Birch, E. and Cary, R. A. Elemental carbon – based method for monitoring occupational exposures to particulate diesel exhaust. *Aerosol Sci. and Techn.*, 1996, 25, 221-241.
- [6] Bond, T. C.; Anderson, T. L.; Campbell, D. Calibration and intercomparison of filter-based measurements of visible light absorption by aerosols. *Aerosol Sci. Tech.* 1999, 30(6), 582-600.
- [7] Bond, T. C.; Streets, D. G.; Yarber, K. F.; Nelson, S. M.; Woo, J.-H.; Klimont, Z. A technology-based global inventory of black and organic carbon emissions from combustion. *Journal of Geophysical Research*, 2004, 109 (D14).
- [8] Bond, T. C. and Bergstrom R. W. Light absorption by carbonaceous particles: An investigative review. *Aerosol Sci. and Techn.*, 2006, 40, DOI:10.1080/02786820500421521
- [9] Cachier, H.; Bremond, M. P.; Buat-Ménard, P. Determination of atmospheric soot carbon with a simple thermal method. *Tellus* 1989, 41B, 379–390.
- [10] Cavalli, F.; Viana, M.; Yttri, K. E.; Genberg, J.; Putaud, J. P. Toward a standardised thermal-optical protocol for measuring atmospheric organic and elemental carbon: the EUSAAR protocol. *Atmospheric Meas. Tech.* 2010, 3, 79-89.
- [11] Caseiro, A.; Marr, I. L.; Claeys, M.; Kasper-Giebl, A.; Puxbaum, H.; Pio, C. A. Determination of saccharides in atmospheric aerosol using anion-exchange high-performance liquid chromatography and pulsed amperometric detection. *Journal of Chromatography A*, 2007, doi:10.1016/j.chroma.2007.09.038.
- [12] Caseiro, A.; Bauer, H.; Schmidl, C.; Pio, C. A.; Puxbaum, H.: Wood burning impact on PM10 in three Austrian regions, 2009. *Atmospheric Environment*, 2009, 43(13), 2186-2195.

- [13] Chow J. C.; Watson, J. G.; Chen, L.-W. A.; Chang, M. C. O.; Robinson, N. F.; Trimble, D.; Kohl, S. The IMPROVE_A Temperature Protocol for Thermal/Optical Carbon Analysis: Maintaining Consistency with a Long-Term Database. *J. of the Air & Waste Manag. Assoc.*, 2007, 57, 1014-1023.
- [14] Coen, M. C.; Weingartner, E.; Apituley, A.; Ceburnis, D.; Fierz-Schmidhauser, R.; Flentje, H.; Heinzinger, J. S.; Jennings, S. G.; Moerman, M.; Petzold, A.; Schmid, O.; Baltensperger, U. Minimizing light absorption measurement artifacts of the Aethalometer: evaluation of five correction algorithms. *Atmos. Meas. Tech.*, 2010, 3, 457-474.
- [15] Dobovicnik, T.; Zgajnar-Gotvajn, A. Correlation among combustion influence in Ljubljana basin. 2008, 130p, UDK: 66:504.7:546.264-546-231(043.2)
- [16] Favez, O.; El Haddad, I.; Piot, C.; Boréave, A.; Abidi, E.; Marchand, N.; Jaffrezo, J.-L.; Besombes, J.-L.; Personnaz, M.-B.; Sciare, J.; Wortham, H.; George, C.; D'Anna, B. Inter-comparison of source apportionment models for the estimation of wood burning aerosols during wintertime in an Alpine city (Grenoble, France). *Atmos. Chem. Phys.*, 2010, 10, 5295-5324.
- [17] Gundel, L. A.; Dod, R. L.; Rosen, H.; Novakov, T.: The relationship between optical attenuation and black carbon concentration for ambient and source particles. *Science of the Total Environment*, 1984, 36, 197-202.
- [18] Hallquist, M.; Wenger, J. C.; Baltensperger, U.; Rudich, Y.; Simpson, D.; Claeys, M.; Dommen, J.; Donahue, N. M.; George, C.; Goldstein, A. H.; Hamilton, J. F.; Herrmann, H.; Hoffmann, T.; Iinuma, Y.; Jang, M.; Jenkin, M. E.; Jimenez, J. L.; Kiendler-Scharr, A.; Maenhaut, W.; McFiggans, G.; Mentel, Th. F.; Monod, A.; Prévôt, A. S. H.; Seinfeld, J. H.; Surratt, J. D.; Szmigielski, R.; Wildt, J. The formation, properties and impact of secondary organic aerosol: current and emerging issues. *Atmos. Chem. Phys.*, 2009, 9, 5155–5236.
- [19] Hansen, A. D. A.; Rosen, H.; Novakov, T. Real-time measurement of the absorption coefficient of aerosol particles. *Applied Optics*, 1982, 21, 3060-3062.
- [20] Hansen, A. D. A.; Rosen, H.; Novakov, T.: The Aethalometer – An Instrument for the Real-Time Measurements of Optical Absorption by Aerosol particles. *The Science of the Total Environment*, 1984, 36, 191-196.
- [21] Hansen, A. D. A. and Rosen, H.: Individual measurements of the emission factor of aerosol black carbon in automobile plums. *J. Air Waste Manage. Assoc.*, 1990, 40, 1654-1657.
- [22] Heintzenberger, J.: Size-segregated measurements of particulate elemental carbon and aerosol light absorption at remote Arctic locations. *Atmos. Environ.* 1982, 16, 2461-2469.
- [23] Hellén, H.; Hakola, H.; Haaparanta, S.; Pietarila, H.; Kauhaniemi, M.: Influence of residential wood combustion on local air quality. *Science of Total Environment* 2008, 393 (2-3), 283-290.
- [24] Hitzemberger, R.; Dusek, U.; Berner, A.: Black carbon measurements using an integrating sphere technique. *J. Geophys. Res.* 1996, 101, 19601-19606.

- [25] Hitzenberger, R.; Tohno, S.: Comparison of black carbon (BC) aerosols in two urban areas (Uji, Japan and Vienna, Austria) – concentrations and size distributions. *Atmos. Environ.* 2001, 35, 2153-2167.
- [26] Hoffer, A., Gelencser, A., Guyon, P., Kiss, G., Schmid, O., Frank, G.P., Artaxo, P., Andreae, M.O. Optical properties of humic like substances (HULIS) in biomass-burning aerosols. *Atmospheric Chemistry and Physics*, 2006, 6, 3563-3570 .
- [27] Hornig, J.F., Soderberg, R.H., Barefoot, A.C., III, Galasyn, J.F., 1985. Wood smoke analysis: vaporization losses of PAH from Plters and levoglucosan as a distinctive marker for wood smoke. In: Cooke, M., Dennis, A.J., (Eds.), *Polynuclear Aromatic Hydrocarbons: Mechanisms, Methods, and Metabolism*. Battelle Press, Columbus, pp. 561-568.
- [28] Iinuma, Y.; Engling, G.; Puxbaum, H.; Herrmann, H. A highly resolved anion-exchange chromatographic method for determination of saccharidic tracers for biomass combustion and primary bio-particles in atmospheric aerosol. *Atmospheric Environment*, 2009, 43, 1367–1371.
- [29] Jacobson, M. Z. Studying the effects of aerosols on vertical photolysis rate coefficient and temperature profiles over an urban airshed. *J. Geophys. Res.*, 1998, 103, 10593-10604.
- [30] Jankowski, N.; Schmidl, C.; Marr, I.L.; Bauer, H.; Puxbaum, H.: Compensation of methods for the quantification of carbonate carbon in atmospheric PM₁₀ aerosol samples. *Atmos. Environ.*, 2008, 42, 8055-8064.
- [31] Jeong, C.-H.; Hopke, P. K.; Kim, E.; Lee, D.-W. The comparison between thermal-optical transmittance elemental carbon and Aethalometer black carbon measured at multiple monitoring sites. *Atmos. Environ.*, 2004, 38, 5193-5204.
- [32] Kim, J.; Bauer, H.; Dobovicnik, T.; Hitzenberger, R.; Lottin, D.; Ferry, D.; Petzold, A. Constraining optical properties and refractive index of combustion aerosol particles through combined experimental and modeling studies, (unpublished yet)
- [33] Kirchstetter, T. W.; Novakov, T.: Evidence that the spectral dependence of light absorption by aerosols is affected by organic carbon. *J. Geophys. Res.*, 2004, 109, D21208; DOI: 10.1029/2004JD004999.
- [34] Kirchstetter, T. W.; Novakov, T.: Controlled generation of black carbon particles from a diffusion flame and applications in evaluating black carbon measurement methods. *Atmospheric Environment*, 2007, 41, 1874-1888.
- [35] Kistler, M.; Schmidl, C.; Padouvas, E.; Giebl, H.; Lohninger, J.; Ellinger, R.; Bauer, H.; Puxbaum, H. Odor, gaseous and PM₁₀ emissions from small scale combustion of wood types indigenous to Central Europe. *Atmospheric Environment*, 2012, 51, 86-93.

- [36] Kochbach, A.; Li, Y.; Yttri, K. E.; Cassee, F. R.; Schwarze, P. E.; Namork, E.: Physicochemical characterization of combustion particles from vehicle exhaust and residential wood smoke. *Particle and Fibre Toxicology*. 2006, 3, 1. DOI: 10.1186/1743-8977-3-1.
- [37] Lanz, V. A.; Alfarra, M. R.; Baltensperger, U.; Buchmann, B.; Hueglin, C.; Szidat, S.; Wehrli, M. N.; Wacker, L.; Weimer, S.; Caseiro, A.; Puxbaum, H.; Prevot, A. S. H. Source Attribution of Submicron Organic Aerosols during Wintertime Inversions by Advanced Factor Analysis of Aerosol Mass Spectra. *Environ. Sci. Technol.*, 2008, 42(1); 214-220. DOI: 10.1021/es0707207.
- [38] Lanz, V. A.; Prévôt, A. S. H.; Alfarra, M. R.; Mohr, C.; De-Carlo, P. F.; Weimer, S.; Gianini, M. F. D.; Hueglin, C.; Schneider, J.; Favez, O.; D'Anna, B.; George, C.; Baltensperger, U. Characterization of aerosol chemical composition by aerosol mass spectrometry in Central Europe: an overview. *Atmos. Chem. Phys. Discuss.*, 2009, 9, 24985-25021, doi:10.5194/acpd-9-24985-2009.
- [39] Levin, Z. and Lindberg, J.D. Size distribution, chemical composition, and optical properties of urban and desert aerosols in Israel. *Journal of Geophysical Research*, 1979, 84, doi: 10.1029/OJGREAO00084000C11006941000001.issn:0148-0227
- [40] Lindberg, J. D.; Douglass, R. E.; Garvey, D. M. Carbon and the optical properties of atmospheric dust. *Appl. Opt.*, 1993, 32, 6077-6081.
- [41] Lioussé, C.; Cachier, H.; Jennings, S. G.: Optical and thermal measurements of black carbon aerosol content in different environments: Variations of the specific attenuation cross-section σ . *Atmos. Environ.*, 1993, 27(8), 1203-1211.
- [42] Locker, H.B., 1988. The use of levoglucosan to assess the environmental impact of residential wood-burning on air quality. Ph.D. Thesis, Dartmouth College, Hanover, NH, 137 pp.
- [43] McDonald, J.D.; Zielinska, B.; Fujita, E.M.; Sagebiel, J.C.; Chow, J.C.; Watson, J.G.: Fine particle and gaseous emission rates from residential wood combustion. *Environmental Science and Technology*, 2000, 34, 2080–2091.
- [44] Peterson, M. R. and Richards, M. H.: Thermal-optical transmittance analysis for organic, elemental, carbonate, total carbon, and OCX2 in PM2.5 by the EPA/NIOSH method, in: *Proceedings, Symposium on Air Quality Measurement Methods and Technology-2002*, edited by: Winegar, E. D. and Tropp, R. J., Air & Waste Management Association, Pittsburgh, PA, 83-1-83-19, 2002.
- [45] Petzold, A.; Kopp, C.; Niessner, R.: The dependence of the specific attenuation cross-section on black carbon mass fraction and particle size. *Atmos. Environ.* 1997, 31(5), 661-672.
- [46] Puxbaum, H. Thermo gas-analyzer for the characterization of carbonaceous and sulphurous compounds in atmospheric particles. *Fresenius Zeitschrift fuer Analytische Chemie*. 1979, 298, 250-259.

- [47] Puxbaum, H.; Caseiro, A.; Sánchez-Ochoa, A.; Kasper-Giebl, A.; Claeys, M.; Gelencsér, A.; Legrand, M.; Preunkert, S.; Pio, C.: Levoglucosan levels at background sites in Europe for assessing the impact of biomass combustion on the European aerosol background, *J. Geophys. Res.*, 2007, 112, D23S05.
- [48] Roberts, A.F., 1970. A review of kinetics data for the pyrolysis of wood and related substances. *Combustion and Flame* 14, 261-272.
- [49] Sandradewi, J.; Prévôt, A. S. H.; Weingartner, E.; Schmidhauser, R.; Gysel, M.; Baltensperger, U.: A study of wood burning and traffic aerosols in an Alpine valley using a multiwavelength Aethalometer. *Atmospheric Environment*, 2008a, 42, 101-112.
- [50] Sandradewi, J.; Prévôt, A. S. H.; Alfarra, M. R.; Szidat, S.; Wehril, M. N.; Ruff, M.; Weimer, S.; Lanz, V. A.; Weingartner, E.; Perron, N.; Caseiro, A.; Kasper-Giebl, A.; Puxbaum, H.; Wacker, L.; Baltensperger, U.: Comparison of several wood smoke markers and source apportionment methods for wood burning particulate mass. *Environ. Sci. Technol.*, 2008b, 42 (9), 3316–3323.
- [51] Schmid, H.; Laskus, L.; Abraham, H.J.; Baltensperger, U.; Lavanchy, V.; Bizjak, M.; Burba, P.; Chachier, H.; Crow, D.; Chow, J.; Gnauk, T.; Even, A.; Brink, H.M.; Giesen, K.P.; Hitzemberger, R.; Hueglin, C.; Maenhaut, W.; Pio, C.; Carvalho, A.; Putaud, J.P.; Sauntry, D.T.; Puxbaum, H.: Results of the “carbon conference” international aerosol carbon round robin test stage I. *Atmospheric Environment*, 2001, 35(12), 2111-2121 .
- [52] Schmidl, C.; Marra, I. L.; Caseiro, A.; Kotianova, P.; Berner, A.; Bauer, H.; Kasper-Giebl, A.; Puxbaum, H.: Chemical characterisation of fine particle emissions from wood stove combustion of common woods growing in mid-European Alpine regions. *Atmospheric Environment*, 2008, 42, 126-141.
- [53] Schmidl, C.; Bauer, H.; Dattler, A.; Hitzemberger, R.; Weissenboeck, G.; Marr, I.L.; Puxbaum, H.: Chemical characterization of particle emissions from burning leaves. *Atmospheric Environment*, 2008b, 42(40), 9070-9079.
- [54] Schnaiter, M.; Horvath, H.; Möhler, O.; Naumann, K.-H.; Saathoff, H.; Schöck, O. W.: UV-VIS-NIR spectral optical properties of soot and soot-containing aerosols. *Aerosol Science*, 2003, 34, 1421-1444.
- [55] Schnaiter, M.; Linke, C.; Möhler, O.; Naumann, K.-H.; Saathoff, H.; Wagner, R.; Schurath, U. Absorption amplification of black carbon internally mixed with secondary organic aerosols. *J. Geophys. Res.* 2005, 110, D19204; doi: 10.1029/2005JD006046.
- [56] Schnaiter, M.; Gimmler, M.; Llamas, I.; Linke, C.; Jäger, C.; Mutschke, H.: Strong spectral dependence of light absorption by organic carbon particles formed by propane combustion. *Atmos. Chem. Phys. Discuss.*, 2006, 6, 1841–1866.

[57] Sergejewa, A.S., 1959. Chemie des Holzes und der Cellulose. Theodor Steinkopff Verlag, Dresden, 143 pp.

[58] Shafizadeh, F., 1984. The chemistry of pyrolysis and combustion. In: Rowell, R. (Ed.), Chemistry of Solid Wood, Adv. Chem Series 207, American Chemical Society, Washington, DC, pp. 489-529.

[59] Simoneit, B. R. T.; Schauer, J. J.; Nolte, C. G.; Oros, D. R.; Elias, V. O.; Fraser, M. P.; Rogge, W. F.; Cass, G. R.: Levoglucosan, a tracer for cellulose in biomass burning and atmospheric particles. Atmospheric Environment, 1999, 33, 173-182.

[60] Virkkula, A.; Mäkelä, T.; Hillamo, R.; Yli-Tuomi, T.; Hirsikko, A.; Hämeri, K.; Koponen, I. K.: A Simple Procedure for Correcting Loading Effects of Aethalometer Data. J. Air & Waste Manage. Assoc., 2007, 57, 1214-1222.

[61] Weingartner, E.; Saathoff, H.; Schnaiter, M.; Streit, N.; Bitnar, B.; Baltensperger, U.: Absorption of light by soot particles: determination of the absorption coefficient by means of Aethalometers. Aeros. Sci. 2003, 34, 1445-1463.

[62] Wonaschütz, A.; Hitzenberger, R.; Bauer, H.; Pournazer, P.; Klatzer, B.; Caseiro, A.; Puxbaum, H.: Application of the Integrating Sphere Method to Separate the Contributions of Brown and Black Carbon in Atmospheric Aerosols. Atmos. Environ. 2009, 43, 1141-1146.

On-line references

[63] Environmental Report Carinthia 2012,

http://www.kiks.ktn.gv.at/260375_DE-PDF-Umweltbericht_2012.pdf – 6. 4. 2013

[64] Janssen, N. A. H.; Gerlofs-Nijland, M. E.; Lanki, T.; Salonen, R. O.; Cassee, F.; Hock, G.; Fischer, P.; Brunekreef, B.; Krzyzanowski, M. WHO Regional office for Europe: Health Effects of Black Carbon, 2012

http://www.euro.who.int/_data/assets/pdf_file/0004/162535/e96541.pdf – 15. 12.2012

[65] U.S. Pat. No. 3,970,430, which issued on Jul. 20, 1976, to John R. Reader, Jr. et al

<http://www.google.si/patents?hl=sl&lr=&vid=USPAT3970430&id=lqEPAAAAEBAJ&oi=fnd&dq=NOx+absorb+in+wavelength&printsec=abstract#v=onepage&q=NOx%20absorb%20in%20wavelength&f=false>

[66] Year book, Klagenfurt 2012

http://www.klagenfurt.at/klagenfurt-am-woerthersee/downloads/Jahrbuch_2012.pdf – 6. 4. 2013

[67] Zahoransky, R.; Kerzenmacher, S.; Benali, G.; Lavigne, R.; Kassab, J.; Henneke, D.: On-line particle emission analysis of the CAST burner using LPME.

<http://www.sootgenerator.com/documents/Zahoransky.pdf>

[68] http://www.esrl.noaa.gov/gmd/aero/instrumentation/neph_desc.html – 11. 5. 2011

[69] <http://www.wodtke.si/toplozracni-polena-vision7.html#ime> – 15. 11. 2012

[70] <http://www.2020site.org/trees/beechn.html> – 15. 11. 2012

[71] www.firestixx.com – 2.5.2013

[72] <http://pminter.eu> – 5. 5. 2013

[73] <http://www.dispergator.com/eng/pellets.htm> – 10.5.2013

[74] www.rika.at – 10. 6. 2013

[75] <http://www.onlineethics.org/cms/23617.aspx> – 10. 6. 2013

[76] <http://www.cdc.gov/niosh/docs/2003-154/pdfs/5040f3.pdf>. – 01/15/13

[77] <http://www.cta.tuwien.ac.at/epa/ea/> – 02/14/2012